JOURNAL OF ENGINEERING & TECHNOLOGY

(A State Level Research Journal)

Volume-2 April-2009

GIT JET

PLATINUM FOUNDATION MANAGED

GANDHINAGAR INSTITUTE OF TECHNOLOGY

A CENTER FOR ENGINEERING AND MANAGEMENT STUDIES

(Approved by AICTE and Affiliated to Gujarat University & Gujarat Technological University)

www.git.org.in
director@git.org.in
PH: 02764 281860/61
FAX: 02764 281862

AT & PO: MOTI BHOYAN,
KHATRAJ-KALOL ROAD,
VIA. VADSAR, TA. KALOL,
DIST. GANDHINAGAR 382721

EDITORIAL BOARD

****

FROM THE DESK OF CHAIRMAN

It gives me a great pleasure to release the second volume of the journal of engineering and technology, published by GIT managed by platinum foundation.

This journal is published annually by the Gandhinagar Institute of Technology with a broad objective of imparting a platform of the research workers in the field of engineering & technology from all over the state to make meaningful contribution to the nation.

There is a need to strengthen the exchange of knowledge between the scientists and research and as Dean of Gujarat Technological University and acting Vice-Chancellor of GTU, I am happy to see the quality of the papers from selected contributors. I am sure this journal will bring research excellence and explore new areas of innovation.

I commend the efforts put in by Prof. Dr. K. N. Sheth and editorial board to bring out the present issue.

March, 2009
Ahmedabad

Prof. M. N. Patel
Dean, Faculty of Engg. & Tech.
Gujarat University and
Acting Vice Chancellor
Gujarat Technological University

IMPROVING THE QUALITY OF RESEARCH PROGRAMMING IN GUJARAT

The universities have been considered excellent centres of research exchange Universities have, in its present era, assumed functions of teaching and advancement of knowledge through research, innovation and creativity.

Research in the discipline of engineering education has a substantial role in improving and strengthening all aspects of education system. Though the volume of research in the field of engineering and technology in Gujarat has increased during last decades, its quality has gradually deteriorated. The function of advancement of knowledge is not receiving the expected attention due to the deterioration in research environment in most of the universities in Gujarat.

Gujarat Technological University has now a challenging role of improving the quality of research programme taken up in the field of engineering, technology and management. GTU will have to encourage enrolment of research scholars and ensure good quality doctoral research and original contribution of knowledge.

Alongwith teaching which is an important function of University teachers, it is crucial for the faculty to extend their intellectual horizons through research and constantly lead the society in the area of their specialization. Excellence is only possible where there is selfless ambition to work for the society and not by undertaking compulsory component of Ph.D. programme or the sake of fulfillment of University / AICTE requirements. In order to improve the quality of education and research, it is essential that both the research guides and research scholars must take up the research project with a sense of devotion, commitment and mission.

To face the challenges of today's recession, advances in technology will prove a successful weapon in the hands of technocrats.

DR. K. N. SHETH
CONVENOR & EDITOR IN CHIEF

CLEANER PRODUCTION VIA CRITICAL ANALYSIS OF TECHNOLOGIES AND POLLUTION CONTROL

Dr. K. N. Sheth,
Director
Gandhinagar Institute of Technology
Ta. Kalol, Dist. Gandhinagar

Dr. S. A. Puranik
Director
Atmiya Institute of Technology & Science,
Rajkot-Gujarat

ABSTRACT

Three typical selected case studies w.r.t. Petrochemicals and Pharmaceutical industries have been considered. Analysis of technologies being employed and recommendations for cleaner production are presented w.r.t. three typical selected cases. It is been concluded that **"Cleaner Production Analysis"** is the need of hour.

Cleaner production analysis for cases under consideration

Route-(I)

Vinyl Chloride can be manufactured by two steps process as under:

Step-(I) Direct chlorination of Ethylene to Ethylene dichloride (EDC)

$$CH_2 = CH_2 + Cl_2 \xrightarrow[65^0C]{(Fecl_2)} ClCH_2 - CH_2Cl$$

ΔH_R = -180 Kj/mole, (exothermic)

Step-(II) Pyrolysis (Thermal cracking) of EDC to vinyl chloride

$$ClCH_2 - CH_2CH_2Cl \xrightarrow[550^0C]{x=60\%} CH_2 = CHCl + HCl$$

ΔH_R = +71 Kj/mole, (endothermic).

- For step-(I): Practically 100% conversion and selectivity above 99%.
- For step-(II): Conversion of EDC to VCM 60% and yield of VCM is above 99%.
- One can say capacity of producing VCM is 50 Ton moles/day. One can also say capacity of plant producing HCl is also 50 Ton moles/day.
- Thus, HCl happens to be co-product which not environmentally friendly.
- Large quantity of liquid effluent containing HCl is generated while separating HCl and VCM by absorption.
- Stringent pollution control measures are required with respect to gaseous pollution due to Cl_2 as well as liquid effluent stream which contains-HCl.

Route-(II)

Step-I Direct chlorination as well as oxy chlorination.

$$CH_2 = CH_2 + Cl_2 \xrightarrow[65^0C]{Fecl_2} ClCH_2 - CH_2Cl$$

ΔH_R = -180 Kj/mole, exothermic

$$CH_2 = CH_2 + 2HCl + \frac{1}{2}O_2 \xrightarrow{240^0C} ClCH_2 - CH_2Cl$$

ΔH_R = -239 Kj/mole, highly exothermic

Step-II: Thermal cracking (Pyrolysis) of EDC to vinyl chloride

$$ClCH_2 - CH_2Cl \xrightarrow[550^0C]{x=60\%} CH_2 = CHCl + HCl$$

ΔH_R = +71 Kj/mole, (endothermic)

- In Step (I), two moles of EDC are obtained but one mole of EDC by direct chlorination and second mole of EDC by oxy chlorination.
- These two moles of EDC are converted to 2 moles of VCM and co-product-HCl obtained is also two moles.
- These two moles of HCl obtained in step-II are recycle to step-I wherein half mole of oxygen is added and it becomes feed stock for step-I.
- Thus in this route-(II), since HCl is fully utilized as a raw material by totally recycling it, it becomes a case of zero % discharge of liquid waste.
- Chlorine quantity requirements are reduced to half, as a result intensity of pollutant-Cl_2 in gaseous effluent stream also gets reduced considerably.

Requirement of raw materials and product produced by Material Balance Principles have been reported in Table-(I). For critical analysis of both routes using MEB Principles from Environmental Point of View, Table-(I) could be utilized conveniently.

Table-(I)

Basis = 10,000 TPD of VCM

		Product		Intermediate	Reactants		Reactants	
	Unit	VCM	HCl*	EDC	C_2H_4	Cl_2	HCl*	O_2
Route-I	TPD	10,000	5,826	25,084	7,094	17,989	-	-
	Kgmol/s	1.851	1.851	2.94	2.94	2.94	-	-
	Unit	VCM	HCl*	EDC	C_2H_4	Cl_2	HCl*	O_2
Route-I	TPD	10,000	5,826	25,084	7,094	8,995	5,826	640
	Kgmol/s	1.851	1.851	2.94	2.94	1.47	1.851	0.462

As could be seen from above Table-(I), product-HCl produced (5826.2 TPD) is recycled as a raw material and it is mixed with 640 TPD of O_2 available from air. Thus 8995.0 TPD of chlorine is produced in the plant. Raw material requirements of Cl_2 thus reduces to half i.e. Instead of 17,989 TPD of raw material Cl_2 only 8995.0 TPD of Cl_2 is required. Generation of liquid waste practically reduces to zero because of HCl recycle. Concentration of Cl_2 pollutant in gaseous stream also reduces to half by use of dilution principle.

It may be noted that liquid effluent generated in the case of Route-II is practically zero. Further, raw material requirement of Cl_2 decreases to half. Thus, Route-II happens to be economically the cheapest route and it is also an environmentally friendly route.

Case Study-II: Formalin Production (Solution of formaldehyde).

37% solution of formaldehyde is called: "Formalin". Formaldehyde can be manufactured by following two processes wherein raw material is methanol (CH_3OH).

Route-I: Oxidation Process:

$$CH_3OH + \tfrac{1}{2}O_2 \xrightarrow[\text{Oxide of Ag.Mo.}]{650^0\,C} HCHO + H_2O \quad \Delta H_R = -156 \text{ Kj/mole.}$$

- Highly exothermic reaction,
- Conversion 80-90%, yield=90%,
- HCHO vapours absorbed in H_2O and

one obtains 37% solution of HCHO called as Formalin.
- Highly energy intensive process, large requirement of cooling water.
- Unreacted methanol separated from formalin by distillation.

Route-II: Dehydrogenation Process:

$$CH_3OH \xrightarrow[Oxides\ of\ Fe,Cr]{600^0 C} HCHO + H_2$$

ΔH_R = 85 Kj/mole

- Highly endothermic reaction,
- Conversion 70-80%, Yield=99%.
- ($HCHO+H_2$) vapours absorbed in H_2O, H_2 gets separated and formalin is formed.
- Highly energy intensive process, large quantity of Heating media required.
- Unreacted methanol separated from formalin by distillation.

Route-I: Produces air emissions such as No_x, CO etc. Hence stringent air pollution control measures required. Also large requirement of cooling media.

Route-II: Happens to be environmentally friendly route as O_2 (from air) not required and has higher yield than route-(I). Also large requirement of heating media.

Cleaner Production Option

As a technological new option, if both is routes-(I) & (II) are combined and oxidation process as well as dehydrogenation process occur simultaneously using shell and tube heat exchanger as a reactor, then heat evolved on tube side wherein oxidation reaction is being carried out can be utilized conveniently to heat the entire mass from shell side wherein dehydrogenation reaction is being carried out. Thus, full energy conservation can be achieved. Energy requirements-cooling media for route-I as well as heating media for route-II reduces to zero.

- Appropriate material balances and energy balances can be done on shell side as well as tube side. Energy requirement from external source for the combined route is, thus, zero.

Critical Analysis:

Basis: 500 TPD of formaldehyde
(**0.1903** Kgmoles of HCHO per sec)

		Oxidation Route	**Combined Route**
CH_3OH required	-	665 TPD	655.25 TPD
Air required	-	1123 TPD	397.44 TPD
Oxygen required	-	234.7 TDP	92.62 TPD
Energy required	-	29.68 Kj/S	zero Kj/S

Temperature of reaction being very high of the order of 600-650^{o}C, some quantity of nitrogen from air is likely to get oxidized to No_x.

Feed stock contains carbon in combined form. Hence, formation of CO, CO_2 by oxidation is likely to occur. Thus, quantity of gaseous stream coming out of plant containing pollutants gets reduced considerably by 65%. Thus, intensity of air pollution gets reduced by a factor of three.

Thus, combined route is likely to be an environmentally friendly route. Heating media and cooling media get generated in plant itself. Energy requirement from external source reduces to zero. Thus, substantial saving is resulted in recurring expenditure. It is a win-win situation for industrialist, pollution control board as well as customer.

In summary, formaldehyde production by combined route is a good example of cleaner production in terms of waste minimization and Energy Conservation.

Case Study-III

Paracetamol Production

Analysis of technologies being employed by Indian industry and recommendations for cleaner production[9,10].

In the phenol route followed by some Indian industries, every ton of paracetamol results into 40,000 liters (approx) of effluent. The yield of paracetamol, based on phenol, obtained is around 60% (l.0t/t phenol). There is tremendous scope of reduction of effluent quantity and improvement of yields.

In the process being adopted, nitrosation is carried out by the reaction of phenol with sodium nitrite in presence of sulphuric acid in a wooden vat. Various chemicals used, per ton of paracetamol include 1050 kg (approx) phenol, 700 kg (approx) sulphuric acid, 1000 kg (approx) sodium nitrite and 170 kg (approx) sodium meta-bisulphite. The low reaction temperature (less than 0°C) is obtained by adding ice into the reaction mass.

The reaction products are filtered and 15,000 lit effluent/ton of paracetamol is discarded. If alloy steel reactor is employed along with chilled brine plant, the effluent could be minimized at least by 10,000 lit/ton of paracetamol. With proper process control, the reaction could be optimized, loss of reactants and products minimized in the effluent, resulting into improved yields.

The reduction of nitrosophcnol to p-aminophenol is carried out with the help of sodium sulphide, generated in situ by the reaction of sulphur with caustic soda, in acidic media and the reduced mass is neutralized with ammonium sulphate. The exothermic reaction is carried out at around 50°C. Various chemicals used, per ton of paracetamol include 900 kg (approx) sulphur, 1750 kg (approx) caustic lye, 1200 kg (approx) hydrochloric acid and 1050 kg (approx) ammonium sulphate. The reaction products are filtered and 8,000 lit effluent (approx)/ton of paracetamol is discarded. The p-aminophenol cake is then purified using activated charcoal in aqueous media and the filtrate generated is of the order of 10,000 lit/ton of paracetamol. If catalytic reduction is carried out with hydrogen and Pd/C catalyst, the effluent could be reduced by around 6,000 lit/ton of paracetamol. With better control of the reaction during catalytic hydrogenation and avoidance of various chemicals used at present, side reactions could be minimized. This would result into improved yield and purer p-aminophenol, requiring less activated carbon and water for its purification and thereby reducing the effluent by at least 6,000 lit/ton of paracetamol. Hydrogen transfer catalysis can offer all these advantages, without handling hydrogen gas. Electrochemical reduction of p-nitrosophenol can also result in less effluent and increased yields.

In the p-nitrochlorobenzene route, followed by many Indian industries, liquid effluent generated is 35,000 liters (approx) for every ton of paracetamol produced The yield of paracetamol, based on p-nitrochlorobenzene is around 75% (0.75 t/t of pNCB). There is scope of reduction of effluent quantity and improvement of yields.

In the process being adopted, hydrolysis is carried out by the reaction of 9% caustic soda solution with p-nitrochlorobenzene. There is no automation for this exothermic reaction. 1335 kg (approx) p-nitrochlorobenzene and 800 kg (approx) caustic soda are used for every ton of paracetamol produced. The reaction mass is filtered and 8,000 litres of highly alkaline filtrate per ton of paracetamol is discarded. With suitable process control and proper design of the reactor, the yields could be optimized, resulting into lower requirement of inputs and generation of lower quantities of effluent.

The sodium salt of p-nitrophenol is then treated with concentrated sulphuric acid (850 kg per ton paracetamol) at 35-45°C. p-Nitrophenol is filtered and 2,000 liters of highly acidic filtrate per ton of paracetamol is discarded. With proper filtration and water wash, alkaline liquor trapped into sodium salt of p-nitrophenol

could be minimized and thereby consumption of sulphuric acid for neutralization could be reduced. The dissolved salts content in the acidic effluent could also be reduced.

p-Nitrophenol is reduced with iron and acetic acid (530 kg and 53 kg per ton of paracetamol respectively) at 90-100°C temperature in wooden vat. The reaction temperature is raised by direct injection of steam. On completion of reduction, water is added to the reaction mass, iron sludge is removed by filtration and the filtrate is pooled to 15°C p-Aminophenol is filtered and the filtrate (9000 lit/ton paracetamol) is collected.

This filtrate, containing p-aminophenol could be re-used in the reduction step 4-5 times before being discharged as effluent. P-aminophenol recovery from the effluent may be increased by further lowering its temperature, using some solvent or by salting out. This would improve the yields. Proper design of the reduction vessel along with optimum stirring speed should also result in the improvement of the yields. The iron sludge could be used for making iron oxide for red oxide primers. Catalytic hydrogenation or electrolytic reduction of p-nitrophenol is likely to give higher yields and avoid solid wastes. Hydrogen transfer catalysis is likely to give all these advantages, without handling hydrogen gas. Pure p-aminophenol is reported to be prepared by adding more p-nitrophenol to the reaction mixture (if the reaction has gone to completion), adjusting the pH between 5.0 and 6.5 and separating the p-nitrophenol phase (for re-use in reduction) and the p-aminophenol could be purified by giving treatment with carbon in aqueous hydrochloric acid solution and it could be stabilized by the addition of sodium sulphite.

The acetylation of p-aminophenol to crude paracetamol is carried out by the addition of 1000 kg (approx) acetic anhydride/ton of paracetamol. No attempt is made to control the temperature of this exothermic reaction. The temperature could increase to around 80°C. After cooling, crude paracetamol is filtered and 4,000 lit (approx) filtrate/ton of paracetamol is discarded. The crude paracetamol is given charcoal treatment and pure paracetamol is recrystallized in water, generating 8,000 lit/ton (approx) paracetamol effluent. The wet cake of paracetamol is centrifuged, dried and packed. The temperature control during acetylation may ensure complete acetylation of p-aminophenol and reduction of side products formation.

The filtrate, after filtration of crude paracetamol, is dilute acetic acid solution containing unreacted p-aminophenol and paracetamol. Secondary acetylation may ensure that the conversion of p-aminophenol is complete. With solvent extraction, paracetamol could be recovered and dilute acetic acid could find some uses. The filtrate obtained after filtration of pure paracetamol could be re-used in the purification step 3-4 times before being discharged as effluent. Paracetamol could be recovered from this effluent by lowering its temperature or by solvent extraction or by salting out. This would improve the yields.

P-aminophenol obtained as reduction product is also reported to be acetylated without isolation. Simultaneous reduction and acetylation1 of p-nitrosophenol with hydrogen in presence of catalyst Pd/C, acetic acid and acetic anhydride can reduce number of process steps, increase the yields and minimize effluents to a large extent.

Modification[1] of acetylation process by pH control during acetylation with acetic anhydride and removal of water with the help of Dean-Stark water trap is reported to maximize the yields of paracetamol. Acetylation could also be modified[2] by dissolving p-aminophenol in acetic acid, treating the mixture with carbon and filtering: treating the filtrate with acetic anhydride and separating paracetamol, recycling the mother liquor alter separation of paracetamol for use as solvent for dissolving p-aminophenol. In addition to reducing the effluent quantity, this process would increase the yields by minimizing loss of paracetamol in the acidic effluent.

During the purification of crude paracetamol by recrystallization from hot water, pH control to 6.5 by the addition of ammonia is reported[3] reducing the solubility of paracetamol in the acidic effluent, thereby increasing the yields.

Recrystallization in aqueous isopropanol[4] containing formamidine sulfinic acid and sodium bisulphite at 85-90°C for 15-20 minutes, cooling the mass to 10°C and filtering the mixture is reported to give better yields. This would help in reducing the effluent quantity and improving yields.

Purification of crude paracetamol may be attempted, without the addition of sodium bisulphite and sodium hydrosulphite, but by aerating with hydrogen peroxide/peracetic acid, followed by charcoal treatment to remove iron oxides and oxidation by-products.

In addition to improvements suggested above in the production processes followed by the Indian Industry, using phenol and p-nitrochlorobenzene as the basic raw materials, the production of p-aminophenol by electrolytic reduction of nitrobenzene[5], and coupling of phenol with diazotized aniline in dilute sodium hydroxide, precipitating hydrozobenzene and hydrogenolyzing, in methanol is also reported.

There is a mention of isomerization[6] of p-aminophenol in high yields to paracetamol in the presence of acetic acid or phosphoric acid. Paracetamol is reported[5] to have been prepared by Beckmann rearrangement of p-hydroxy-aceto-phenoxy oxine in the presence of thionyl chloride in potassium iodide-ethyl acetate solvent with 99.44% conversion.

It is reported[7] that the reaction of hydroquinone, acetamide and HZSM-5 zeolite gave 93.6% conversion of hydroquinone with 45.9 mole % of selectivity to paracetamol. The single step reaction of hydroquinone and a ammonium acetate is reported[8] to give paracetamol with a selectivity of 75% on hydroquinone.

These new processes[7] offer simplification in reaction steps and may be evaluated from techno-economic angle especially with respect to variable cost. All the relevant details W.R.T. cleaner production options are available in details in a technical paper of AKA Rathi & Puranik[9,10].

From the above critical discussion it is Crystal Clear that there is tremendous scope for reduction in effluent quantity and improvement of yields by use of process optimization of various parameters.

Conclusions

“Cleaner Production” appears to be the need of hour. By performing critical analysis of various technical options available for the production of various chemicals, methodologies can be appropriately suggested for reducing the quantity of effluent generated in a particular process. Thus, an environmentally friendly route can be suggested. It also automatically results in reduction in the cost of production in many cases.

In this technical paper only three typical case studies have been considered. However, there is tremendous scope to perform “Cleaner Production Options” for other chemicals under different sectors like Petrochemicals, Fertilizers, Dye & Intermediates, Solvents, Pesticides, Plastics, rubber etc. inclusive of inorganic chemicals.

References

1. Dhanutirto Haryanto et al. (FMIPA, ITC, Bandung), Acta Pharm Indones, 9(2), 79-85, 1984.
2. Schulman H L et al. (Mallinckrodt Inc), Pat U S 3,917,695, 4 Nov 1975, 4pp.
3. Young D W (Sinclair research Inc.), Pat U S 3,113,150, 3 Dec 1963.
4. Keel B L et al. (Monsanto-Co), Pat U S 4,474,985, 2 Oct 1984, 4pp.
5. Fruchey O S (Hoechst Celances Corpn), Pat U S 4,855,499, 8 Aug 1989, 4pp.
6. Akieda H et al. (Mitsui Toatsu Chemical), Pat E P 435,263,3 Jul 1991, 15pp.
7. Clerici M G et al. Pat E P 321,020, 21 Jun 1989, 4pp.
8. Ratnaswamy P, Chem Weekly, 14 Dec 1993, 60.
9. Rathi AKA and Puranik S. A., Research & Industry, 1994, Vol. 39, Sept., P-143-146.
10. Rathi AKA and Puranik S. A., Chem. Engg. World, 1994, Vol. XXIX, No. 10, Oct. P45 to 52.

DEVELOPMENT AND COMPARISON OF COMPOUND PARABOLIC CONCENTRATING SOLAR COLLECTORS

Dr. P. K. Shah
Mechanical Engineering Department
Govt. Engineering College, Bhuj

Dr. L. N. Patel
Principal
S. P. College of Engineering, Visnagar

ABSTRACT

Compound parabolic concentrator (CPC) is the most popular non-imaging type solar collector. Its development is cited in the introduction. Geometric expressions for the quantities like concentration ratio, arc length, aperture width, collector height etc. are derived for the CPC having cylindrical absorber with a gap between absorber and reflector. These expressions form a mathematical model, which is used to generate a large amount of data. The characteristic curves are plotted which are useful for selection of CPC for a particular application. Various CPC configurations are compared. Noting some latest applications of CPC ends the paper.

NOMENCLATURE

C = concentration ratio
F(θ') = angular acceptance
H = height of CPC
L = reflector arc length
W = aperture width
n = average number of reflections
r_e = radius of envelope
r_o = outside radius of the absorber
x, y = cartesian co-ordinates
θ = angle between the line joining any point on absorber with origin and the negative y-axis
θ' = incident angle
θ_c = half acceptance angle
θ_t = angle between CPC axis and extreme ray

INTRODUCTION

Solar collectors used for collecting solar energy are divided into two main types, flat plate collectors (FPC) and concentrating collectors. The concentrating collectors may further be classified as (1) focusing or imaging type collectors e.g. cylindrical parabolic concentrators and (2) non-focusing or non-imaging type concentrators e.g. compound parabolic concentrators.

In CPC, the rays, after reflection, are not focused at a point or line but are simply collected on absorber (receiver) surface. So it is known as non-focusing type concentrator. The basic two-dimensional CPC having flat absorber is shown in Fig. 1. It has two different parabolic surfaces, which work as reflectors. The rays incident in the range of acceptance angle $2\theta_c$ are fully accepted. AF and BG are known as shadow lines. Central vertical line is called optic axis. The ratio of aperture area to absorber area is known as concentration ratio C. This ratio for FPC is 1, for CPC it is 2 to 10 and for focusing collectors it is greater than 10.

Thus concentration ratio for CPC is in the moderate range, so the temperature obtained in CPC is also in the moderate range. Temperature obtained in FPC is 55^o to 100^o C, in CPC 100^o to 200^o C and in focusing collector it is greater than 200^o C. The moderate temperature available in CPC is useful in large number of practical applications. So CPCs are much popular. A part of diffuse radiation (=1/C) is also accepted by CPC.

It can be proved that the maximum concentration C_{max} achieved by any concentrator is limited to $1/\sin\theta_c$ by second law of Thermodynamics. This is known as ideal concentration. CPC achieves this ideal concentration while the other concentrators fall short of it. CPC does not need a continuous tracking of the sun unlike the focusing collectors but it necessitates only a few tilt adjustments per year.

The upper portion of the reflectors does not collect much energy, so it is a practice to truncate the reflector to about 1/2 to 1/3 of its full height. This way, a large amount reflector material is saved only with a slight loss in concentration ratio.

The rays incident on aperture may either fall directly on the absorber or may reach the absorber after one or more reflections from the reflector. A term average number of reflections n is defined as the average of numbers of reflections experienced by all rays. CPC with smaller value of n will be more efficient. Truncation decreases n, thus making the collector more efficient. One more term known as angular acceptance function F(θ') is defined as a fraction of the rays incident on the aperture at an angle θ' that reaches the absorber. By truncation, some more rays are accepted beyond $2\theta_c$.

The basic CPC with flat absorber was, first of all, developed by Winston [1] in 1974. Rabl [2] derived the expressions for height H, reflector are length L, aperture width W and average number of reflections n for full & truncated CPCs. The graphs of L/W → C, H/W → C and n→ C (L and H are divided by W to make them dimensionless) are plotted for various acceptance angles and for various degrees of truncation for each acceptance angle. These graphs provide a good design data. Carvalho et al. [3] derived the expression for F(θ') and plotted the graphs of F(θ') → θ' for a known acceptance angle with various degrees of truncation.

CPC WITH CYLINDRICAL ABSORBER

The main drawback in CPC with flat absorber is that there is a back loss from the backside of the absorber. The development of CPC having cylindrical absorber is presented by Rabl [4], where this loss is prevented as the absorber is covered by reflector from all sides. This CPC is shown in Fig. 2. AG is the mirror image of AF. Of course, for ideal concentration, the shape of the reflector will no longer remain a parabola, but it has to be changed. For ideal concentration, the portion of the reflector from the bottom of the absorber to the point where shadow line touches the reflector (arc AB) should be involute to the absorber and remaining portion (arc BF) should be such that the ray incident on it at an angle θ_c should, after reflection, be a tangent to the cylindrical absorber. The expression for reflector shape satisfying these conditions is presented by Baum & Gordon [5]. This expression is:-

$$x = r_o\left(\sin\theta - M(\theta)\cos\theta\right)$$
$$y = -r_o\left(\cos\theta + M(\theta)\sin\theta\right) \quad (1)$$

where $M(\theta) = \theta$ for involute portion (2)

$$= \frac{\theta + \theta_c + \frac{\pi}{2} - \cos(\theta - \theta_c)}{1 + \sin(\theta - \theta_c)}$$

for the remaining portion (3)

The center of the absorber & the optic axis are considered as origin and y-axis respectively for the co-ordinate system.

In this case, the graphs of L/W→ C and H/W→C are plotted by McIntire [6] and that of F(θ') → θ' and n → C are plotted by Carvalho et al. [3].

CPC WITH CYLINDRICAL ABSORBER HAVING A GAP BETWEEN ABSORBER AND REFLECTOR

In the previous case, absorber touches the reflector. So, there is conduction heat loss from absorber to reflector. To avoid this heat loss, a gap should be created between the absorber and reflector. One of the methods to create a gap, as suggested by Winston [7], is to lift the absorber from reflector. The glass envelope can also be provided over the cylindrical absorber tube, which may help in reducing convection loss to some extent. This type of CPC is shown in Fig. 3. Of course, as the gap is there, some rays will escape through the gap and so gap losses are created. McIntire [8] has presented the faceted design of reflector portion below the absorber, which eliminates gap losses. Of course, here, due to multi-reflections, average number of reflections increases which decreases the optical efficiency slightly.

As the position of the absorber is changed, it is necessary to redesign the reflector shape to achieve the ideal concentration.

McIntire [8] has presented the expression for this reflector shape. It is

$$x = r_o\left(\sin\theta - M'(\theta)\cos\theta\right)$$
$$y = -r_o\left(\cos\theta + M'(\theta)\sin\theta\right) \qquad (4)$$

where $M'(\theta) = \theta + \beta$ for involute portion (5)

$$\beta = \sqrt{\left(\frac{r_e}{r_o}\right)^2 - 1} - \cos^{-1}\frac{r_o}{r_e} \qquad (6)$$

and

$$M'(\theta) = \frac{\theta + \theta_c + \frac{\pi}{2} + 2\beta - \cos(\theta - \theta_c)}{1 + \sin(\theta - \theta_c)}$$

for the remaining portion (7)

Of course, for these CPCs the geometric expressions for L, H, W, C, n & F(θ') as well as the characteristic curves of L/W → C, H/W → C n → C and F(θ') → θ' which are of utmost importance from the viewpoint of selection of CPC for a particular application and the saving of reflector material, are not available.

This is done in the following sections.

GEOMETRIC CHARACTERISTICS

CPC having cylindrical absorber with a gap between absorber and reflector is shown in Fig. 3. It is truncated from GF to G'F'. So the angular acceptance of radiation increases from θ_c to θ_t. The extreme ray is incident at an angle θ_t . It can be said that $\theta_t = \theta_c$ for full CPC. The glass envelope is provided over the absorber. The expressions for various quantities for truncated CPC are derived as under.

Concentration Ratio C

$$C = \frac{1}{\pi}\left[-\cos\theta_t + \frac{2\pi + \theta_c - \theta_t + 2\beta + \sin(\theta_c + \theta_t)}{1 - \cos(\theta_c + \theta_t)}\sin\theta_t\right]$$

Arc Length L

It is two times the arc length AF'.

$$L = r_0\left[\begin{array}{l}\left(\theta_c + \frac{\pi}{2} - \cos^{-1}\frac{r_0}{r_e}\right)\left(\theta_c + \frac{\pi}{2} + \cos^{-1}\frac{r_0}{r_e} + 2\beta\right) \\ + \left(2\pi + \theta_c - \theta_t + 2\beta\right)\left(\frac{\cos\theta_m}{\sin^2\theta_m} - \ln\tan\frac{\theta_m}{2}\right) - \\ 2\left(1 - \cos ec\,\theta_m\right) - 4\left(G - S\right)\end{array}\right] \qquad (9)$$

where $\theta_m = \frac{\theta_c + \theta_t}{2}$

(10)

$G = 0.91597$ .It is Catalan's constant (11)

$$S = \sum_{k=1}^{\infty} \frac{\sin\left[(2k-1)\theta_m\right]}{(2k-1)^2} \quad (12)$$

Aperture Width W

$$W = 2\pi r_o C \quad (13)$$

Height H

$$H = r_o\left[\pi C \cot\theta_t + \operatorname{cosec}\theta_t + (\pi/2 + \beta)\right] \quad (14)$$

Average Number Of Reflections n

$$n = \frac{1}{4\pi}\left[\left(\theta_c + \frac{\pi}{2} - \cos^{-1}\frac{r_o}{r_e}\right)\left(\theta_c + \frac{\pi}{2} + \cos^{-1}\frac{r_o}{r_e} + 2\beta\right)\right] + \frac{1}{\sqrt{2}\pi}\int_{\theta_t+\frac{\pi}{2}}^{\frac{3\pi}{2}-\theta_t} \frac{\left(\theta + \theta_c + \frac{\pi}{2} + 2\beta - \cos(\theta - \theta_c)\right)\left(1 - \sin\frac{\theta - \theta_c - \pi/2}{2}\right)}{\left(1 + \sin(\theta - \theta_c)\right)^{\frac{3}{2}}} d\theta \quad (15)$$

Angular Acceptance F(θ')

The expression for F(θ') will remain the same as that used for gapless design [3] as it is purely a geometric property and depends only on the field of view of the aperture i.e. on acceptance angle & on truncation. This expression is

$$F(\theta') = 1$$

for $\theta' \le \theta_c$

$$= \frac{1}{2} + \frac{1 - \frac{\sin\theta'}{\sin\theta_t}(1 + \pi\cos)\theta_t}{2\pi C\cos\theta'}$$

for $\theta_c < \theta' \le \theta_t = 0$

for $\theta' > \theta_t$ (16)

CHARACTERISTIC CURVES

Equations (8) through (16) form a mathematical model. Using these equations a computer program is prepared to find the values of L/W, H/W, C and n for various values of θ_c starting from 5° to 60° at an interval of 2.5° with truncation in each case from θ_c to 80° in steps of 2.5°. The following values are used in calculations. r_o = 2.535 cm, r_e = 3.3 cm

The value of S in Eq. (12) is approximated by taking k from 1 to 50. The integration appearing in Eq. (15) is done numerically.

A separate program is prepared to find F(θ') for θ_c = 9.2° with truncations from θ_t = 20° to 80° in steps of 10°. For each truncation, F(θ') is obtained for θ' starting from 10° to the corresponding θ_t in steps of 2.5° and also for 9.2°.

Thus, a large amount of data is generated. The graphs of L/W → C, H/W → C n → C and F(θ') → θ' are plotted using these data. These graphs are shown in Fig. 4, Fig. 5, Fig. 6 and Fig. 7 respectively.

SELECTION OF CPC

Above graphs are much useful for selection of a CPC for a particular application. e.g. Suppose a CPC having θ_c = 20° is selected. For this CPC, when it is un-truncated, C = 3.05, L = 1.768 m, H= 0.785 m, W = 0.486 m, n = 1.37 (point A in Fig. 4, point B in Fig. 5 and point C in Fig. 6). When it is truncated to approximately ½ of its full height, say H/W = 0.8 (point D in Fig. 4, point E in Fig. 5 and point F in Fig. 6), C = 2.65, L = 0.862 m, H = 0.335 m, W = 0.422 m, n= 1.11. This shows a reduction in concentration ratio by 13.11% while arc length is reduced by 51.24%. Thus, with this truncation, approximately 50% material is saved by only 13% loss in

concentration ratio. Average number of reflections decreases from 1.37 to 1.11, which improves optical efficiency. Also the field of view is somewhat increased which may be observed from Fig. 7.

A vertical line from point A to point G on the curve of $\theta_c = 15^o$ is drawn in Fig. 4. Going from A to G, 46.8% of reflector material is saved without any loss in concentration ratio, but a field of view is slightly reduced and number of tilt adjustments per year is increased.

Thus, a selection can be made depending upon the requirement.

COMPARISON

In this paper, three designs of CPCs viz. (1) CPC with flat absorber (2) CPC with cylindrical absorber without gap and (3) CPC with cylindrical absorber having a gap are considered. CPC with absorber has back losses. So, it is not much used. CPC with gapless design has conduction loss to the reflector. Also the values of arc length and average number of reflections are comparatively higher. So the third type i.e. the CPC with a gap between absorber and reflector is a better selection.

This CPC also seems attractive in comparison of faceted design from the viewpoints of simplicity in construction and average number of reflections. Of course, some radiation is lost due to the gap.

All CPCs have lower thermal losses as compared to that in FPC.

CPC does not need utmost accuracy in fabrication, as it is a non-focusing type concentrator.

APPLICATIONS OF CPCs

As moderate temperature of 100^o to 200^o C is generally attained in CPC, there are vast applications of CPCs where this range of temperature is needed. Some of them are listed here.

- water heating
- space heating
- industrial process heat
- process steam generation in textile industry, dairy and hosiery
- steam generation for running small engines
- small sized electricity generating systems
- drive irrigation pumps
- photovoltaics (simple or dielectric concentrator)
- boiler for vapor absorption system
- space application
- CPC type integrated collector storage system
- second stage concentrator

Over and above this, CPCs have been used in some latest applications. Few of them are as under.

- laser pumping [9]
- development of high flux solar furnace
- detoxification of contaminated water [10]
- sun protection system [11]
- heliostat [12]

CONCLUSION

It is observed that CPCs have many advantages over the other collectors. CPC with a gap between absorber and reflector is better than the other CPC designs. Truncation has many advantages. Characteristic curves should be used for selection of CPC for a particular application. Fabrication of CPC is easier. It is possible to make use of CPC for a large number of applications. CPCs have been used in many latest applications. There is still further scope for CPC to be used in newer applications in future.

REFERENCES

[1] Winston, R., 1974, "Solar Concentrators of a Novel Design," Solar Energy, 16, pp. 89 –95.

[2] Rabl, A., 1976, "Optical and Thermal Properties of Compound Parabolic Concentrators," Solar Energy, 18, pp. 497 – 511.

[3] Carvalho, M. J., Collares-Pereira, M. C., Gordon, J. M. and Rabl, A., 1985, "Truncation of CPC Solar Collectors and its Effect on Energy Collection," Solar Energy, 35, pp. 393 – 399.

[4] Rabl, A., 1976, "Solar Concentrators with Maximal Concentration for Cylindrical Absorbers," Applied Optics, 15, pp. 1871-1873.

[5] Baum, H. P. and Gordon, J. M., 1984, "Geometric Characteristics of Ideal Non-imaging (CPC) Solar Collectors with Cylindrical Absorber," Solar Energy, 33, pp. 455 – 458.

[6] McIntire, W. R., 1979, "Truncation of Non-imaging Cusp Concentrators," Solar Energy, 23, pp. 351 – 355.

[7] Winston, R., 1978, "Ideal Flux Concentrators with Reflector Gaps," Applied Optics, 17, pp. 1668 – 1669.

[8] McIntire, W. R., 1984, "Design Parameters for Concentrators without Gap Losses," Solar Energy, 32, pp. 439 – 441.

[9] Jenkins, D., O'Gallagher, J. and Winston, R., 1997, "Attaining and Using Extremely High Intensities of Solar Energy with Non-imaging Concentrators," Advances in Solar Energy, 11, pp. 43 – 108.

[10] Ajona, J. I. and Vidal, A., 2000, "The Use of CPC Collectors for Detoxification of Contaminated Water: Design, Construction and Preliminary Results," Solar Energy, 68, pp. 109 – 120.

[11] Yogi Goswami, D. and Boer, K. W., 2001, "Sun Protection System Based on CPCs with Total Internal Reflection," Advances in Solar Energy, 14, pp. 17 – 32.

[12] Chen, Y. T., Chong, K. K., Lim, C. S., Lim, B. H., Tan, K. K., Aliman, O., Bligh, T. P., Tan, B. K. and Ismail, G., 2002, "Report of the First Prototype of Non-imaging Focusing Heliostat and its Application in High Temperature Solar Furnaces," Solar Energy, 72, pp. 531 – 544.

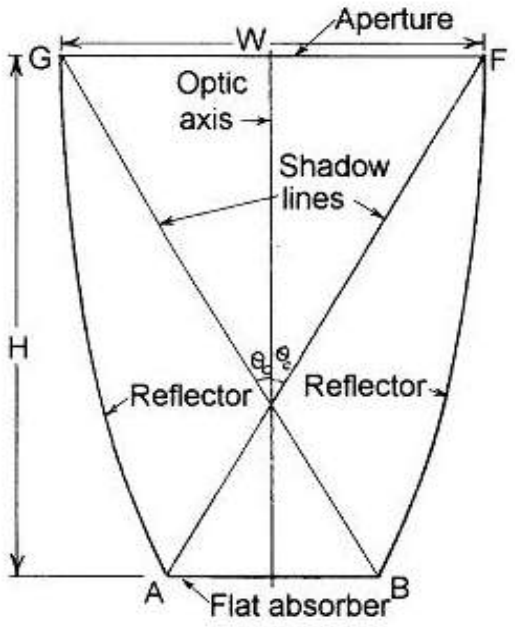

Fig. 1 CPC with flat absorber

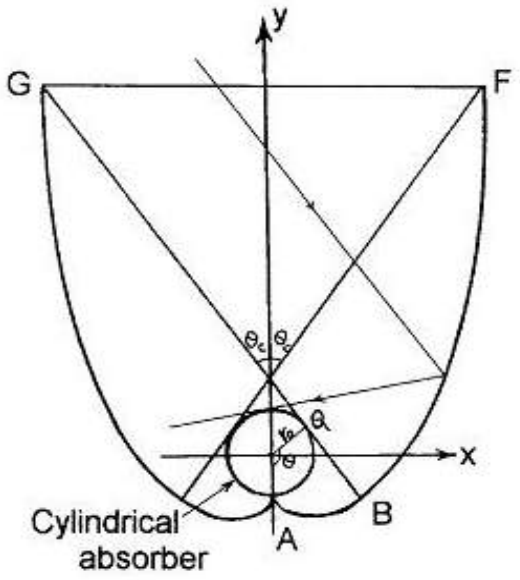

Fig. 2 CPC with cylindrical absorber

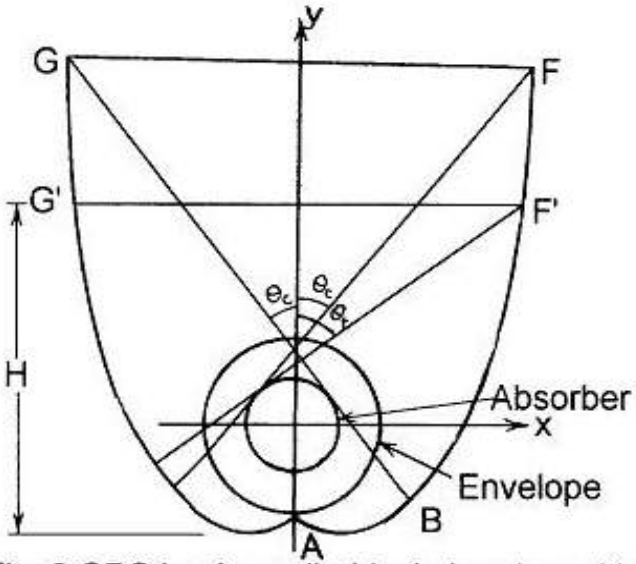

Fig. 3 CPC having cylindrical absorber with a gap

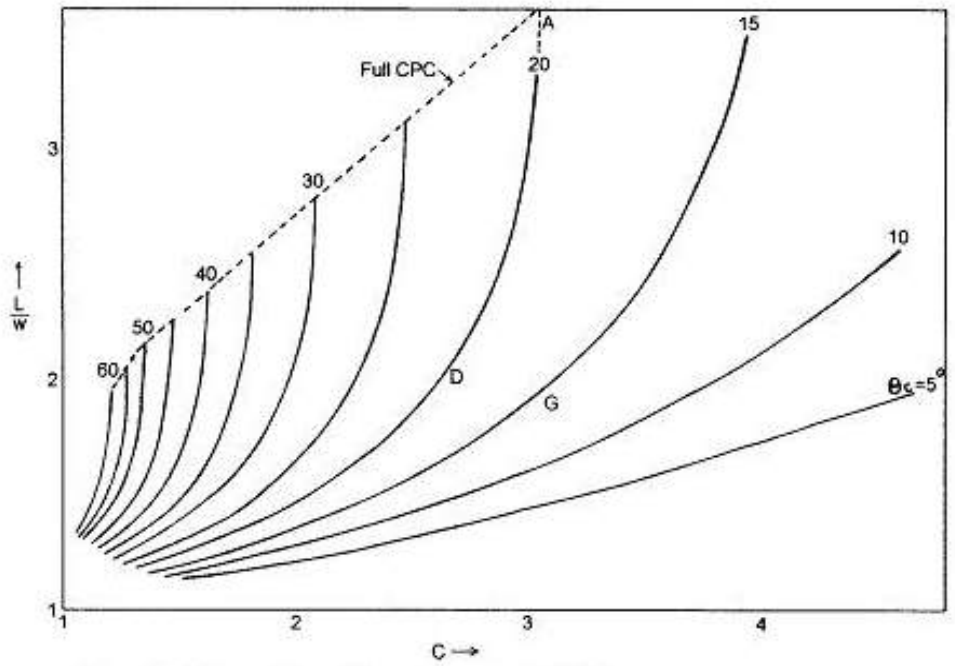

Fig. 4 L / W ⟶ C for full and truncated CPC for various θ_c

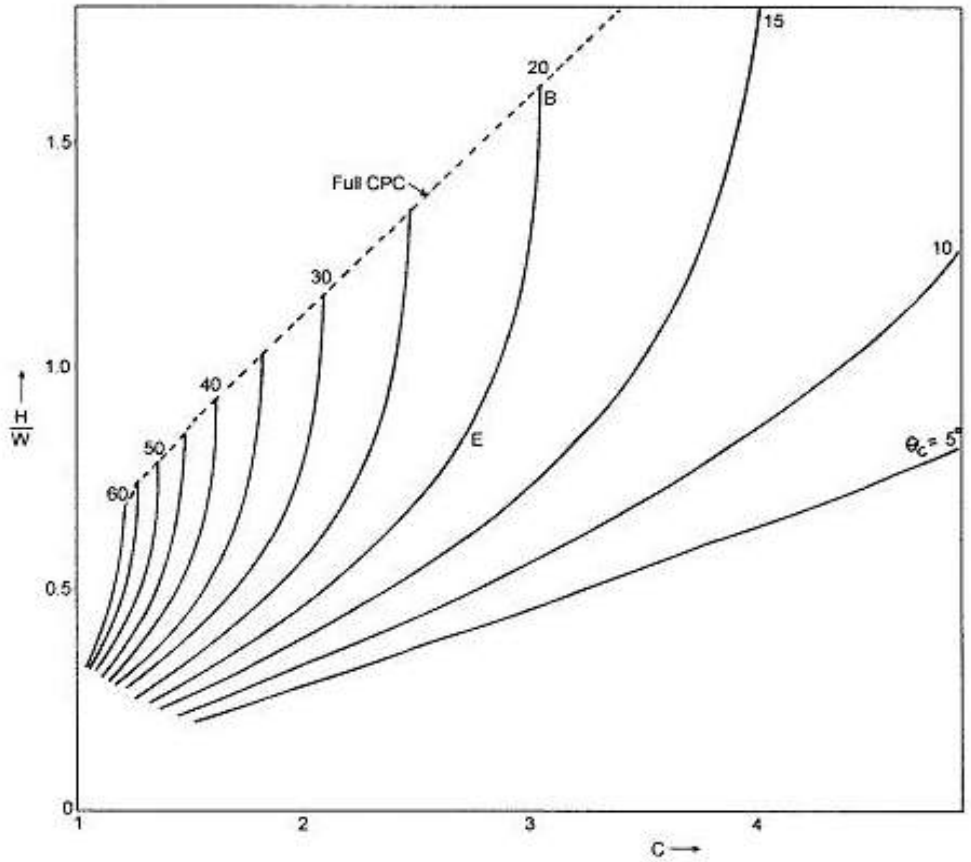

Fig. 5 H / W ⟶ C for full and truncated CPC for various θ_c

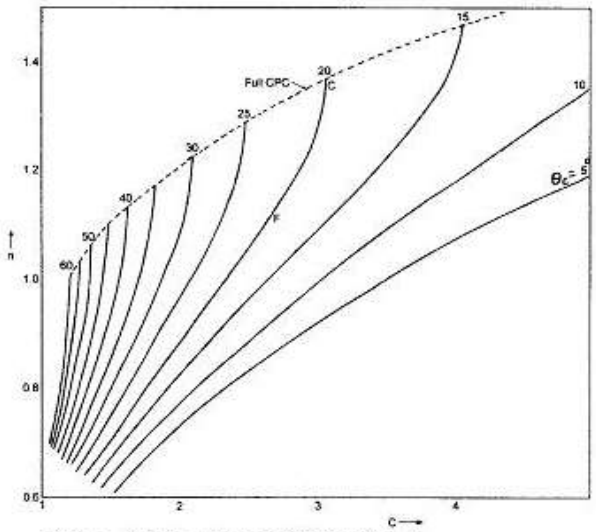

Fig. 6 n⟶C for full and truncated CPC for various θ_c

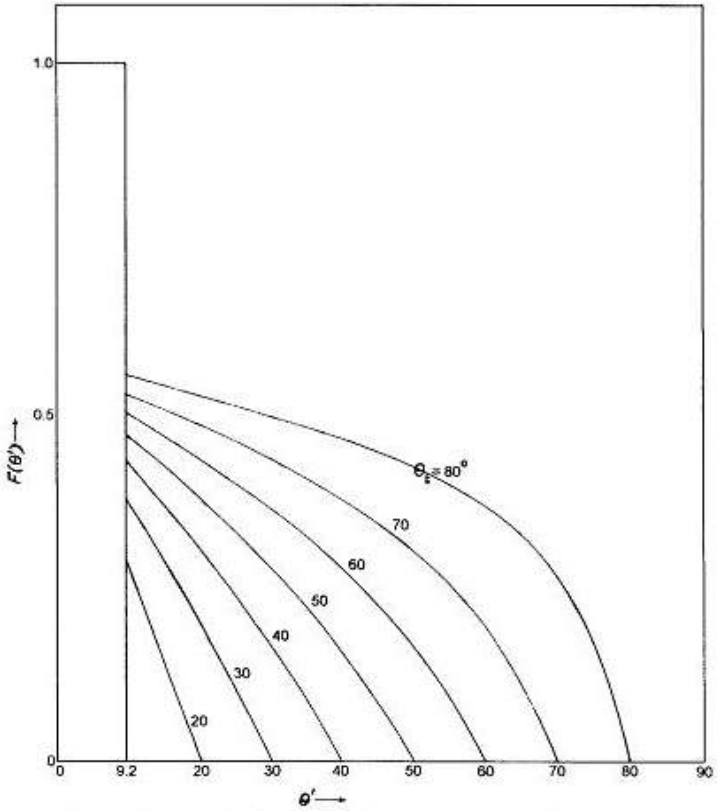

Fig. 7 F(θ′) for CPC with $\theta_c = 9.2^\circ$ for various degrees of truncation

COMPARISON OF SCHEDULING ALGORITHMS FOR INPUT QUEUED CROSSBAR SWITCHES

Heena Patel, Mehul C. Patel
PG students, EC Department,
L. D. College of Engg, Ahmedabad

Mihir V. Shah
Sr. lecturer, EC Department
L. D. College of Engg, Ahmedabad

ABSTRACT

Crossbar architectures with input queued buffer are widely used to implement high performance network switches and routers. A Scheduling algorithm is used to configure the crossbar switch for deciding the order in which packets will be served. Several scheduling algorithms were proposed for input-queued crossbar switches. In this paper, we present the MATLAB simulation of input queued crossbar switches with PIM, RRM and iSLIP scheduling algorithms. We have simulated scheduling algorithms for 4x4 and 8x8 crossbar switches with four different traffic models using MATLAB 7.0.

The simulation results show that iSLIP saves loss of packet due to buffer overflow and thus increases the throughput by 2% to 4% compared to PIM and RRM with less delay variance compared to PIM and RRM.

Index Terms : Crossbar switches, QoS (Quality of Service), Scheduler, VOQ (Virtual output Queuing)

INTRODUCTION

Crossbars (NxN) switches play a major role in the design of high speed interconnection networks. Architecture of a single-stage, non-blocking switch fabric has three basic parts as shown in figure 2.

1. Queue Structure – Input queuing is increasingly used for high bandwidth switches and routers. If an input-queued switch employs a single FIFO queue at each input, as shown in figure 1 then Head of Line blocking (HOL) problem limits the throughput to 58.6% [2].

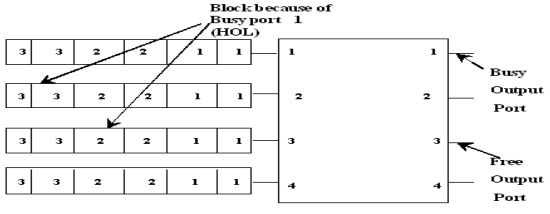

Figure1. An input buffered single FIFO queue switch

In figure 1 HOL blocking occurs when a cell at the head of queue waiting for a busy output blocks a cell behind it that is destined to an idle output. To solve the Head of Line (HOL) problem, virtual output queuing (VOQ) is used as shown in figure 2. [6], [7].

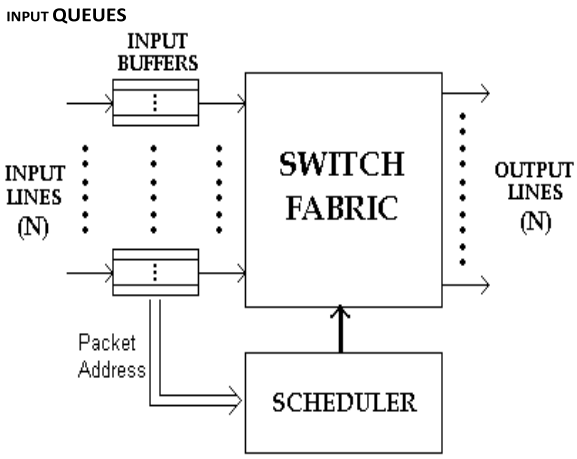

Figure 2. NxN crossbar switch with VOQ structure

Each input maintains N FIFO Virtual output Queues (VOQs) one for each output. Qij denotes the VOQ at input i containing cells destined to output j.

2. Crosspoint Switch – A crossbar switch can transfer cells between multiple ports simultaneously by operating multiple cross points.

3. Scheduler – It is a critical device selecting configurations for the switch fabric to transfer cells from inputs to outputs. Scheduler manages cell transfer and solves contentions within the switching fabric. Switch throughput can be increased from 58.6% to 100% with a centralized scheduling algorithm [5].

In this implementation, we assume that the fabric handles fixed size cells but variable sized cells can also be routed by using some sort of cell dissembler and assembler. Each input port competes for multiple output ports but can communicate with only one at a time. Likewise, each output port vies for multiple input ports but can communicate with only one at a time. The scheduling problem for NxN crossbar switch with VOQ is defined as follows: for each input port i, there are n request lines going to the scheduler: $R_{i,1}$; $R_{i,2}$; ; ; $R_{i,n}$. $R_{i,j}$ = 1 indicates that there is a request from input port i to switch a cell to output port j. Correspondingly, there are n grant lines produced by the scheduler: $G_{i,1}$; $G_{i,2}$; ; ; ; $G_{i,n}$. $G_{i,j}$ = 1 means that the scheduler has granted the request from input port i to switch a cell to output port j depending on the scheduling algorithm. To ensure that each input delivers at most one cell into the crossbar fabric, and that each

output receives at most one cell, the conditions $\Sigma^{n}_{j=1} G_{i,j} \leq 1$; for $1 \leq i \leq n$ and $\Sigma^{n}_{i=1} G_{i,j} \leq 1$; for $1 \leq j \leq n$ must hold, respectively. [3]

Rest of the paper first discusses scheduling algorithms in section 2, simulations results in section 3. Section 4 describes comparison, while Section 5 presents our conclusion. Section 6 presents references.

Scheduling Algorithms

There is a centralized scheduler in the N×N switch that considers requests from all the input queues and determines the best realizable configuration for the crossbar. The scheduler's decision is determined by a scheduling algorithm. This scheduling algorithm has to be fast, efficient (good throughput), easy to implement in hardware, fair in serving all the inputs and having low latency.

The scheduling problem in input queued switches is nothing but a bipartite graph matching problem as shown in figure 3, with M inputs and N outputs.(M would be equal to N for an N×N switch with VOQ). Requests from different inputs to various outputs can be seen as edges in bipartite graph as shown in figure 3. Graph G is bipartite if its nodes are divided into two sets, and each edge has an end in one of the sets. Switch inputs and outputs form the two sets of nodes of the bipartite graph and the edges are the connections required by the queued cells.

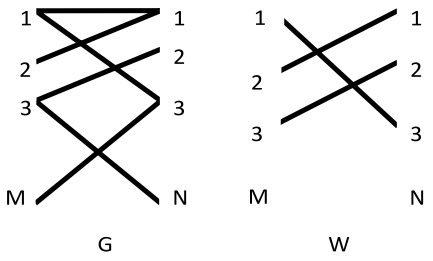

Figure3: Bipartite graph G, and a matching W on it.

a. Parallel Iterative Matching (PIM):

PIM algorithm was developed by DEC system research centre. It is based on randomness (to avoid starvation) and iteration [8]. This algorithm converges on a conflict-free match in multiple iterations;

where each iteration consists of three steps operate in parallel on each input and output.

Request- All unmatched inputs send requests to every output for which they have queued cell;

Grant- If an unmatched output receives any request, it grants at random one of its requesting input;

Accept- If an input receives a grant, it accepts it but if it receives multiple grants then it accepts one by selecting an output randomly among those that granted its request. These three steps are repeated for the inputs that are not paired with any outputs, until they converge to a maximal match. A maximal match is one in which each node is either matched or has no edge to an unmatched node.

b. Round Robin Matching (RRM):

RRM is perhaps the simplest and most obvious form of iterative round-robin scheduling algorithms. The three steps of RRM arbitration are as shown in figure 4.

Request- Each input sends a request to every output for which it has a queued cell.

Grant- If an output receives any requests, it chooses the one that appears next in a fixed, round robin schedule starting from the highest priority element. The output notifies each input whether or not its request was granted. The pointer to the highest priority element of the round-robin schedule is incremented (modulo N) to one location beyond the granted input.

Accept- If an input receives a grant, it accepts the one that appears next in a

fixed, round-robin schedule starting from the highest priority element. The pointer to the highest priority element of the round-robin schedule is incremented (modulo N) to one location beyond the accepted output.

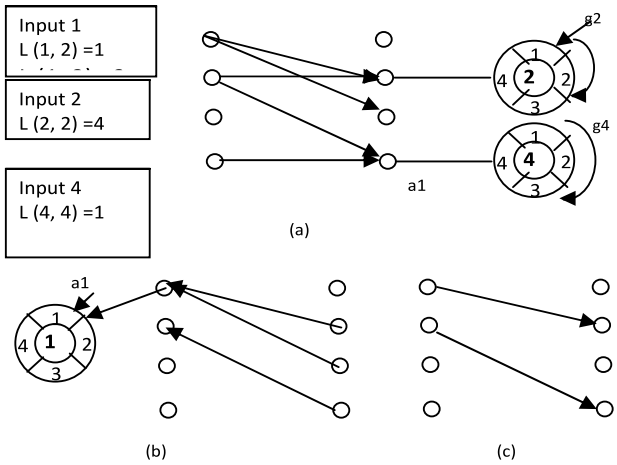

Figure 4: RRM (a) Request (b) Grant (c) Accept. [9]

c. ITERATIVE SERIAL LINE INPUT- iSLIP

iSLIP is an iterative algorithm, achieved by making a small variation to the RRM scheme [8]. iSLIP achieves this by not moving the grant pointers unless the grant is accepted. The Grant step of RRM is changed to:

Grant- If an output receives any requests; it chooses the one that appears next in a fixed round-robin schedule, starting from the highest priority element. The output notifies each input whether or not its request was granted. The pointer to the highest priority element of the round-robin schedule is incremented (modulo N) to one location beyond the granted input if, and only if, the grant is accepted in Step of grant.

Those inputs and outputs not matched at the end of one iteration are eligible for matching in the next iteration.

SIMULATIONS

We simulated PIM, RRM and iSLIP scheduling algorithms for 4x4, and 8x8 crossbar switches with four different traffic models using MATLAB 7.0. For each traffic model, algorithms were simulated for 1000 time slots and results

were taken by averaging the outcomes for 100 times. We have measured three parameters throughput efficiency, delay variance and average latency.

Efficiency –Efficiency of the algorithms were measured by ((passed packets + packets in buffer) / (total no of packets))*100.

Average latency – Average latency refers to the time spent by a packet from the point it enters the switch to when it leaves. Latency should be less for a good scheduling algorithm.

Delay variance – For all the scheduling algorithms, minimum delay is 0 time slot, which means a packet is being scheduled immediately. The maximum delay is poor measure since it is susceptible to statically anomalies of the simulation. Therefore, we use variance as a measure of fairness.

A. With i.i.d. Bernoulli arrivals and uniformly distributed destinations: In this traffic model cell arrives as i.i.d. (independent and identically distributed) Bernoulli arrivals and cell destinations distributed uniformly over all outputs.

B. With i.i.d. Bernoulli arrivals and non-uniformly distributed destinations. Real traffic is not usually uniformly distributed over all outputs, but is asymmetric. In this traffic model cell arrives as i.i.d. (independent and identically distributed) Bernoulli arrivals and cell destinations distributed normally over some outputs with variance.

C. With bursty arrivals and uniformly distributed destinations: Real traffic is not only asymmetric it is highly correlated from cell to cell and so it is also bursty. We illustrate the effect of burstiness on scheduling algorithms using an on-off arrival process modulated by a two state Markov chain. The source alternatively produces a burst of full cells followed by an idle period of empty cells.

D. With bursty arrivals and non-uniformly distributed destinations: In this traffic model input generated using an on-off arrival process modulated by a two state Markov chain. The bursts and idle periods contain a geometrically distributed number of cells.

As shown in figure 5, throughput of iSLIP as a function of offered load increases by 10% to 20% compared to PIM and RRM algorithm while the delay variance of RRM algorithm increase by 20 to 70 time slots compared to iSILP and PIM as shown in figure 6 for traffic model A. Delay variance of iISLIP algorithm as a function of offered load reduces by 10 to 20 time slots compared to PIM algorithm.

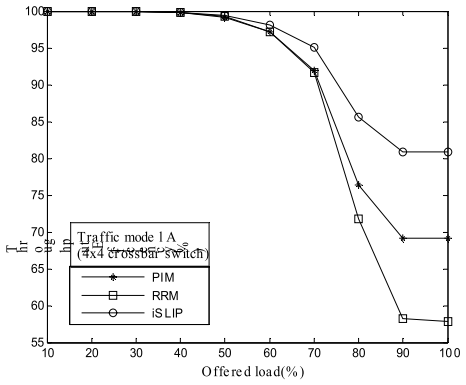

Figure5. Throughput increments (%) in 4x4 switch

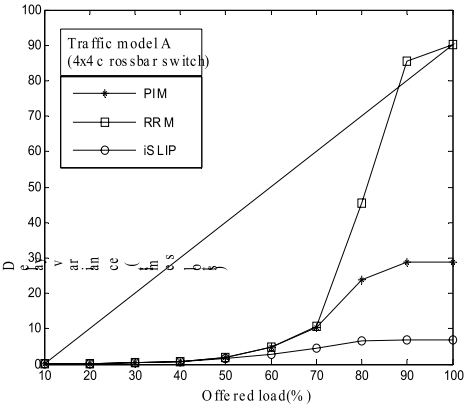

Figure6. Delay variance in timeslots in 4x4 switch

As shown in figure 7, throughput of iSLIP as a function of offered load increases by 1.2% to 1.4% compared to PIM and RRM algorithm. Delay variance of the iSLIP is less compared to PIM and RRM by 1.5 to 4 time slots compared to RRM as shown in figure 8 for traffic model D.

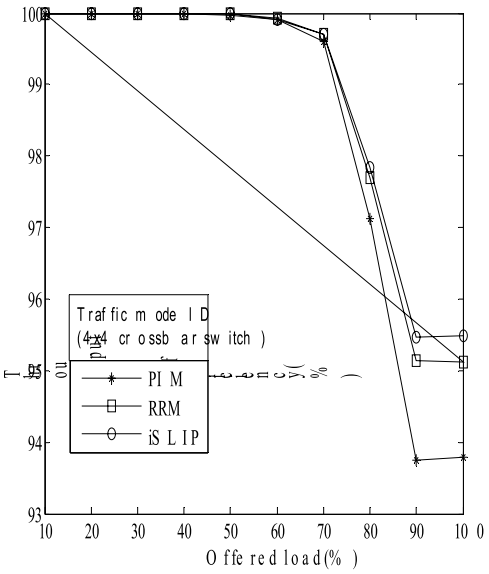

Figure7. Throughput increments (%) in 4x4 switch

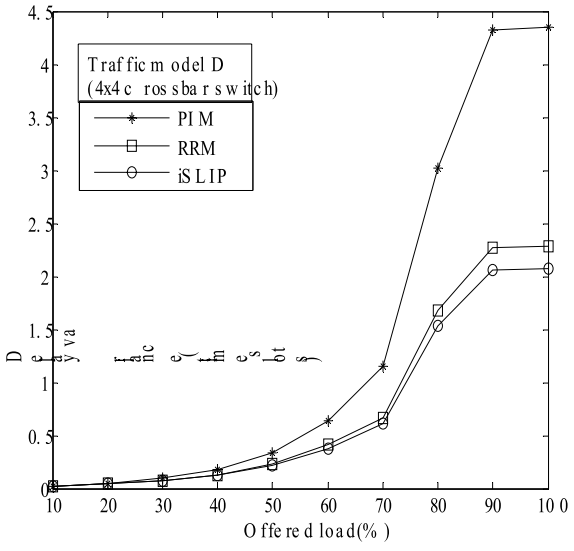

Figure8. Delay variance in timeslots in 4x4 switch

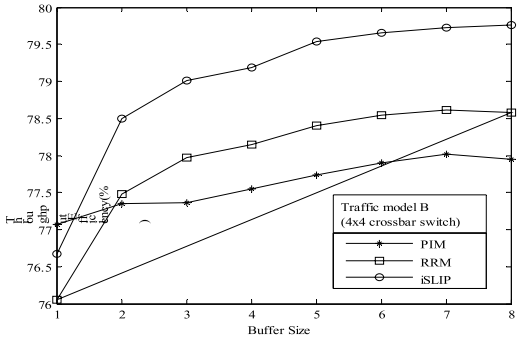

Figure9. Throughput increments (%) in 4x4 switch

As shown in figure 9, throughput of iSLIP as a function of buffer size increases by 0.5% to 1.5% compared to PIM and RRM algorithm for traffic model B.

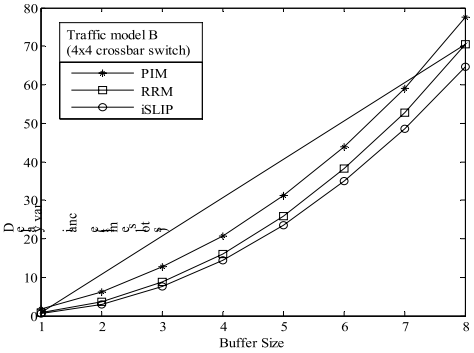

Figure10. Delay variance in timeslots in 4x4 switch

Delay variance of PIM algorithm increases by 5 to 10 time slots compared to iSLIP and RRM algorithms as shown in figure 10.

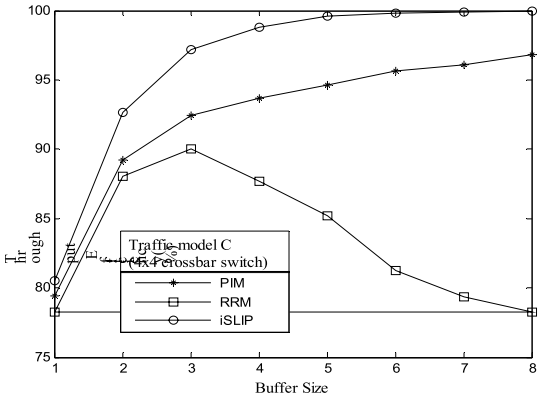

Figure11. Throughput increments (%) in 4x4 switch

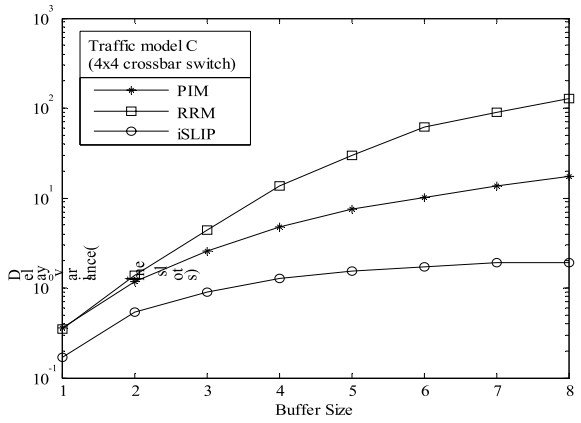

Figure12. Delay variance in timeslots in 4x4 switch

As shown in figure 11, throughput of iSLIP as a function of buffer size increases by 3% to 21% compared to PIM and RRM algorithm for traffic model C. Delay variance of ISLIP algorithm reduces by 20 to 40 time slots as shown in figure 12. Here the delay variance is shown in log scales.

As shown in figure 13, throughput of iSLIP (8x8) as a function of buffer size increases by 14% to 25%compared to PIM and RRM algorithm for traffic model. Delay variance of iISLIP algorithm as a function of buffer size reduces by 30 to 40 time slots compared to PIM and iSLIP

algorithm as shown in figure 14.

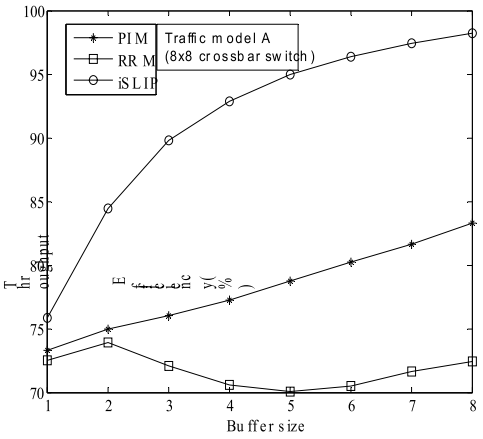

Figure13. Throughput increments (%) in 8x8 switch

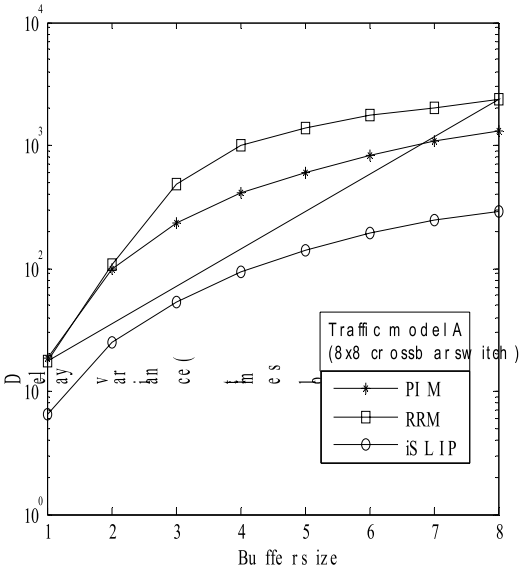

Figure14. Delay variance in timeslots in 8x8switch

As shown in figure 15, throughput of iSLIP as a function of buffer size increases by 1% to 1.5% compared to PIM and RRM algorithm for traffic model A. As shown in figure 16, delay variance of PIM algorithm as a function of buffer size increases by 1.5 to 4 time slots compared to RRM and iSLIP algorithm.

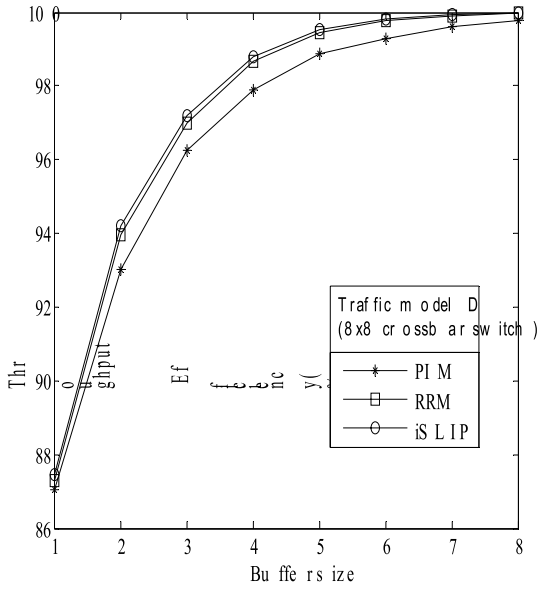

Figure15. Throughput increments (%) in 8x8 switch

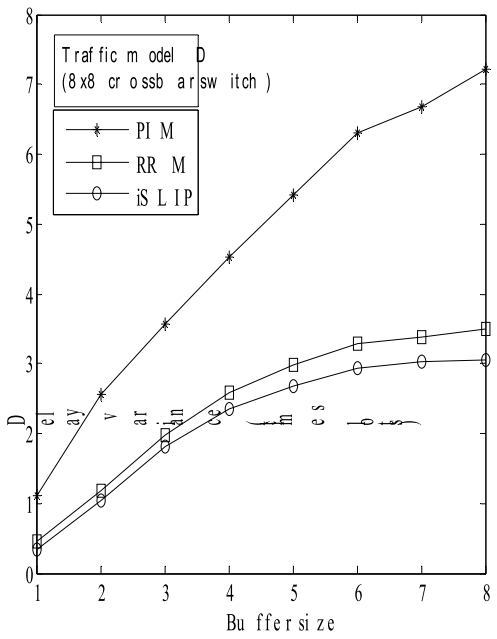

Figure16. Delay variance in timeslots in 4x4 switch

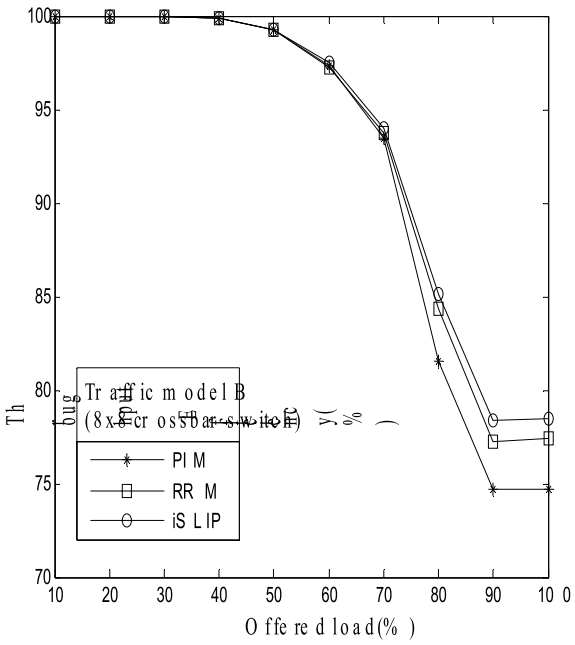

Figure17. Throughput increments (%) in 8x8 switch

As shown in figure 17, throughput of iSLIP as a function of offered load increases by 1% to 4% compared to PIM and RRM algorithm and delay variance is less compared to 2 to 7 time slots, for traffic model A.

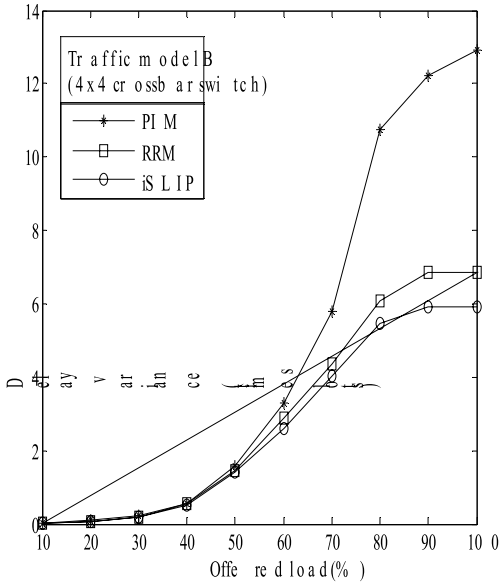

Figure18. Delay variance in timeslots in 8x8switch

As shown in figure 19, throughput of iSLIP, as a function of offered load increases by 14% to 19% compared to PIM and RRM algorithm for traffic model A.

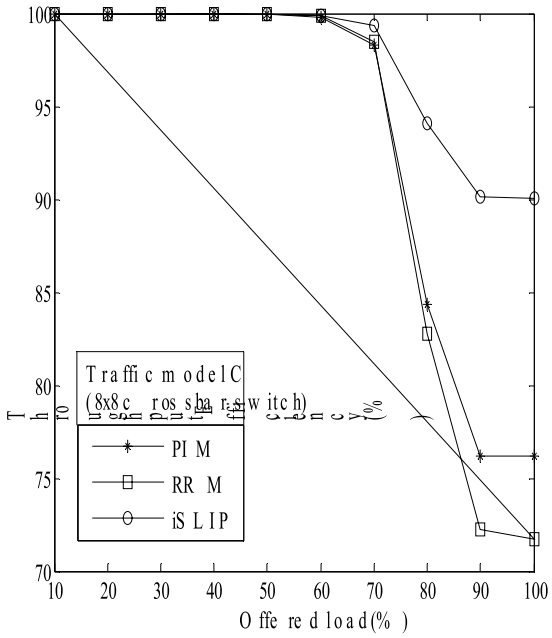

Figure19. Throughput increments (%) in 8x8 switch

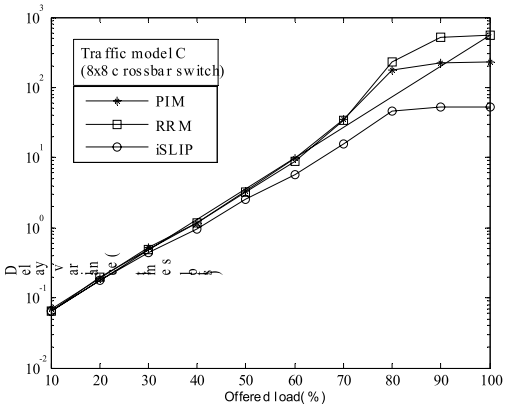

Figure20. Delay variance in timeslots in 8x8switch

As shown in figure 20, delay variance of iSLIP algorithm as a function of offered load reduces by 130 to 500 timeslots compared to PIM and RRM algorithm.

Comparison

RRM algorithm removes the unfairness and complexity inherent in the PIM algorithm; it performs well on a single iteration and converges to a maximal match in an average of O(log N) iterations. [1] The reason for the poor performance of RRM lies in the rules for updating the pointers at the output arbiters. So, the RRM algorithm performs poorly under heavy traffic due to a synchronization phenomenon described in [8].This small change to the RRM algorithm makes iSLIP capable of handling heavy loads of traffic and eliminates starvation of any connections with a simplicity and easiness to implement in hardware. The algorithm converges in an average of O(log N) and a maximum of N iterations.

Conclusion

Comparison criteria for the scheduling algorithms are simplicity, fairness and

starvation free with high efficiency to serve input packets with lower delay variance. In this paper, it has been shown that the iSLIP has fair efficiency with lower delay variance compared to PIM and RRM algorithms.

REFERENCES

[1]T. E. Anderson, S. S. Owicki, J. B. Saxe, and C.P.Thacker, "High speed switch scheduling for local area networks," ACM Transactions on Computer Systems, pp. 319-352, November 1993.

[2]M. J. Karol, M.G. Hluchyj and S.P. Morgan, "Input vs. output queueing on a space-division cell switch", IEEE Transaction on Communications, Vol. 35, No. 12, pp. 1347-1356, 1987.

[3]J. Hurt, A. May, X. Zhu, and B. Lin, "Design and implementation of high-speed symmetric crossbar schedulers," Proc. IEEE International Conference on Communications (ICC'99), Vancouver, Canada, June 1999, pp. 253-258.

[4]A. Mekkittikul and N. McKeown, "A practical scheduling algorithm to achieve 100% throughput in input-queued switches," Proc. IEEE INFOCOM 1998, vol. 2, Apr. 1998, San Francisco, pp. 792-799.

[5]N. McKeown, V. Anamtharam, and J. Warland, "Achieving 100% throughput in an input-queued switch," Proc. INFOCOM'96, San Francisco, March 1996, pp. 296-302.

[6]H. S. Chi and Y. Tamir, "Decomposed arbiters for large crossbars with multi-queue input buffers" Proc. of International Conference on Computer Design, Cambridge, Massachusetts, October 1991, pp. 233-238.

[7]Y. Tamir and H.C. Chi, "Symmetric crossbar arbiters for VLSI communication switches," IEEE Transactions on Parallel and Distributed Systems, vol. 4, no. 1, pp. 13-27, January 1993.

[8]N. McKeown, "The iSLIP scheduling algorithm for input-queuedswitches," IEEE Transactions on Networking, vol. 7, no. 2, pp. 188-201, April 1999.

DIGITAL ON/OFF AM MODULATOR

Amit R. Sharma
Asst. Professor, Electronics & Communication Department
Gandhinagar Institute of Technology
Moti Bhoyan, Ta. Kalol, Dist. Gandhinagar

ABSTRACT

This project report describes the Digital design of a module called "DIGITAL ON/OFF AM MODULATOR" in FPGA using VHDL. This module is a part of "ZigBee Light Transmitter". The key function of this "AM Modulator" is to modulate the serial input data stream coming from base band coder. It generates 8 bit sinus signal of 13.56 MHz. It is a type of ASK modulation or on/off keyed modulation. Bit "1" is transmitted by a signal of one of particular amplitude, bit "0" is transmitted by a signal of another amplitude and if there is no data at the input it transmits a constant value. The Amplitude of the transmitted carrier wave is controlled by microcontroller using wishbone interface.

Introduction

Modulation is the process of facilitating the transfer of information over a medium. I.e. Voice cannot be sent very far by just screaming. To extend the range of sound, we need to transmit it through a medium other than air, such as a phone line or radio. The process of converting information so that it can be successfully sent through a medium is called modulation. In amplitude modulation the amplitude of the signal is changed in response to information and all else is kept fixed.

The basic principle of radio transmission is to convert the voice frequencies coming into the microphone to radio frequencies, so that they can be radiated as an electromagnetic wave. At the receiver the electromagnetic wave can be intercepted and the original voice frequency is recovered. The electromagnetic radiation takes many forms. Light is electromagnetic radiation. The infrared signal from our TV remote control is electromagnetic radiation. The heat given off by a bar radiator is electromagnetic radiation. The whole secret of radio communication is to place information on to the signal, to convey intelligence or a message from one point to another.

The audio frequencies from a human voice range up to about 3000Hz of course the human voice can make sounds above this range, but for voice radio communications we do not need to use those higher voice frequencies. All of the intelligence we need is contained in the voice frequencies below 3000 Hz.

Amplitude Modulation (AM):-

In amplitude modulated (AM) systems, the modulated audio is applied to the radio frequency carrier in such a way that the total power of the transmitted wave is made to vary in amplitude, in accordance or in sympathy with the power of the modulating audio.

There are three parts to a communications system.

1. The information also called the base band
2. The medium
3. The carrier

Information can be defined in two forms, digital or analog. Analog signal is considered continuous. Its signal amplitude can take on any number of values between the signals maximum and minimum .Voice is analog and can take any number of volume levels between its dynamic ranges which is the range of volumes your vocal cords can produce. Digital devices converts' analog signal to digital signal by the process of sampling and quantization. The analog signal is first sampled and then quantized in levels and then each level is converted to a binary number. I.e. we may quantize our voice in 16 levels. Each of these levels can be represented by four bits.

The medium is thing the signal travels through. It can be air, space or wires of all sorts. Each of these medium offers its own unique set of advantages and distortions that determine what is used as carrier. A short wire in a chip for example may not need a carrier at all A Signal through space such as for satellite transmission may need a very high frequency carrier that can overcome space loss and other losses. It can be light in optical communication or microwave for mobile communication.

Amplitude shift keying

$$s(t) = m(t) A_c \cos(2\pi f_c t) = \begin{cases} A_c \cos(2\pi f_c t) & m(nT_b) = 1 \\ 0 & m(nT_b) = 0 \end{cases}$$

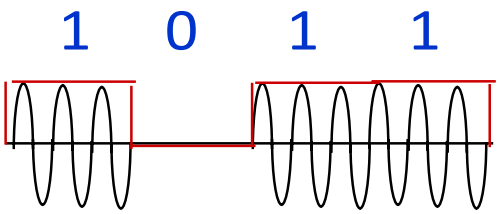

Fig – 1 AM modulation

All of the techniques vary a parameter of a sinusoid to represent the information which we wish to send .A sinusoid has three different parameters than can be varied. These are its amplitude phase and frequency. But since we are dealing with Amplitude Modulator we will discuss amplitude modulation.

Project description

Recently a standard called Zigbee, for wireless sensor networks has been established. The standard supports different data packets to handle different network topologies. A lite version of the standardized wireless sensor node will be developed and this project will design and implement a module that performs on/off AM Modulation of a Bit-stream.

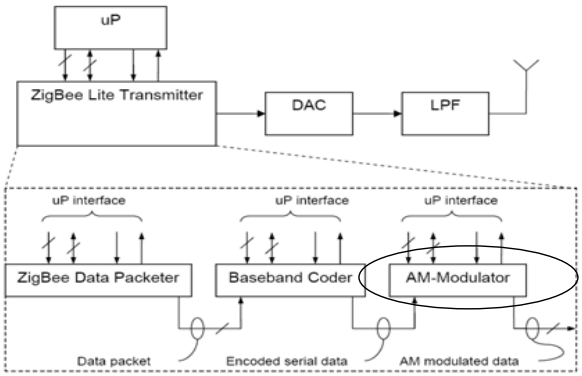

Fig – 2 Modulation of a Bit-stream

In this project a dedicated hardware module is developed that performs on/off AM modulation of the bit-stream The incoming signal would be coming from baseband coder as a stream of bits i.e. 0 and 1.The function of this module is to modulate this incoming signal. In this case the bit 1 is transmitted by a signal of one particular amplitude and bit 0 is transmitted by a signal of other particular amplitude while other parameters like phase and freq of the signal is kept constant. The coding is done in VHDL and it has to be implemented using FPGA. The maximum clock freq is of 100 MHz and the modulated signal should be 8 bit sinus signal of 13 MHz.

Hardware design

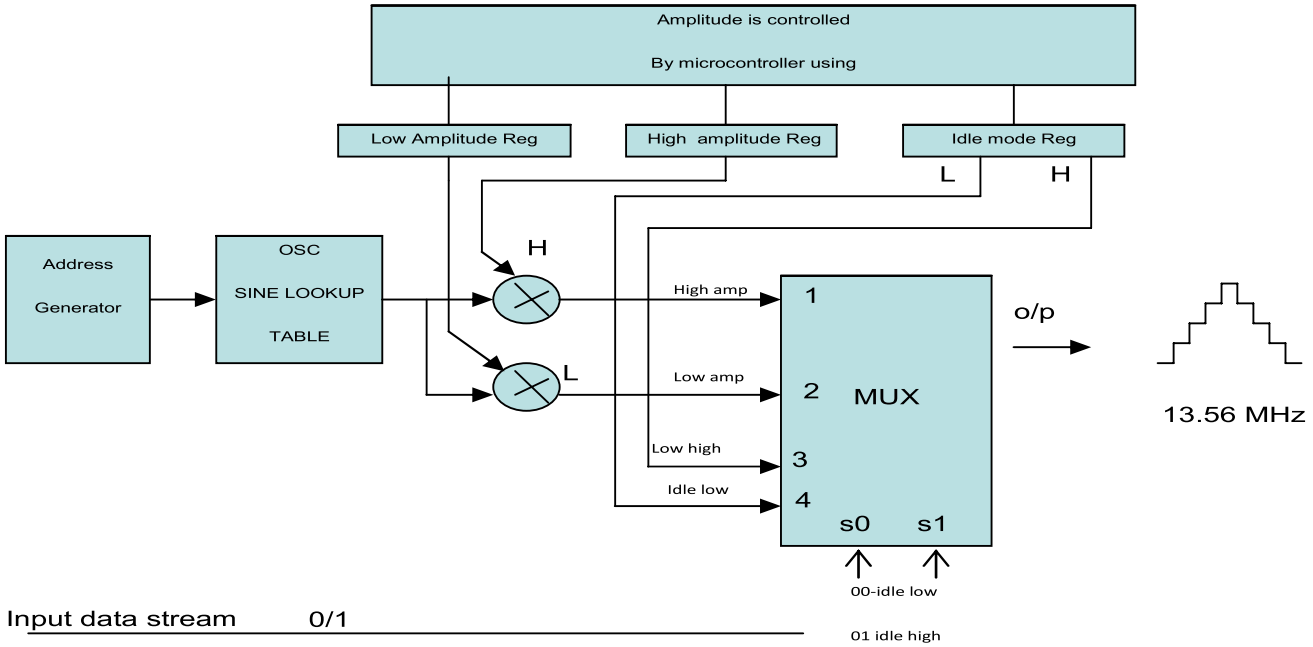

Fig – 3 Functional Block Diagram of AM Modulator

Address generator and sine lookup table:

The look up table keeps the record of amplitude of sine wave from 0 to 255. The address of Register 1 is 00000000 and the address of Register 255 is 11111111. At each address stored is the data of Amplitude of sine wave. The oscillator will generate sine signal of 13.56 MHz.

High Amplitude Register

It's an eight bit register which is used to store the high amplitude value of 8 bit.

Low Amplitude Register

It's an eight bit register which is used to store the low amplitude value of 8 bit.

Idle Amplitude Register

It's also an eight bit register which is used to store a constant value amplitude value of 8 bit.

Multiplier

It performs an 8 bit multiplication of generated sine wave and amplitude value by using shift and adds. If 8 bit sine value is multiplied with 8 bit value in high amplitude register then we get sine wave of high amplitude which acts as an first input to Mux ,which is to be transmitted when input bit is "1".And hence similar results can be derived for low amplitude and constant value.

4x1 Mux

A 4x1 mux is used for selecting the output. The output can display four types of value like high Amplitude, low Amplitude idle high and idle Low which is stored in Register. If the input is 1 then (s0, s1) = (1, 1) is selected and high Amplitude sine wave will appear at the output of mux. If the input is 0 then (s0, s1) = (1, 0) is selected and Low Amplitude sine wave will appear at the output of mux. If there is no input then idle mode is selected and a const value (no sine wave) appears at the output of mux.

Software design

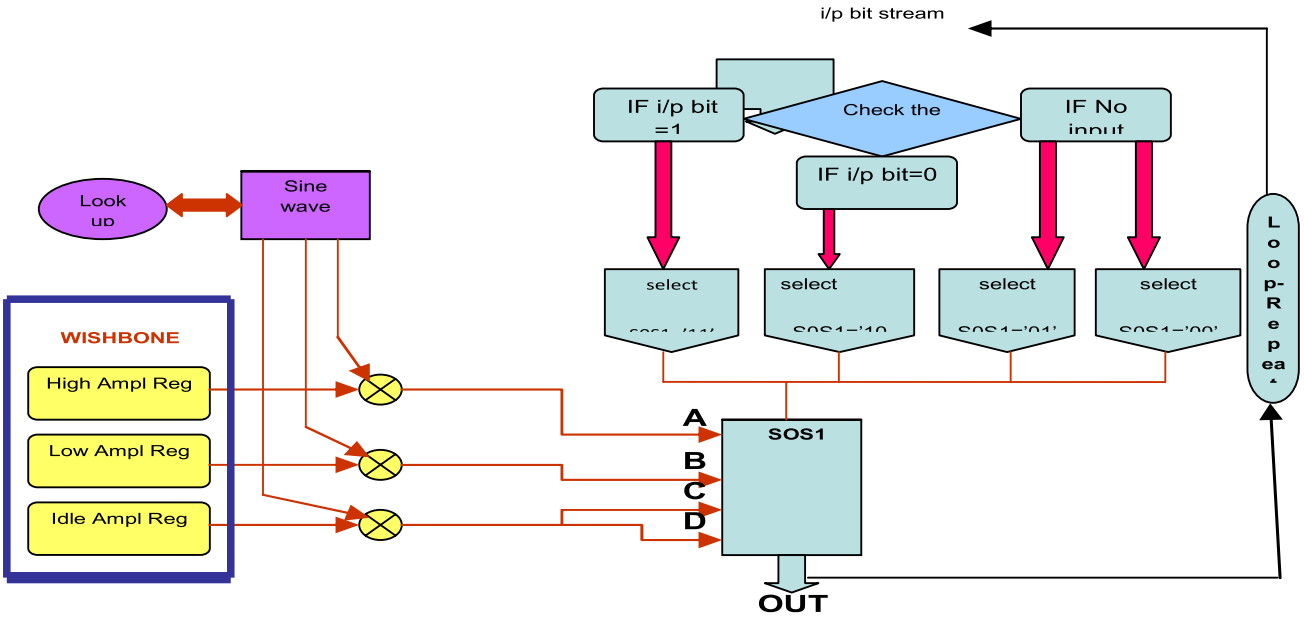

Fig - 4 Data Flow Diagram for AM Modulator

The software module is divided into various sub modules which are listed below:-

1. sine wave counter(acts as counter for oscillator)
2. sine package (look up table)
3. Register1 (storing 8 bit of data)
4. Register2 (storing 8 bit of data)
5. Multiplier1 (performing two 8 bit of multiplication)
6. Multiplier2 (performing two 8 bit of multiplication)
7. Modulator
8. Final (inter connecting the signal)
9. Convert (for extracting 8 bit of MSB for 16 bit of output result)

The first and second sub module constitute oscillator for generating sine wave of 12.5 MHz. The third and fourth sub modules are used for storing two 8 bit data which will constitute the amplitude of the sine wave. The fifth and sixth sub module are used for multiplying two 8 bit of data. The modulator sub module consists of mux and conditional statement. Depending on the input data it would transmit different signal at the output. The final sub module is used for inter connecting all the signals. Since two 8 bit of data is multiplied, hence the output would be a 16 bit therefore convert sub module is used to extract 8 bit MSB and give it at the output. The VHDL code can be seen from web page.

Input/output waveform

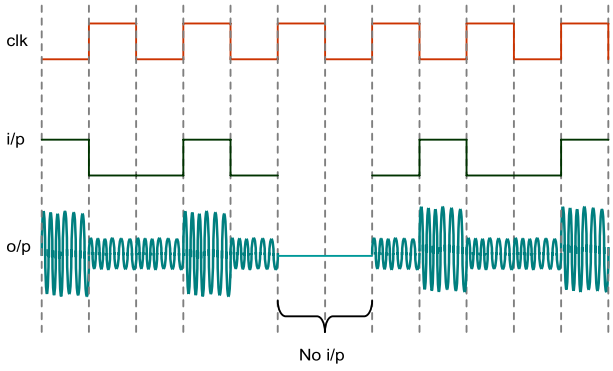

Fig – 5 Input / output wave form

Synthesis report HDL Synthesis Report : Macro Statistics

Sr.	Item	Numbers
1	FSMs	: 1
2	Multipliers	: 2
3	8x8-bit multiplier	: 2
4	Adders/Subtractors	: 2
5	7-bit adder	: 1
6	1-bit addsub	: 1
7	Registers	: 8
8	1-bit register	: 6
9	8-bit register	: 2
10	Multiplexers	: 3
11	1-bit 2-to-1 multiplexer	: 1
12	8-bit 2-to-1 multiplexer	: 1
13	16-bit 2-to-1 multiplexer	: 1

Device utilization summary : Selected Device: 3s4000fg900-5

Sr.	Item	Numbers	Percent
1	Number of Slices:	11 out of 27648	0%
2	Number of Slice Flip Flops	6 out of 55296	0%
3	Number of 4 input LUTs:	19 out of 55296	0%
4	Number of bonded IOBs	11 out of 633	1%
5	Number of MULT18X18s:	2 out of 96	2%
6	Number of GCLKs:	1 out of 8	12%

Timing Summary : Speed Grade: 5

Minimum period	2.725ns (Maximum Frequency: 366.973MHz)
Minimum input arrival time before clock	03.470ns
Maximum output required time after clock	11.521ns
Maximum combinational path delay	07.385ns

Results and discussions

Initially the program was implemented using Matlab, the output of Matlab program is shown in fig-A below. Then the program was implemented using VHDL code .The code was synthesized and simulated using xilinx and modelsim. The output is shown below .In both the case the results are favorable . As can be seen from the results below in both the cases we are able to vary the amplitude of carrier signal depending on the input signal.

The carrier freq obtained is of 12.5 MHz with maximum clock frequency of 100 MHz. Hence from the results it can be said that we have successfully completed the project.

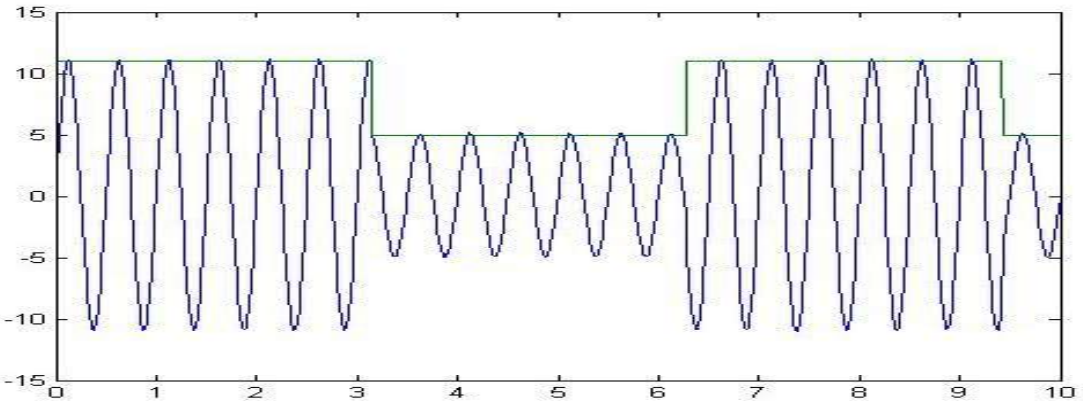

Fig – 6 Output of mat lab program

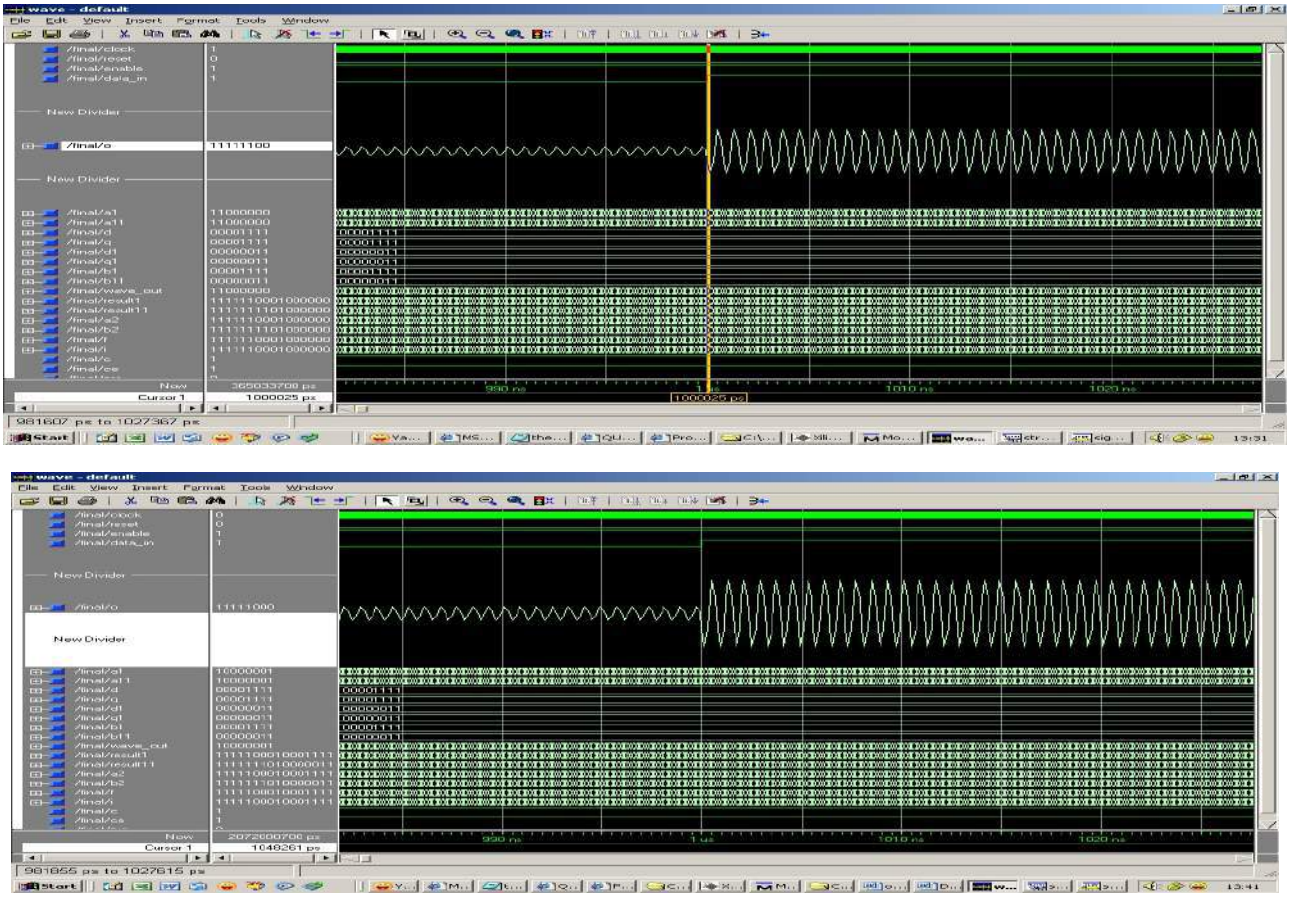

Fig – 7 Output from Xilinx ISE 9.1i & Modelsim-6 using VHDL code

Limitations of performance

1. The Maximum Clock freq is 100 MHz.
2. The Output Generated Sine wave is of 12.05 MHz.
3. The wishbone Interface should be used for generating the amplitude of sine wave
4. The Programming is done in VHDL and shall be implemented using FPGA

References

1. By I. Janiszewski, b Hoppe, and H Meuth., "Numerical controlled Oscillators with Hybrid Function Generators", Minlman publications-1998
2. http://radioelectronicsschool.com
3. www.complextoreal.com
4. www.classradio.com

COMMON RANDOM FIXED POINTS OF RANDOM MULTIVALUED OPERATORS ON POLISH SPACES

Yogita R. Sharma,
Lecturer, Mathematics Department
Gandhinagar Institute of Technology
Ta. Kalol, Dist. Gandhinagar

V. H. Badshah
School of studies in Mathematics
Vikram University
Ujjain, M.P.

ABSTRACT

In this paper common random fixed point theorem of random multivalued operators on polish spaces is given by using functional expression.

Keywords: Fixed point; Multivalued mapping; Polish space.

Introduction

Random fixed point theorems are of fundamental importance in probabilistic functional analysis. They are stochastic generalization of classical fixed point theorems and are required for the theory of random equations. In a separable metric space random fixed point theorems for contractive mapping were proved by Spacek [1], Hans [2, 3], Mukherjee [4]. Itoh [5, 6] extended several fixed point theorems, i.e., for contraction, nonexpensive, mappings to the random case. Thereafter, various stochastic aspects of Schauder's fixed point theorem have been studied by Sehgal and Singh [7] and Lin [8]. Afterwards Beg and Shahzad [9], Badshah and Sayyad [10] studied the structure of common random fixed points and random coincidence points of a pair of compatible random operators and proved the random fixed points theorems for contraction random operators in polish spaces.

Preliminaries

Let (X, d) be a Polish space; that is a separable, complete metric space and (Ω, a) be a measurable space. Let 2^X be a family of all subsets of X and CB(X) denote the family of all non empty closed bounded subsets of X. A mapping $T:\Omega\to 2^X$, is called measurable, if for any open subset C of X, $T^{-1}(C)=\{\omega\in\Omega: T(\omega)\cap C\neq\phi\}\in a$ mapping $\xi:\Omega\to X$, is said to be measurable selector of a measurable mapping $T:\Omega\to 2^X$, if ξ is measurable and for any $\omega\in\Omega$, $\xi(\omega)\in T(\omega)$. A mapping $f:\Omega\times X\to X$ is called a random operator if for any $x\in X$, $f(.,X)$ is measurable. A mapping $T:\Omega\times X\to CB(X)$, is called random multivalued operator if for every $x\in X$, $T(.,X)$ is measurable. A measurable mapping $\xi:\Omega\to X$, is called the random fixed point of a random multivalued operator $T:\Omega\times X\to CB(X)$ ($f:\Omega\times X\to X$), if for every $\omega\in\Omega$, $\xi(\omega)\in T(\omega,\xi(\omega))$ $(f(\omega,\xi(\omega))=\xi(\omega))$. Let $T:\Omega\times X\to CB(X)$ be a random operator and $\{\xi_n\}$ a sequence of measurable mappings $\xi_n:\Omega\to X$. The sequence is said to be asymptotically T-regular, if $d(\xi_n(\omega),T(\omega,\xi_n(\omega)))\to 0$.

$$\leq \frac{\alpha(\omega)}{\left(d(\xi_o(\omega),\ \xi_1(\omega))\ +\ d(\xi_1(\omega),\ \xi_2(\omega)\right)^2} \times$$

$$\left\{\left(d(\xi_o(\omega),\ \xi_1(\omega))+\ d(\xi_1(\omega),\right)\xi_2(\omega))\ \left(\ d(\xi_o(\omega),\ \xi_1(\omega)\right)^2\right.$$
$$\left.-\ d(\xi_o(\omega),\ \xi_1(\omega)d(\xi_1(\omega),\ \xi_2(\omega))+\left(d(\xi_1(\omega),\ \xi_2(\omega)\right)^2\right\}$$

$$+\beta(\omega)\ d(\xi_o(\omega),\xi_1(\omega)$$

$$\leq \alpha(\omega)\frac{\left(d(\xi_o(\omega),\ \xi_1(\omega))\right)^2+\left(\ d(\xi_1(\omega),\ \xi_2(\omega))\right)^2}{\left(d(\xi_o(\omega),\ \xi_1(\omega))\ +\ d(\xi_1(\omega),\ \xi_2(\omega)\right)}\ +\beta(\omega)\ d(\xi_o(\omega),\ \xi_1(\omega)$$

$$\leq \frac{\alpha(\omega)\left\{\left(d(\xi_o(\omega),\ \xi_1(\omega))\ +\ d(\xi_1(\omega),\ \xi_2(\omega)\right)\right\}^2-2d(\xi_o(\omega),\ \xi_1(\omega)d(\xi_1(\omega),\ \xi_2(\omega))}{\left(d(\xi_o(\omega),\ \xi_1(\omega))\ +\ d(\xi_1(\omega),\ \xi_2(\omega)\right)}$$

$$+\beta(\omega)\ d(\xi_o(\omega),\xi_1(\omega)$$

$$\leq \alpha(\omega)\left(d(\xi_o(\omega),\ \xi_1(\omega))+d(\xi_1(\omega),\ \xi_2(\omega)\right)+\beta(\omega)\ d(\xi_o(\omega),\ \xi_1(\omega)\cdot$$

So, $$\left(1-\alpha(\omega)\right)\ d(\xi_1(\omega),\ \xi_2(\omega))\leq\left(\alpha(\omega)+\beta(\omega)\right)d(\xi_o(\omega),\ \xi_1(\omega)\ \cdot$$

Thus, $$d(\xi_1(\omega),\ \xi_2(\omega))\leq k(\omega)d(\xi_o(\omega),\ \xi_1(\omega),$$

where, $$k\ =\ k(\omega)=\frac{\left(\alpha(\omega)+\beta(\omega)\right)}{\left(1-\alpha(\omega)\right)}<1\ .$$

By the Lemma 2.3 of Beg & Shahzad [9] in the same manner, we obtain a measurable mapping $\xi_3:\Omega\longrightarrow X$ such that for all $\omega\in\Omega$, $\xi_3(\omega)\in S(\omega,\ \xi_2(\omega))$ and

$$d(\xi_2(\omega),\ \xi_3(\omega))\leq\frac{\alpha(\omega)\left\{d(\xi_1(\omega),\ \xi_2(\omega))^3+d(\xi_2(\omega),\ \xi_3(\omega))^3\right\}}{\left(d(\xi_1(\omega),\ \xi_2(\omega))+d(\xi_2(\omega),\ \xi_3(\omega))\right)^2}$$
$$+\beta(\omega)d(\xi_1(\omega),\ \xi_2(\omega))\cdot$$

Hence,

$$d(\xi_2(\omega),\ \xi_3(\omega))\leq\alpha(\omega)\left\{d(\xi_1(\omega),\ \xi_2(\omega))+d(\xi_2(\omega),\ \xi_3(\omega))\right\}$$
$$+\beta(\omega)d(\xi_1(\omega),\ \xi_2(\omega)),$$

or,

$$\left(1-\alpha(\omega)\right)d(\xi_2(\omega),\ \xi_3(\omega))\leq\left(\alpha(\omega)+\beta(\omega)\right)d(\xi_1(\omega),\ \xi_2(\omega)\ \cdot$$

Thus,

$$d(\xi_2(\omega),\ \xi_3(\omega))\leq k^2d(\xi_o(\omega),\ \xi_1(\omega)\ .$$

Similarly, proceeding in the same way, by induction, we get a sequence of measurable mappings $\xi_n:\Omega\longrightarrow X$, such that for n > 0 for any $\omega\in\Omega$.=

Definition (1) If f is a single valued self-mapping of a set X. Then a point of X which remains invariant under the mapping f, is called fixed point of f in X.

Example (2) : Let a single valued mappings f : $R^+ \to R^+$ is defined by $f(x) = x^2$, then 0 and 1 are the fixed points of the mapping f in R^+.

Definition (3) : Let X is a non-empty set. A point $x \in X$ is said to be a fixed point of a multi-valued mapping $F : X \to 2^X$ if and only if X is contained in its image i.e. x Fx.

Example (4) : Let $X = [0, 1]$, and $F : X \to 2^X$ such that $F(x) = \left[0, \frac{x}{2}\right]$, for all $x \in X$, Then 0 is the fixed point of F.

MAIN RESULTS

In this section we give stochastic version of a result of Beg & Shahzad [11].

Theorem (1). Let X be a Polish space. Let $T, S : \Omega \times X \to CB(X)$ be two continuous random multivalued operators. If there exist measurable mappings $\alpha, \beta : \Omega \to (0, 1)$ such that

$$H(S(\omega, x), T(\omega, y)) \leq \alpha(\omega) \frac{d(x, S(\omega, x))^3 + d(y, T(\omega, y))^3}{(d(x, S(\omega, x)) + d(y, T(\omega, y)))^2} + \beta(\omega)\, d(x, y),$$

for each $x, y \in X$, $\omega \in \Omega$ and $\alpha, \beta \in R^+$ with $2\alpha + \beta < 1$, there exists a Common random fixed point of S and T (hence H represents the Hausdorff metric on CB(X) induced by the metric d).

Proof. Let $\xi_o : \Omega \to X$ be an arbitrary measurable mapping and choose a measurable mapping $\xi_1 : \Omega \to X$ such that $\xi_1(\omega) \in S(\omega, \xi_o(\omega))$ for each $\omega \in \Omega$. Then for each $\omega \in \Omega$.

$$H(S(\omega, \xi_o(\omega)), T(\omega, \xi_1(\omega)))$$

$$\leq \alpha(\omega) \frac{d(\xi_o(\omega), S(\omega, \xi_o(\omega)))^3 + d(\xi_1(\omega), T(\omega, \xi_1(\omega)))^3}{(d(\xi_o(\omega), S(\omega, \xi_o(\omega))) + d(\xi_1(\omega), T(\omega, \xi_1(\omega))))^2}$$

$$+ \beta(\omega)\, d(\xi_o(\omega), \xi_1(\omega)).$$

Further, there exists a measurable mapping $\xi_2 : \Omega \to X$ such that for all $\omega \in \Omega$,

$$\xi_2(\omega) \in T(\omega, \xi_1(\omega)) \text{ and}$$

$$d(\xi_1(\omega), \xi_2(\omega))$$

$$\leq \alpha(\omega) \frac{d(\xi_o(\omega), \xi_1(\omega))^3 + d(\xi_1(\omega), T(\omega, \xi_1(\omega)))^3}{(d(\xi_o(\omega), \xi_1(\omega)) + d(\xi_1(\omega), \xi_2(\omega))^2} + \beta(\omega)\, d(\xi_o(\omega), \xi_1(\omega)),$$

$$\xi_{2n+1}(\omega) \in S(\omega, \xi_{2n}(\omega)), \quad \xi_{2n+2}(\omega) \in T(\omega, \xi_{2n+1}(\omega))$$

and

$$d(\xi_n(\omega), \xi_{n+1})(\omega) \leq k(d\ \xi_{n-1}(\omega), \xi_n)(\omega) \leq \cdots \leq k^n d(\xi_o(\omega), \xi_1(\omega)).$$

Further, for m > n,

$$d(\xi_n(\omega), \xi_m(\omega)) \leq d\ \xi_n(\omega), \xi_{n+1})(\omega) + \cdots + d(\xi_{m-1}(\omega), \xi_m(\omega))$$

$$\leq (k^n + k^{n+1} + \cdots + k^{m-1})\, d(\xi_o(\omega), \xi_1(\omega))$$

$$d(\xi_n(\omega), \xi_m(\omega)) \leq \left(\frac{k^n}{1-k}\right) d\ (\xi_o(\omega),\ \xi_1(\omega))$$

Which tends to zero as $n \to \infty$. It follows that $\{\xi_n(\omega)\}$ is a Cauchy sequence and there exists a measurable mapping $\xi : \Omega \to X$ such that $\xi_n(\omega) \to \xi(\omega)$ for each $\omega \in \Omega$.=φt= implies that $\xi_{2n+1}(\omega) \to \xi(\omega)$ and $\xi_{2n+2}(\omega) \to \xi(\omega)$. Thus, we have for any $\omega \in \Omega$,

$$d(\xi(\omega), S(\omega, \xi(\omega))) \leq d(\xi(\omega), \xi_{2n+2}(\omega)) + d(\xi_{2n+2}(\omega), S(\omega, \xi(\omega)))$$

$$\leq d(\xi(\omega), \xi_{2n+2}(\omega)) + H(T(\omega, \xi_{2n+1}(\omega)), S(\omega, \xi(\omega))),$$

therefore,

$$d(\xi(\omega), S(\omega, \xi(\omega))) \leq d(\xi(\omega), \xi_{2n+2}(\omega))$$

$$+ \alpha(\omega) \frac{d(\xi(\omega), S(\omega, \xi(\omega)))^3 + d(\xi_{2n+1}(\omega), T(\omega, \xi_{2n+1}(\omega)))^3}{(d(\xi(\omega), S(\omega, \xi(\omega))) + d(\xi_{2n+1}(\omega), T(\omega, \xi_{2n+1}(\omega))^2}$$

$$+ \beta(\omega)\, d(\xi(\omega), \xi_{2n+1}(\omega)).$$

Taking $n \to \infty$, we have

$$d(\xi(\omega), S(\omega, \xi(\omega))) \leq \alpha(\omega)\, d(\xi(\omega), S(\omega, \xi(\omega))).$$

Hence,

$$\xi(\omega) \in S(\omega, \xi(\omega)) \text{ for all } \omega \in \Omega.=$$

Similarly, for any $\omega \in \Omega$,

$$d(\xi(\omega), T(\omega, \xi(\omega))) \leq \alpha(\omega)\, d(\xi(\omega), \xi_{2n+1}(\omega)) + H(S(\omega, \xi_{2n+1}(\omega)), T(\omega, \xi(\omega)))$$

$$\leq \alpha(\omega)\, d(\xi(\omega), T(\omega, \xi(\omega))).$$

Hence,

$$\xi(\omega) \in T(\omega, \xi(\omega)) \text{ For all } \omega \in \Omega.=$$

Corollary (2). Let X be a Polish space. Let $T : \Omega \times X \to CB(X)$ be a continuous random multivalued operators. If there exist measurable mappings $\alpha, \beta : \Omega \to (0, 1)$ such that for each $x, y \in X, \omega \in \Omega$.

$$H(T(\omega, x), T(\omega, y)) \leq \alpha(\omega) \frac{d(x, T(\omega, x))^3 + d(y, T(\omega, y))^3}{(d(x, T(\omega, x)) + d(y, T(\omega, y)))^2}$$

$$+ \beta(\omega)\, d(x, y).$$

Then there exists a sequence $\{\xi_n\}$ of measurable mappings $\xi_n : \Omega \to X$ which is asymptotically T-regular and converges to a random fixed point of T.

Remark (3).Theorem (1) is in continuation of Beg and Shahzad [9], Badshah and Sayyad [10] investigations and proves the existence of the common random fixed point of the multivalued generalized contractions with functional expressions.

Reference

1. Spacek, A. 1955. Zulfallige Gleichungen. Czechoslovak Mathematical Journal 5: 462-466.
2. Hans, O. 1957. Reduzierende Zufallige Transformationen. Czechoslovak Mathematics Journal 7: 154-158.
3. Hans, O. 1961. Random operator equations. Proceedings of the 4th Berkeley symposium in Mathematics and Statistical Probability, Vol. II :180-202.
4. Mukherjee, A. 1968. Random transformations of Banach spaces. Ph. D. Dissertation. Wayne State University, Detroit, Michigan,USA.
5. Itoh, S. 1977. A random fixed point theorem for a multivalued contraction mapping. Pacific Journal Mathematics 68: 85-90.
6. Itoh, S. 1979. Random fixed point theorem with applications to random differential equations in Banach spaces. Journal of Mathematical Analysis and Application 67: 261-273.
7. Sehgal, V.M. & Singh, S.P. 1985. On random approximation and a random fixed point theorem for a set valued mappings. Proceedings of the American Mathematical Society 95: 91-94.
8. Lin, T.C. 1988. Random approximations and random fixed point theorems for non-self maps. Proceedings of the American Mathematical Society 103:1129-1135.
9. Beg, I. & Shahzad, N. 1993. Random fixed points of random multivalued operators on Polish spaces. Nonlinear Analysis 20: 835-847.
10. Badshah, V. H. & Sayyad, F. 2000. Random fixed points of random multivalued operators on Polish spaces. Kuwait Journal of Science and Engineering 27: 203-208.
11. Beg, I. & Shahzad, N. 1995. Common random fixed points of random multivalued operators on metric spaces. Bollettino U.M.I. 7: 493-503.3

MAGNETIC FLUID BASED SQUEEZE FILM BEHAVIOR BETWEEN TRANSVERSELY ROUGH CURVED PLATES

Nikhilkumar D. Abhangi
Lecturer, Mathematics Department
Gandhinagar Institute of Technology
Ta. Kalol, Dist. Gandhinagar

G. M. Deheri,
Department of Mathematics
Sardar Patel University,
Vallabh Vidyanagar, Gujarat

Rakesh M. Patel
Department of Mathematics,
Gujarat Arts and Science College,
Ellis Bridge, Ahmedabad, Gujarat

ABSTRACT

An endeavor has been made to analyze the magnetic fluid based squeeze film behavior between two transversely rough curved plates, when the curved upper plate approaches the stationary curved lower plate. The lubricant used is a magnetic fluid in the presence of an external magnetic field oblique to the radial axis. The roughness of the bearing surface is modeled by a stochastic random variable with nonzero mean, variance and skewness. The associated Reynolds equation is solved with appropriate boundary conditions to obtain the pressure distribution, which is, then used to get the expression for load carrying capacity. To present a comparative study we consider the curvature of exponential form, hyperbolic form and secant form to represent the film thickness. The results are presented graphically. It is found that the load carrying capacity increases with increasing magnetization. It is seen that the bearing suffers in general, owing to the surface roughness. It is observed that negatively skewed roughness increases the load carrying capacity. Same is the case with negative variance. The adverse effect induced by the standard deviation, positive variance and positive skewness can be compensated up to certain extent by the magnetization parameter taking an appropriate choice of curvature parameters. This article makes it clear that the roughness must be given due consideration while designing the bearing system even if a proper choice of curvature parameters has been taken into consideration.

Key Words: Magnetic Fluid, Squeeze film, Transverse roughness, Reynolds equation, Load carrying capacity.

Nomenclature

a	Radius of the plates
H	Lubricant film thickness
c_1	Constant of integration
P	Pressure distribution
B	Curvature parameter of the upper plate
C	Curvature parameter of the lower plate
H	Magnitude of the magnetic field
P	Non-dimensional pressure
W	Load carrying capacity
H_0	Central distance
h_0	Normal Velocity
$\overline{W}$	Dimensionless load carrying capacity
μ	Fluid viscosity
$\overline{\mu}$	Magnetic susceptibility
μ_0	Permeability of the free space
σ^*	Non-dimensional standard deviation
α^*	Non-dimensional variance
ε^*	Non-dimensional skew ness

Introduction

The performance of squeeze film behavior between various geometrical configurations of flat surfaces was discussed by Archibald [1]. Murti [2] analyzed the behavior of squeeze film trapped between curved circular pates describing the film thickness by an expression of an exponential function. He also dealt with the squeeze film behavior between a curved upper plate and a flat lower plate and established that the load carrying capacity rose sharply with the curvature in the case of concave pads. Modifying the approach of Murti [2], Gupta and Vora [3] analyzed the performance of squeeze film behavior between curved annular plates. In all the above cases the lower plate was taken to be flat. Ajwaliya [4] considered the problem of squeeze film behavior taking the lower plate also to be curved. He also studied the squeeze film between curved annular plates choosing the curvature of an exponential form to represent the film thickness.

All the above studies considered conventional lubricant. Verma [5] and Agrwal [6] investigated the squeeze film performance by taking a magnetic fluid as a lubricant. Subsequently, Bhat and Deheri [7] analyzed the squeeze film between porous annular disks using a magnetic fluid lubricant with the external magnetic field oblique to the lower disk. They concluded that the application of magnetic fluid lubricant enhanced the performance of the squeeze film bearing system. However, they assumed that the plates were flat. But in actual practice, the flatness of the plate does not endure owing to elastic, thermal and uneven wear effects. With this end in view Bhat and Deheri [8] discussed the effect of magnetic fluid lubricant on the configuration of Ajwaliya [4], considering the two plates determined by exponential functions. They found that magnetic fluid lubricant improved the performance of the bearing.

Further, Bhat and Deheri [9] investigated the magnetic fluid based squeeze film behavior in curved porous circular disks. Patel and Deheri [10] analyzed the performance of magnetic fluid based squeeze film between two curved plates lying along the surfaces determined by secant functions. In addition, Patel and Deheri [11] studied the magnetic fluid based squeeze film between curved plates along the surfaces governed by hyperbolic functions. In the above three studies it was found that the magnetic fluid lubricant enhanced the performance of the bearing system.

By now, it is well-known that bearing surfaces particularly after having some run in and wear develop roughness. In order to study and analyze the effect of roughness of the bearing surfaces on the performance of the squeeze film bearings various methods have been resorted to. Several investigators have proposed a stochastic approach to mathematically model the random character of the roughness (Tzeng and Seibel [12], Christensen and Tonder [13, 14, 15]). Christensen and Tonder [13, 14, 15] presented a comprehensive general analysis for surface roughness (both transverse as well as longitudinal) based on a general probability density function by developing the approach if Tzeng and Seibel [12]. Subsequently, this method of Christensen and Tonder [13, 14 and 15] formed the basis of the analysis to study the effect of surface roughness on the performance of the bearing system in a number of investigations (Ting [16], Prakash and Tiwari [17], Prajapati [18], Guha [19], Gupta and Deheri [20]). Also, Andharia, Gupta and Deheri [21- 22] dealt with the analysis of the effect of surface roughness on the performance of a squeeze film bearing using the general stochastic analysis for describing the random roughness.

However, in these discussions conventional lubricants were used.

Efforts have been directed to present a comparative study on the behavior of magnetic fluid based squeeze film between transversely rough curved circular plates lying along the surfaces determined by different trigonometric functions and exponential function.

Analysis

The configuration of the bearing system is shown in Figure-1. The assumptions of usual hydrodynamic lubrication theory are taken into consideration in the development of the analysis.

The bearing surfaces are assumed to be transversely rough. The thickness $h(x)$ of the lubricant film is:-

$$h(x) = \bar{h}(x) + h_s$$

where $\bar{h}(x)$ is the mean film thickness and h_s is the deviation from the mean film thickness characterizing the random roughness of the bearing surfaces. h_s is considered to be stochastic in nature and governed by the probability density function:-

$$f(h_s), \quad -c \le h_s \le c$$

where c is the maximum deviation from the mean film thickness. The mean α, standard deviation σ and the parameter ε which is the measure of symmetry associated with the random variable h_s are determined by the relations

$$\alpha = E(h_s),$$

$$\sigma^2 = E[(h_s - \alpha)^2],$$

and

$$\varepsilon = E[(h_s - \alpha)^3]$$

where E denotes the expected value defined by:-

$$E(R) = \int_{-c}^{c} R f(h_s) dh_s$$

The axially symmetric flow of the magnetic fluid between the plates under an oblique magnetic field:-

$$\bar{H} = (H(r)\cos\phi(r,z), 0, H(r)\sin\phi(r,z))$$

whose magnitude H vanishes at $r = a$ has been taken into consideration. The following three cases have been subjected to investigations.

Case-1: We assume that the upper plate lying along the surface, given by

$$z = h_0\left(\exp(-Br^2)\right), \qquad 0 \le r \le a$$

approaches with normal velocity $\dot{h}_0 = dh_0/dt$ to the lower plate lying along the surface:-

$$z = h_0\left[\left(\exp(-Cr^2)\right) - 1\right]; \quad 0 \le r \le a$$

The film thickness $h_1(r)$ is given by

$$h_1(r) = h_0[\exp(-Br^2) - \exp(-Cr^2) + 1];$$
$$0 \le \quad \le a \qquad \ldots\ldots\ldots\ldots\ldots (1)$$

We obtain the dimensionless film thickness

$$\bar{h}_1 = \left[\exp(-BR^2) - \exp(-CR^2) + 1\right] \ldots (2)$$

by the introduction of the dimensionless quantities

$$\bar{h}_1 = \frac{h_1}{h_0}, \quad R = \frac{r}{a}, \quad B = Ba^2, \quad C = Ca^2$$

Case-2: Here the surface of the upper plate determined by

$$z = h_0\left[\frac{1}{1 + Br}\right]; \quad 0 \le r \le a$$

approaches to the lower plate lying along the surface

$$z = h_0\left[\frac{1}{1+Cr} - 1\right]; \quad 0 \le r \le a$$

with the normal velocity $\dot{h}_0$. The central film thickness $h_2(r)$ then is defined by

$$h_2(r) = h_0\left[\frac{1}{1+Br} - \frac{1}{1+Cr} + 1\right];$$

$$0 \le r \le a \qquad \ldots\ldots\ldots (3)$$

whose dimensionless form is

$$\bar{h}_2 = \left[\frac{1}{1+\boldsymbol{B}R} - \frac{1}{1+\boldsymbol{C}R} + 1\right]$$

where $\bar{h}_2 = \frac{h_2}{h_0}$, $\qquad \ldots\ldots\ldots (4)$

Case-3: Lastly, we have the surface of the upper plate determined by

$$z = h_0[\sec(Br^2)]; \quad 0 \le r \le a$$

approaching the lower plate lying along the surface

$$z = h_0[\sec(Cr^2) - 1]; \quad 0 \le r \le a$$

with the normal velocity $\dot{h}_0$. Here the central film thickness $h_3(r)$ is defined by

$$h_3(r) = h_0[\sec(Br^2) - \sec(Cr^2) + 1] \quad \ldots (5)$$

whose dimensionless form is given by

$$\bar{h}_3 = [\sec(\boldsymbol{B}R^2) - \sec(\boldsymbol{C}R^2) + 1]$$

where $\bar{h}_3 = \frac{h_3}{h_0}$, $\qquad \ldots\ldots\ldots (6)$

Now the associated modified Reynolds equation governing the film pressure p turns out to be

$$\frac{1}{r}\frac{d}{dr}\left[rh^3\frac{d}{dr}\left(p - 0.5\mu_0\bar{\mu}H^2\right)\right] = 12\mu h_0$$

Taking for example, $\qquad \ldots\ldots\ldots (7)$

$$H^2 = a(a-r) \qquad \ldots\ldots\ldots (8)$$

and remembering that the magnetic field comes out of a potential, it can be shown that ϕ satisfies the first order partial differential equation

$$\cot\varphi\frac{\partial\varphi}{\partial r} + \frac{\partial\varphi}{\partial z} = \frac{1}{2(a-r)}$$

whose solutions are

$$c_1\,\mathrm{cosec}^2\varphi = a - r \text{ and}$$
$$z = -2c_1\sqrt{(a - c_1^{\,2} - r)}.$$

Solving the equation (7) using expressions (1), (3), (5) and (8) under the boundary conditions

$$P(1) = 0, \qquad \frac{dP}{dR} = -\frac{\mu^*}{2} \quad \text{w}$$

Hence; R=0

we obtain the pressure distribution in dimensionless form for the three cases respectively, as

$$P = 0.5\mu^*(1-R) - 6\int_0^R \frac{R}{G(\bar{h}_1)}dR \qquad \ldots\ldots\ldots (9)$$

where

$$G(\bar{h}_1) = \bar{h}_1^{\,3} + 3\bar{h}_1^{\,2}\alpha^* + 3\bar{h}_1(\sigma^{*2} + \alpha^{*2}) + \varepsilon^* + 3\sigma^{*2}\alpha^* + \alpha^{*3}$$

$$P = 0.5\mu^*(1-R) - 6\int_0^R \frac{R}{G(\bar{h}_2)}dR \quad \ldots (10)$$

where

$$G(\bar{h}_2) = \bar{h}_2^{\,3} + 3\bar{h}_2^{\,2}\alpha^* + 3\bar{h}_2(\sigma^{*2} + \alpha^{*2}) + \varepsilon^* + 3\sigma^{*2}\alpha^* + \alpha^{*3}$$

$$P = 0.5\mu^*(1-R) - 6\int_0^R \frac{R}{G(\bar{h}_3)}dR$$

$$\ldots\ldots\ldots (11)$$

Where,

$$G(\bar{h}_3) = \bar{h}_3^{\,3} + 3\bar{h}_3^{\,2}\alpha^* + 3\bar{h}_3(\sigma^{*2} + \alpha^{*2}) + \varepsilon^* + 3\sigma^{*2}\alpha^* + \alpha^*$$

The load carrying capacity W is obtained from the relation

$$W = 2\pi \int_0^a rp(r)dr$$

whose non-dimensional form in the three cases respectively, is given by

$$\overline{W} = \frac{\mu^*}{12} + 3\int_0^1 \frac{R^3}{G(\bar{h}_1)}dR \qquad \ldots\ldots\ldots (12)$$

$$\overline{W} = \frac{\mu^*}{12} + 3\int_0^1 \frac{R^3}{G(\bar{h}_2)}dR \qquad \ldots\ldots\ldots (13)$$

and

$$\overline{W} = \frac{\mu^*}{12} + 3\int_0^1 \frac{R^3}{G(\bar{h}_3)}dR \qquad \ldots\ldots\ldots (14)$$

Results and discussion

Expressions for the dimensionless pressure and load carrying capacity for all the three cases are presented respectively in Eq.s (9)-(14). These expressions depend on various parameters such as μ^* , σ^* , ε^*, α^*, B and C. Setting μ^* to be equal to zero we get the corresponding non-magnetic cases for the respective rough bearing system. Further, taking roughness parameters to be zero we get the corresponding case of non-magnetic smooth bearing system. Lastly, considering only the roughness parameters to be zero we get the corresponding magnetic fluid based smooth bearing system analyzed in [23], [11] and [10].

However, load carrying capacity increases significantly in all the cases with respect to the magnetization. Further, it is clearly seen that the effect of magnetization is most sharp in the hyperbolic case. The five figures Figure 2-6 indicate that the effect of $\mu*$ is almost negligible upto the value of 0.01 for the exponential case and hyperbolic case while in the case of secant function the effect of $\mu*$ is negligible upto 0.001.

The bearing suffers in general owing to the surface roughness. The load carrying capacity decreases with respect to the standard deviation associated with roughness for all the cases which can be seen from Figure 7-10. This negative effect is more in the case of the surface determined by the hyperbolic functions. The negatively skewed roughness increases the load carrying capacity for all the shapes, while positive $\varepsilon*$ decreases the load carrying capacity (cf. Figure 11-13). This effect of $\varepsilon*$ is comparatively sharp in the hyperbolic case. Almost similar are the trends for the variance (cf. Figure 14-15).

A symmetric nature (Figure 16) is observed in the case of the secant function with respect to the curvature parameters. The load carrying capacity decreases and then increases with respect to the lower plate curvature parameter while exactly the opposite happens with respect to the upper plate curvature parameter. The upper plate curvature parameter increases the load carrying capacity while the lower plate curvature parameter decreases the load carrying capacity in the hyperbolic case and exponential case. Comparatively this effect is less for exponential shape, as can be seen from Figure 16 in the respective cases.

Some of the figures tend to suggest that the adverse effect induced by the standard deviation, positive variance and

positive skewness can be compensated upto some extent by the magnetization parameter by considering an appropriate choice of curvature parameters.

However, this compensation is upto a considerably large extent in the case of negatively skewed roughness especially, when negative variance is involved. The decreased load carrying capacity due to the lower plate curvature parameter gets further decreased owing to the standard deviation of the roughness. The increased load carrying capacity introduced by the upper plate curvature parameter gets substantially increased by the positive effect of magnetization in the case of negatively skewed roughness.

Conclusion

This article makes it clear that the roughness must be given due consideration while designing such magnetic fluid based bearing system, albeit a proper choice of curvature parameter has been taken into consideration. Even if a strong magnetic field is brought in and an appropriate choice for curvature parameters is made, roughness needs to be accounted for from longevity point of view.

References

[1] Archibald, F.R., Load capacity and time relations for squeeze films, Transactions of ASME, Vol. 78, (1956), p.p A231-245.

[2] Murti, P.R.K., Squeeze films in curved circular plates, ASME, Journal of Lubrication technology, Vol.97, (1975), p.p.650-654.

[3] Gupta, J.L. and Vora, K.H., Analysis of squeeze film between curved annular plates, Journal of lubrication technology, Vol. 102, (1980), p.p.48-53.

[4] Ajwaliya, M.B., On certain theoretical studies in hydrodynamic and electromagnetohydroynamic lubrication, Ph. D. thesis, (1984), S.P. University, V. V. Nagar.

[5] Verma, P.D.S., Magnetic fluid based squeeze film, International Journal of Engineering Sciences, Vol. 24(3), (1986), p.p. 395-401.

[6] Agrwal, V.K., Magnetic fluid based porous inclined slider bearing, Wear, Vol. 107, (1986), p.p. 133-139.

[7] Bhat, M.V. and Deheri, G.M., Squeeze film behavior in porous annular disks lubricated with magnetic fluid, Wear, Vol. 151, (1991), p.p. 123-128.

[8] Bhat, M.V. and Deheri, G.M., Magnetic fluid based squeeze film between two curved circular plates, Bulletin of Calcutta Mathematical Society, Vol. 85, (1993), p.p. 521-524.

[9] Bhat, M.V. and Deheri, G.M., Magnetic fluid based squeeze film in porous circular disks, Journal of Magnetism and Magnetic Materials, Vol. 127, (1993), p.p. 159-162.

[10] Patel, R.M. and Deheri, G.M., Magnetic fluid based squeeze film between two curved plates lying along the surfaces determined by secant functions, Indian Journal of Engineering and Material Sciences, Vol. 9, (2002), p.p. 45-48.

[11] Patel, R.M. and Deheri, G.M., An analysis of Magnetic fluid based squeeze film between curved plates, Jour. Nat. Acad. Math. Vol. 16(2002), p.p. 74-84.

[12] Tzeng, S.T. and Seibel, E. Surface roughness effect on slider bearing lubrication, Trans. ASME, J. Lubr. Tech., (1967), 10, p.p 334-338.

[13] Christensen, H. and Tonder, K.C., Tribology of rough surfaces: Stochastic models of hydrodynamic lubrication. SINTEF report no. 10/69 – 18, 1969.

[14] Christensen, H. and Tonder, K.C., Tribology of rough surfaces: Parametric study and comparison of lubrication models. SINTEF report no. 22/69 -18, 1969.

[15] Christensen, H. and Tonder, K.C., The hydrodynamic lubrication of rough bearing surfaces of finite width. ASME-ASLE Lubrication conference, Cincinnati, Ohio, 1970, paper no. 70-Lub-7.

[16]Ting, L.L., Engagement behavior of lubricated porous annular disks. Part 1: Squeeze film phase, surface roughness and elastic deformation effects. Wear, 1975, 34, p.p. 159-182.
[17]Prakash, J. and Tiwari, K., Roughness effects in porous circular squeeze plates with arbitrary wall thickness. Lubr. Technol., (1983), 105, p.p. 90-95.
[18] Prajapati, B.L., Behavior of squeeze film between rotating porous circular plates: surface roughness and elastic deformation. Pure Appl. Math. Sci., (1991), 33(1-2), p.p. 27-36.
[19]Guha, S.K., Analysis of dynamic characteristic of hydrodynamic journal bearings with isotropic roughness effects. Wear, (1993), 167, p.p 173-179.
[20]Gupta, J.L. and Deheri, G.M., Effect of roughness on the behavior of squeeze film in a spherical bearing, Tribology Transactions, (1996), 39, p.p. 99-102.
[21]Andharia, P.I., Gupta, J.L. and Deheri, G.M., Effect of longitudinal surface roughness on hydrodynamic lubrication of slider bearings. In Proceedings of Tenth International Conference on Surface modification Technologies, The Institute of Materials, (1997), p.p. 872-880.
[22]Andharia, P.I., Gupta, J.L. and Deheri, G.M., Effects of transverse roughness on the behavior of squeeze film in a spherical bearing, Int. J. of Applied Mechanics and Engineering, Vol. 4, No. 1, (1999), p.p. 19-24.

Hyperbolic Shape

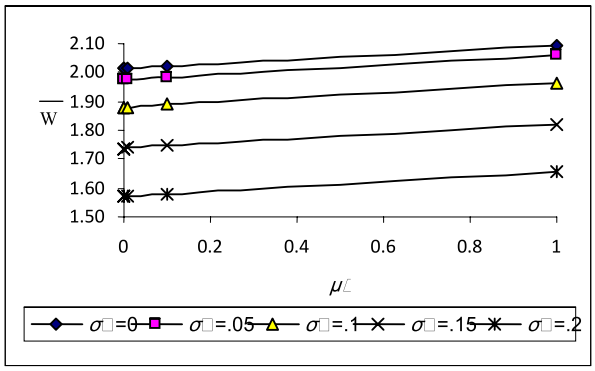

Figure 2: Variation of Load carrying capacity with respect to μ and σ^*

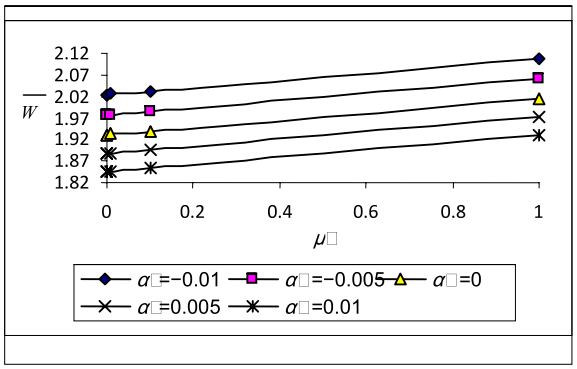

Figure 5: Variation of Load carrying capacity with respect to μ and α^*

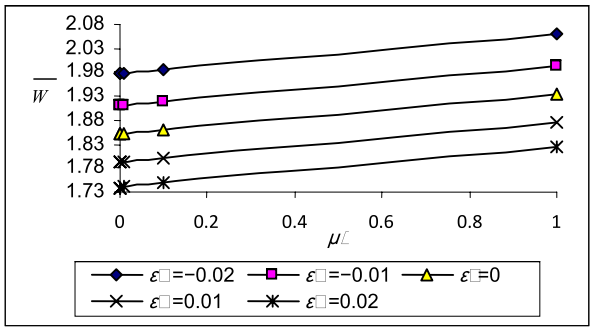

Figure 3: Variation of Load carrying capacity with respect to μ and ε^*

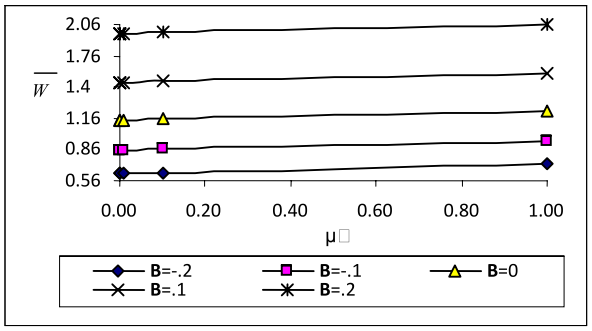

Figure 6: Variation of Load carrying capacity with respect to μ and β

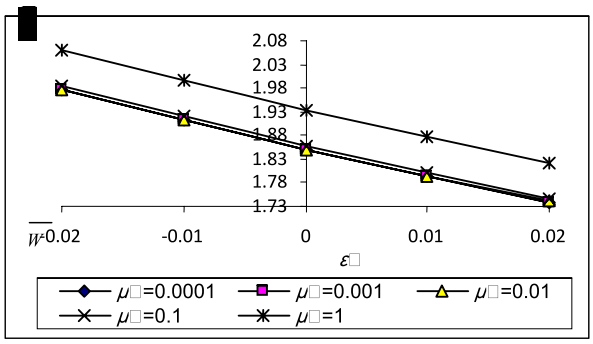

Figure 4: Variation of Load carrying capacity with respect to ε^* and μ

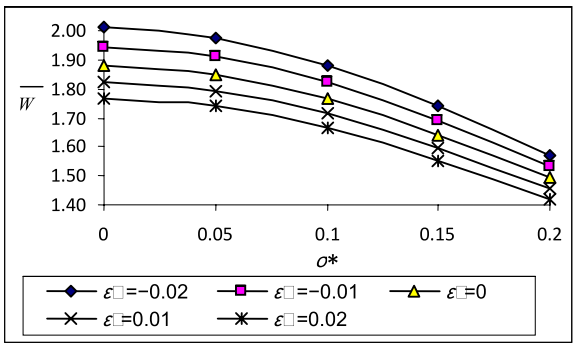

Figure 7: Variation of Load carrying capacity with respect to σ^* and ε^*

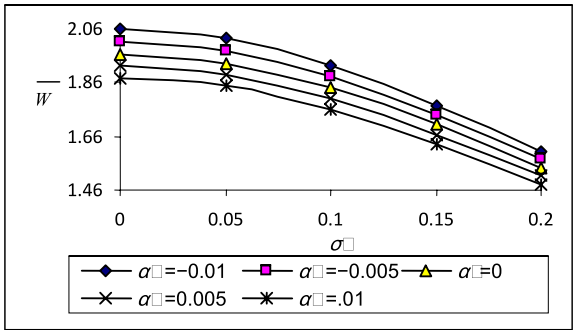

Figure 8: Variation of Load carrying capacity with respect to σ and α^*

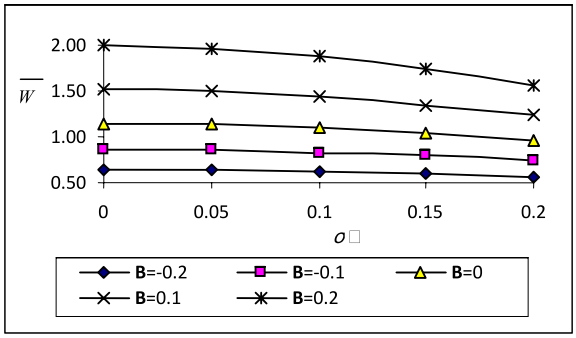

Figure 9: Variation of Load carrying capacity with respect to σ and B

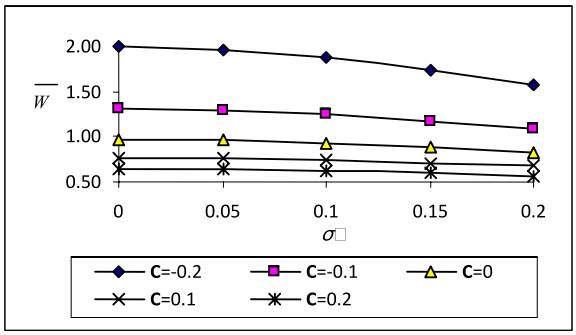

Figure 10: Variation of Load carrying capacity with respect to σ and C

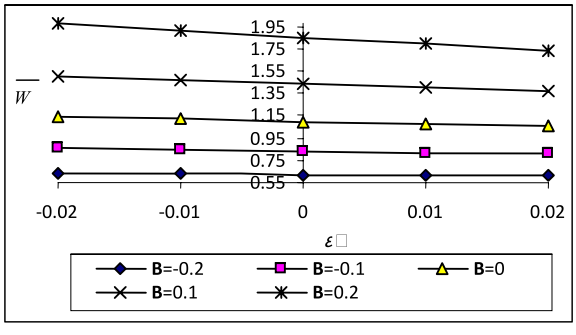

Figure 11: Variation of Load carrying capacity with respect to ε^* and B

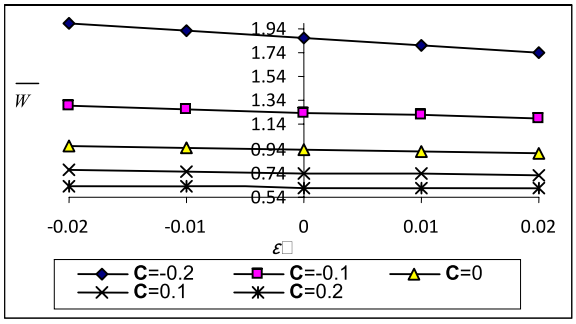

Figure 12: Variation of Load carrying capacity with respect to ε^* and C

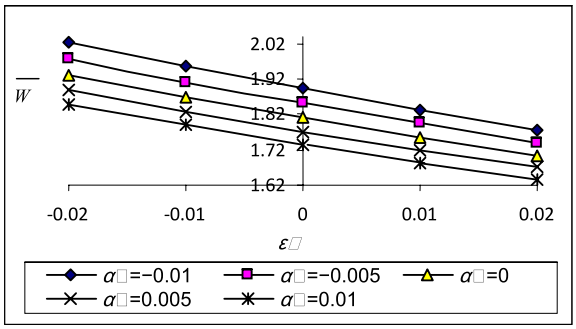

Figure 13: Variation of Load carrying capacity with respect to ε^* and α^*

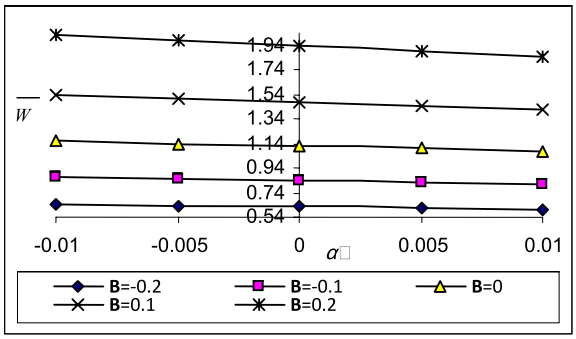

Figure 14: Variation of Load carrying capacity with respect to α^* and B

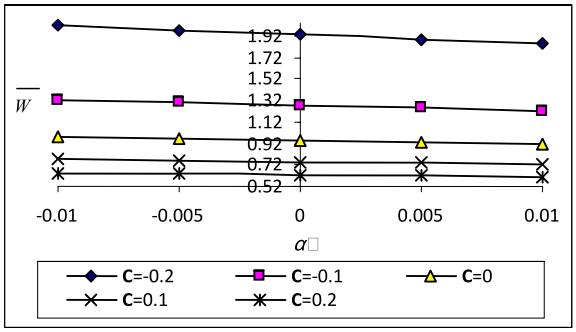

Figure 15: Variation of Load carrying capacity with respect to α^* and C

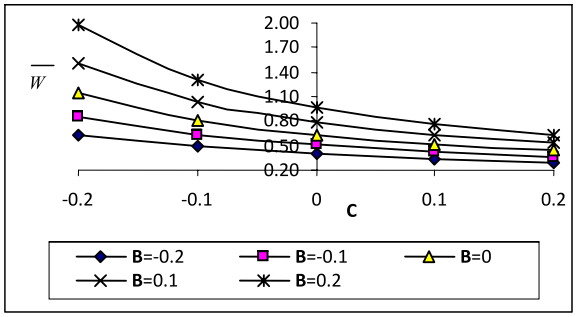

Figure 16: Variation of Load carrying capacity with respect to C and B

Exponential Shape

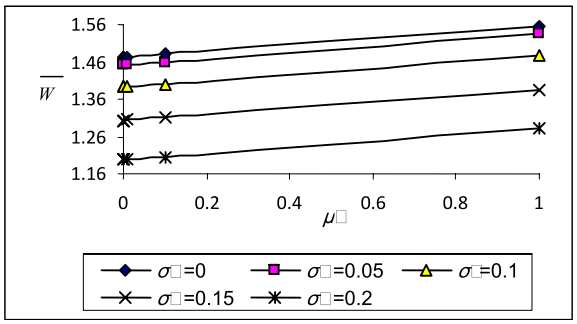

Figure 2: Variation of Load carrying capacity with respect to μ and σ^*

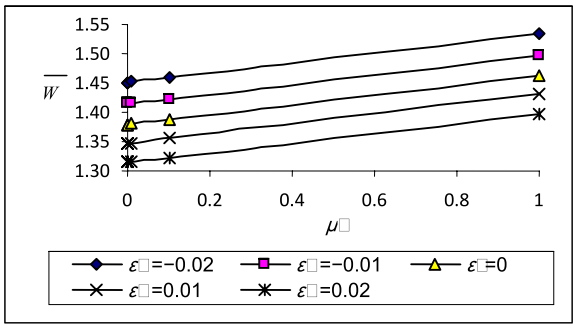

Figure 3: Variation of Load carrying capacity with respect to μ and ε^*

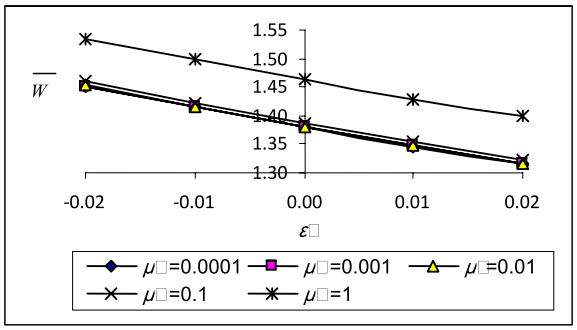

Figure 4: Variation of Load carrying capacity with respect to $\varepsilon^*$and μ

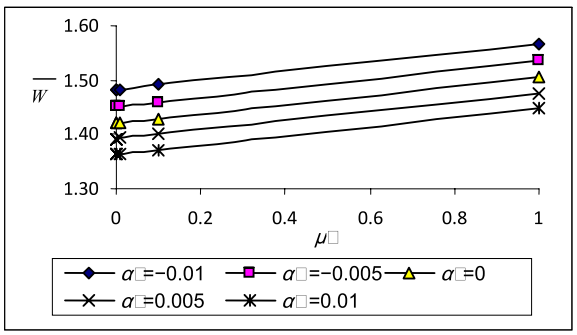

Figure 5: Variation of Load carrying capacity with respect to μ and α^*

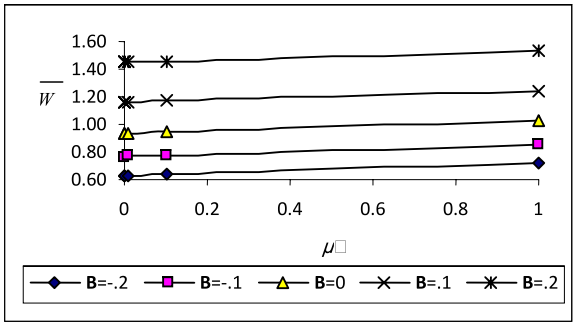

Figure 6: Variation of Load carrying capacity with respect to μ and β

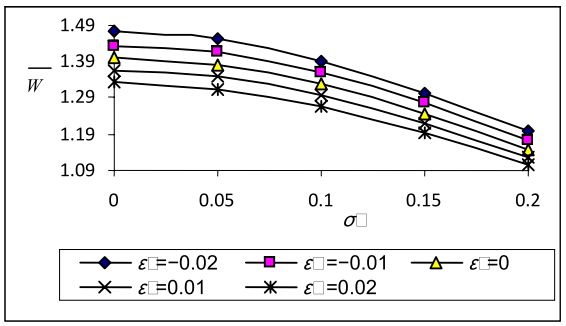

Figure 7: Variation of Load carrying capacity with respect to σ^* and α^*

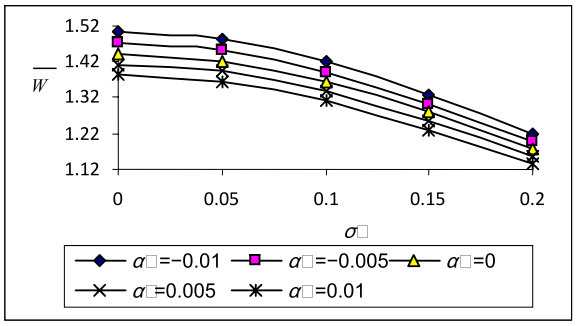

Figure 8: Variation of Load carrying capacity with respect to σ and α^*

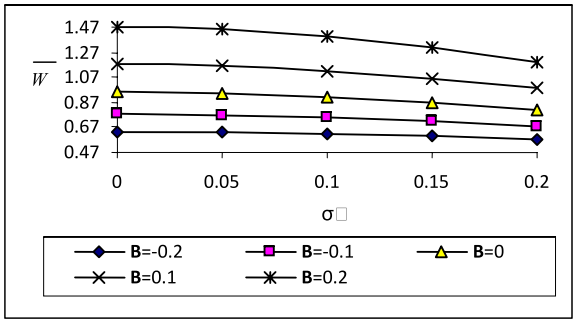

Figure 9: Variation of Load carrying capacity with respect to σ and B

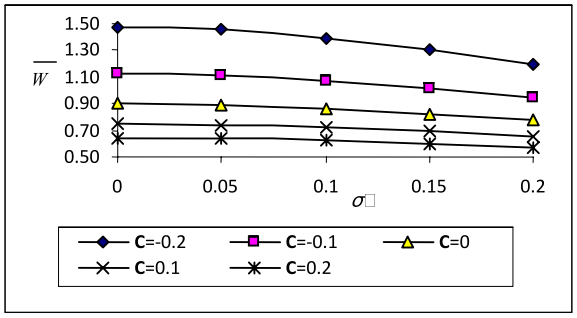

Figure 10: Variation of Load carrying capacity with respect to σ and C

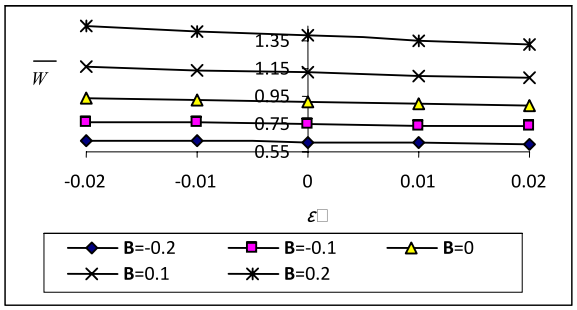

Figure 11: Variation of Load carrying capacity with respect to ε^* and B

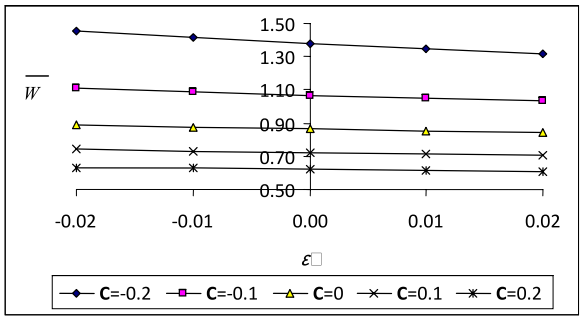

Figure 12: Variation of Load carrying capacity with respect to ε^* and C

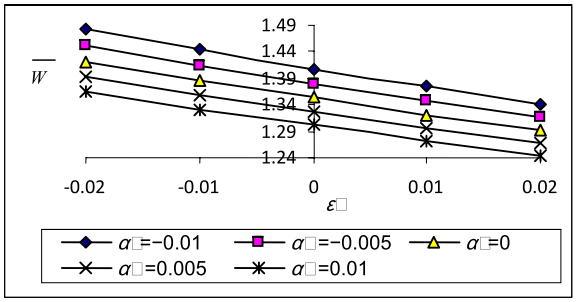

Figure 13: Variation of Load carrying capacity with respect to ε^* and α^*

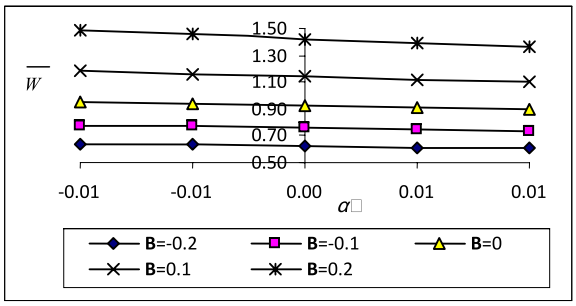

Figure 14: Variation of Load carrying capacity with respect to α^* and B

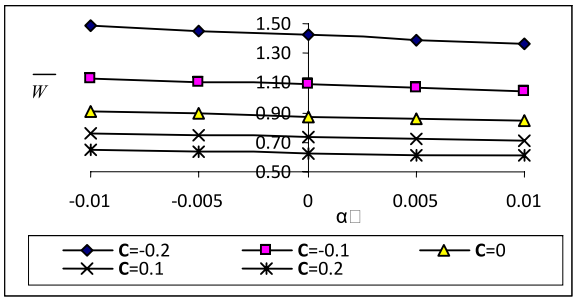

Figure 15: Variation of Load carrying capacity with respect to α^* and C

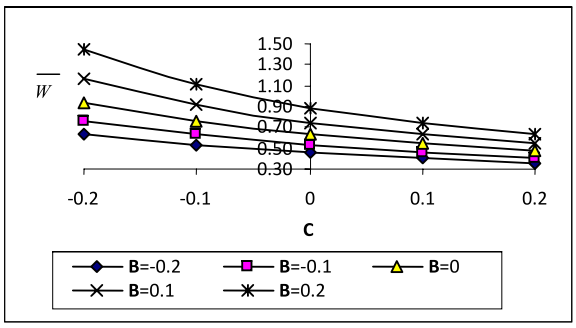

Figure 16: Variation of Load carrying capacity with respect to C and B

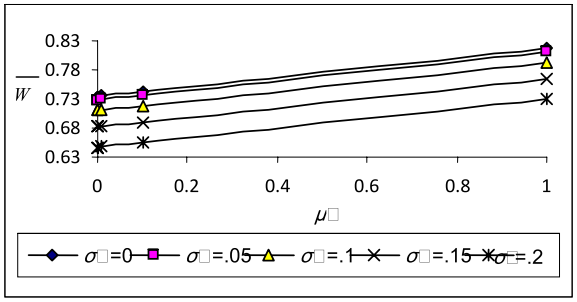

Figure 2: Variation of Load carrying capacity with respect to μ^* and α^*

Secant Shape

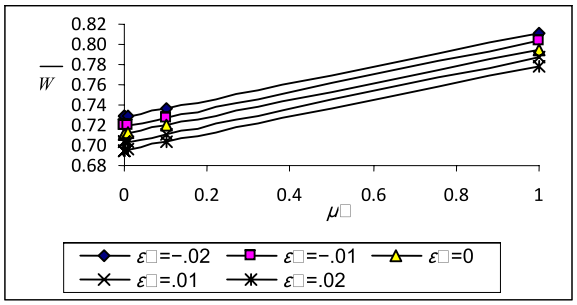

Figure 3: Variation of Load carrying capacity with respect to μ^* and ε^*

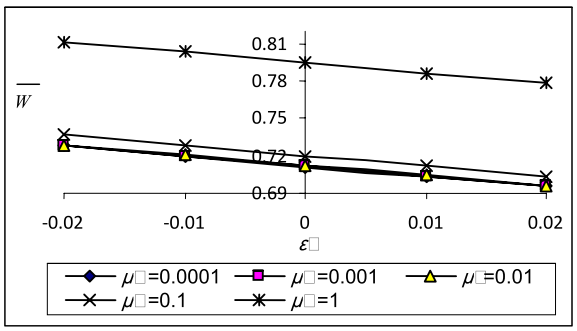

Figure 4: Variation of Load carrying capacity with respect to $\varepsilon^*$and μ^*

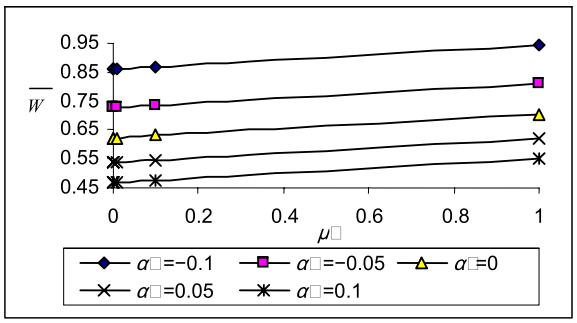

Figure 5: Variation of Load carrying capacity with respect to μ^* and α^*

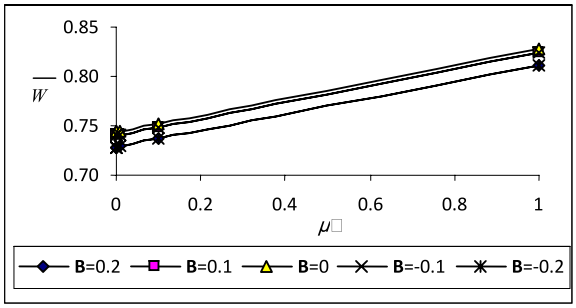

Figure 6: Variation of Load carrying capacity with respect to μ^* and B

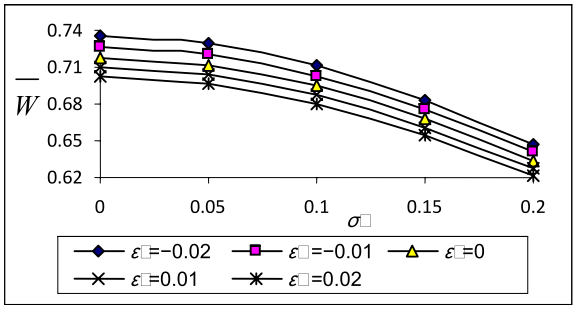

Figure 7: Variation of Load carrying capacity with respect to σ^* and ε^*

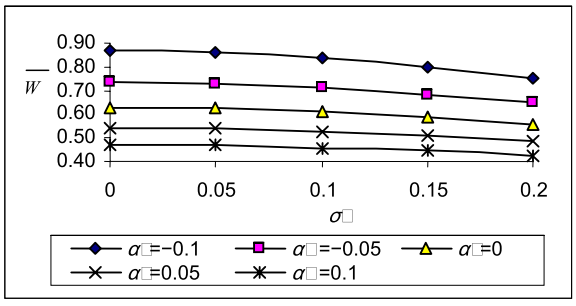

Figure 8: Variation of Load carrying capacity with respect to σ^* and α^*

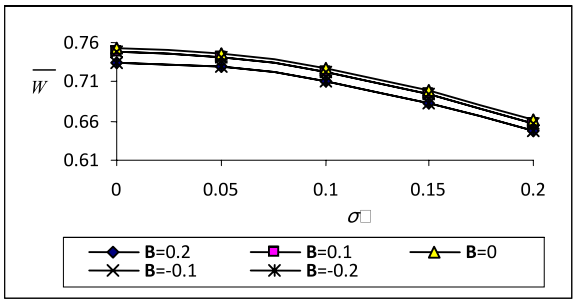

Figure 9: Variation of Load carrying capacity with respect to σ^* and B

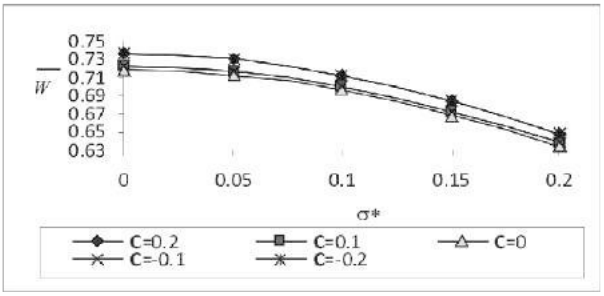

Figure 10: Variation of Load carrying capacity with respect to σ^* and C

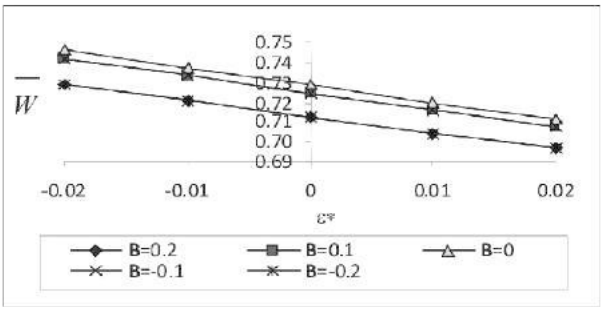

Figure 11: Variation of Load carrying capacity with respect to ε^** and B

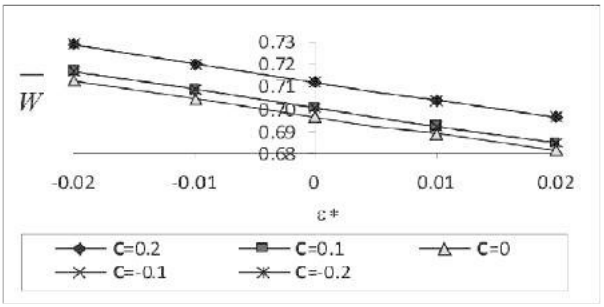

Figure 12: Variation of Load carrying capacity with respect to ε^* and C

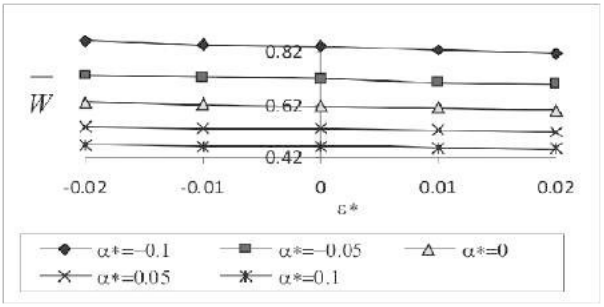

Figure 13: Variation of Load carrying capacity with respect to ε^* and α^*

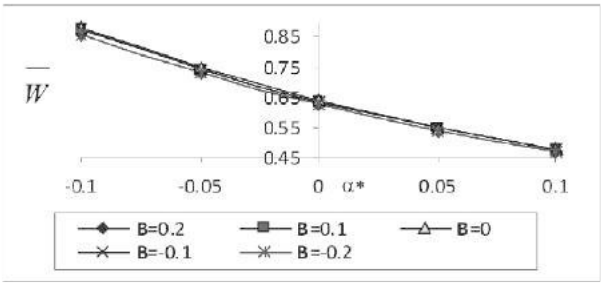

Figure 14: Variation of Load carrying capacity with respect to α^* and B

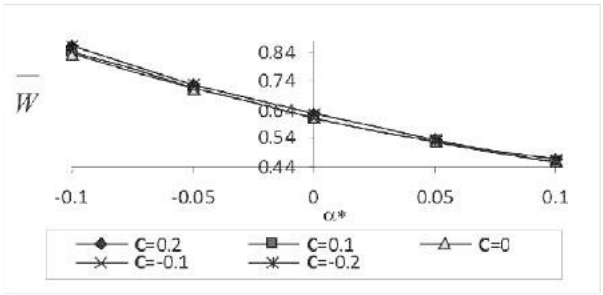

Figure 15: Variation of Load carrying capacity with respect to α^* and C

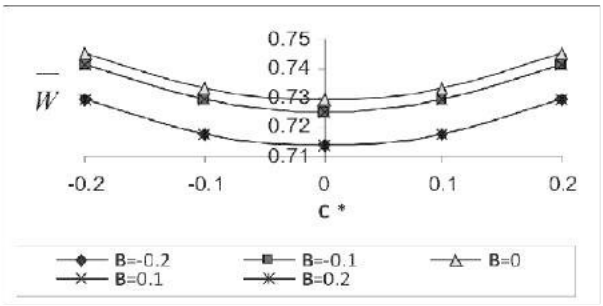

Figure 16: Variation of Load carrying capacity with respect to C and B

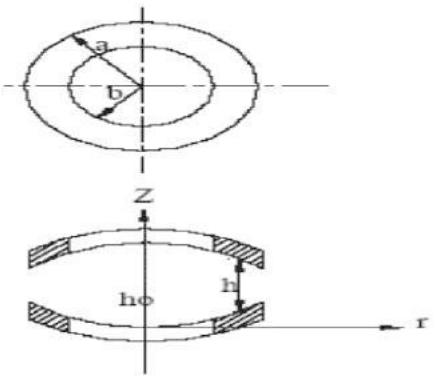

Figure1: Configuration of the bearing system

PERFORMANCE OF AN INFINITELY LONG TRANSVERSELY ROUGH HYDRODYNAMIC SLIDER BEARING

G. M. Deheri
Department of Mathematics,
Sardar Patel University,
Vallabh Vidyanagar-Gujarat

Chandaniben D. Changela
Lecturer, Mathematics Department
Gandhinagar Institute of Technology
Ta. Kalol, Dist. Gandhinagar

H. C. Patel
Government Engineering College
Patan, Gujarat,

Nikhilkumar D. Abhangi
Lecturer, Mathematics Department
Gandhinagar Institute of Technology
Ta. Kalol, Dist. Gandhinagar

ABSTRACT

By now, it is well-known that the standard deviation associated with the roughness plays an important role in the performance of a hydrodynamic slider bearing. Thus, it has been thought appropriate to study and analyze the effect of standard deviation on the performance of an infinitely long transversely rough slider bearing. The concerned Reynolds equation is solved with suitable boundary conditions to get the pressure distribution, in turn which is used to obtain load carrying capacity. Besides, the friction at the runner plate and the bearings surface has been calculated. The results are presented graphically. It is observed that the effect of standard deviation is significantly adverse. Further, the friction decreases at the bearing surface while there is an almost negligible increase at the runner plate. In addition, it is noticed that the aspect ratio has a significantly positive effect in the sense that the load carrying capacity increases and the friction decreases at the bearing surface and the runner plate with respect to increasing values of the aspect ratio. Also, it has been noted that the ratio of outlet film thickness to the bearing length tends to enhance the performance of the bearing system. This article makes it clear that the adverse effect of standard deviation can be compensated upto considerable extent by choosing a proper combination of the aspect ratio and the ratio of outlet film thickness to the length of the bearing.

Nomenclature

h- fluid film thickness at any point
m- aspect ratio
p - lubricant pressure
w- load carrying capacity
h_1 - maximum film thickness
h_2- minimum film thickness
σ - standard deviation
ε - skewness
α - variance
μ- dynamic viscosity of fluid
τ - shear stress
B - width of bearing
F- frictional force
L- length of bearing
P- dimensionless pressure
W- dimensionless load carrying capacity
$\bar{F}$- dimensionless frictional force
$\bar{\tau}$- dimensionless shear stress

Introduction

The fundamental aspect in a hydrodynamic slider bearing is the formation of a conversing wedge of the lubricant. The hydrodynamic slider may be construct at to provide this conversing wedge in a number of ways. Purday [3] showed that the shape of the wedge is not that important and all that matter is in the aspect ratio.

The analysis of hydrodynamic lubrication of non-porous slider is a classical one, for instance one can have a look at Pinkus and Sternlicht [7]. The infinitely long slider bearing is the idealization of a single sector shaped pad of a hydrodynamic thrust bearing. Such a bearing consist of a fixed or pivoted pad and a moving pad which may be plane, stepped, curved or composite shaped. {such bearing are widely use hydrodynamic generators and turbines}. Exact solutions of Reynolds equations thrust slider bearing with various simple film geometries are presented in a number of books and research papers. (Cameron [8], Gross et.al. [15], Bogli [2], Archibald [4], [6], Charnes and Seibel [5], Rayleigh [1], Basu et.al. [23]). Lord Rayleigh [1] applied the calculus of variation to determine the optimum film thickness and he found that the optimum slider profile was a step function.

Plane inclined porous slider bearing was analyzed by Prakash and Vij [13] and it was concluded that the effect of porosity was to decrease the load carrying capacity and friction. Patel and Gupta [16] extended this analysis by considering this problem with slip velocity.

All the above analysis assumes the bearing surfaces to be smooth. However, we know that the bearing surfaces after run-in and wear develop roughness. In order to study and analyze the effect of roughness several investigations have propose a approach to mathematically model the random character of the roughness (Tzeng and Seibel [9], Christensen and Tonder [10], [11] and [12]). Subsequently these approaches of Christensen and Tonder form the basis of the methods to analyze the effect of surface roughness on the performance of the bearing system in a number of investigations (Ting [14], Prakash and Tiwari [17], Prajapati [18], Guha [19], Gupta and Deheri [20]).

The standard deviation associated with the characterization of roughness plays a crucial role especially when the effect of variance and skewness is relatively not that sharp. Here, we propose to analyze the performance of transversely rough infinitely long bearings in which the standard deviation plays a pivoted role.

Analysis

The configuration of the bearing system which is infinite in Z-direction is given below in Figure (1) where in the slider moves with the uniform velocity u in the X-direction.

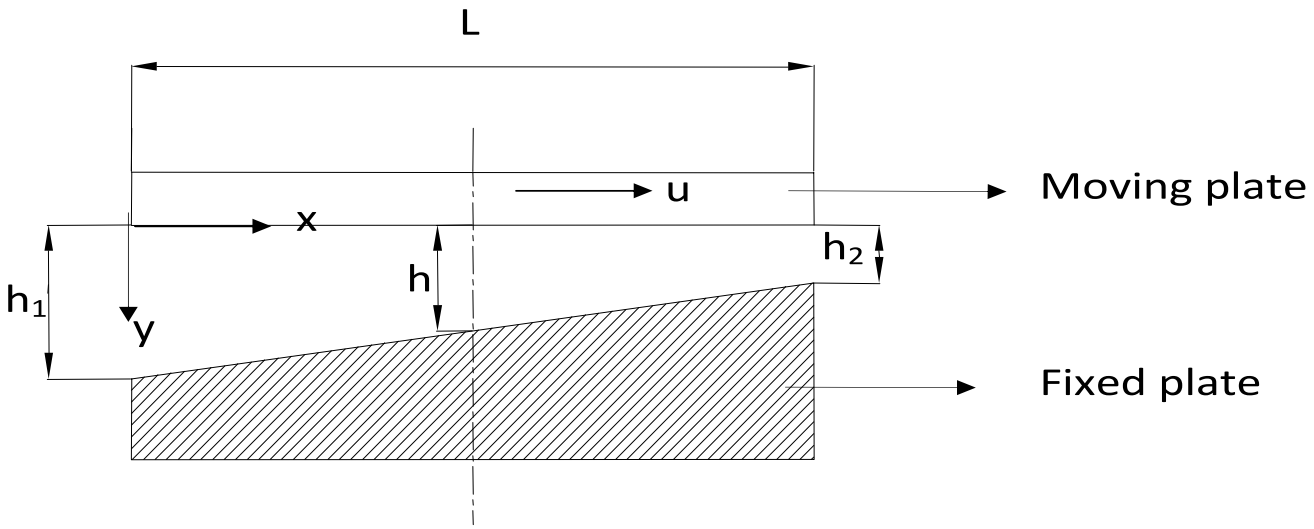

Figure-1 Configuration of the bearing system

The length of the bearing is L and breadth B is in Z-direction. The bearing surfaces are considered to be transversely rough. The thickness $h(x)$ of the lubricant film is

$$h(x) = \bar{h}(x) + h_S$$

Where $\bar{h}(x)$ is the mean film thickness and h_S is the deviation from the mean film thickness characterizing the random roughness of the bearing surfaces. h_s is assumed to be stochastic in nature and governed by the probability density function $f(h_s), -c \le h_s \le c$ where c is the maximum deviation from the mean film thickness. The mean α, the standard deviation σ and the parameter ε, which is the measure of symmetry of the random variable h_s, are defined by the relationships

$$\alpha = E(h_s),$$
$$\sigma^2 = E\left[(h_s - \alpha)^2\right]$$

and

$$\varepsilon = E\left[(h_s - \alpha)^3\right]$$

where, E denotes the expected value defined by

$$E(R) = \int_{-c}^{c} R f(h_s) dh_s$$

The assumptions of usual hydrodynamic lubrication theory are taken into consideration in the analysis. The lubricant film is considered to be is oviscous and incompressible and the flow is laminar. Taking in to account the predominant nature of standard deviation the governing Reynolds equation (C.F.) Basu, Sengupta and Ahuja (2005), Andharia, Gupta and Deheri (2001), Andharia, Gupta and Deheri (1997) turns out to be

$$\frac{dp}{dx} = 6\mu u \left[\frac{h_2\left[1 + m\left(1 - x/L\right)\right] - \lambda h_2}{h_2^3\left[1 + m\left(1 - x/L\right)\right] + 3\sigma^2 h_2\left[1 + m\left(1 - x/L\right)\right]} \right]$$

… … … … … (1)

The associated boundary conditions are

$$P = 0 \text{ at } X = 0, X = L$$

Introducing the dimensionless quantities

$$m = \frac{h_2 - h_1}{L},\ X = \frac{x}{L},\ P = \frac{h_2^3 p}{\mu u L^2},\ \bar{\sigma} = \frac{\sigma}{L},\ \bar{h}_2 = \frac{h_2}{L}$$

and fixing the following symbols

$$C = \frac{\sqrt{1+J^2}}{\sqrt{(1+m)^2+J^2}},\ A = \frac{(m/J)}{1+[(1+m)]/J^2},\ J = \frac{\sqrt{3}\bar{\sigma}}{\bar{h}_2},\ \bar{L} = \frac{L}{h_2},$$

$$\lambda = \left(\frac{\sqrt{3}\bar{\sigma}}{\bar{h}_2}\right)G \qquad G = \frac{\tan^{-1}\left\{\dfrac{\left(m\bar{h}_2/\sqrt{3}\bar{\sigma}\right)}{1+\left(\bar{h}_2/\sqrt{3}\bar{\sigma}\right)^2(1+m)}\right\}}{\ln\left\{\dfrac{(1+m)\sqrt{1+\left(\sqrt{3}\bar{\sigma}/\bar{h}_2\right)^2}}{\sqrt{(1+m)^2+\left(\sqrt{3}\bar{\sigma}/\bar{h}_2\right)^2}}\right\}}$$

we obtain the dimensionless pressure distribution determined by the expression

$$P = \frac{2\sqrt{3}\bar{h}_2^2}{m\bar{\sigma}}\tan^{-1}\left\{\frac{\left(\bar{h}_2/\sqrt{3}\bar{\sigma}\right)[m(1-x)]}{1+\left(\bar{h}_2/\sqrt{3}\bar{\sigma}\right)^2[1+m(1-x)]}\right\} + \frac{2\bar{h}_2^3}{\bar{\sigma}^2}\lambda\ln\left\{\frac{1+m(1-x)\sqrt{1+\left(\sqrt{3}\bar{\sigma}/\bar{h}_2\right)^2}}{\sqrt{[1+m(1-x)]^2+\left(\sqrt{3}\bar{\sigma}/\bar{h}_2\right)^2}}\right\}$$

… … … … … (2)

Where

$$\lambda = \left(\frac{\sqrt{3}\bar{\sigma}}{\bar{h}_2}\right)\left\{\tan^{-1}\left\{\frac{\left(m\bar{h}_2/\sqrt{3}\bar{\sigma}\right)}{1+\left(\frac{\bar{h}_2}{\sqrt{3}\bar{\sigma}}\right)^2(1+m)}\right\}\Bigg/\ln\left\{\frac{(1+m)\sqrt{1+\left(\frac{\sqrt{3}\bar{\sigma}}{\bar{h}_2}\right)^2}}{\sqrt{(1+m)^2+\left(\frac{\sqrt{3}\bar{\sigma}}{\bar{h}_2}\right)^2}}\right\}\right\}$$

The dimensionless load carrying capacity per unit width is given by

$$W = \frac{\bar{h}_2^3}{\mu u L^4} w = \int_0^1 P dx$$

which comes out to be

$$W = \frac{2\sqrt{3}\bar{h}_2^2}{m\bar{\sigma}}\left\{\left(\frac{m^2-1}{m}\right)\tan^{-1}(A) - \frac{J}{2m}\ln(C) - \frac{J\left(\tan^{-1}(A)\right)^2}{\ln\left[C(1+m)\right]}\right\} \quad \text{… (3)}$$

Further, the frictional force per unit width on the lower plane of the moving plate is obtained as

$$\bar{F} = \int_0^1 \bar{\tau} dx$$

where in

$$\bar{\tau} = \left(\frac{h_2}{\mu u} \right) \tau$$

is the non-dimensional shearing stress, while

$$\tau = \frac{dp}{dx}\left(y - \frac{h}{2} \right) + \frac{\mu u}{h}$$

(c.f. Basu, Sengupta and Ahuja (2005)

Hence, the dimensionless frictional force comes out to be

$$\bar{\tau} = \frac{dP}{dX}\bar{L}\{1 + m(1 - X)\}\left(Y - \frac{1}{2} \right) + \frac{1}{[1 + m(1 - X)]}$$

At Y=0 (moving plate) we find that,

$$\bar{\tau} = -\frac{1}{2}\frac{dP}{dX}\bar{L}\{1 + m(1 - X)\} + \frac{1}{[1 + m(1 - X)]}$$

which results in,

$$\bar{\tau} = -\frac{1}{2}\bar{L}d\left[\left(\frac{2\bar{h}_2^3}{\bar{\sigma}^2} \right)\left\{ \frac{1}{1 + \left(\bar{h}_2/\sqrt{3\bar{\sigma}} \right)d^2} \right\} + \left(-6\sqrt{3}m\bar{\sigma} \right)\left\{ \frac{G}{d^2 + \left(\sqrt{3\bar{\sigma}}/\bar{h}_2 \right)} \right\} \right] + \frac{1}{d}$$

Where,

$$d = [1 + m(1 - X)]$$

in turn, which gives

$$\bar{\tau} = \left(\frac{-\bar{h}_2^3\bar{L}}{\bar{\sigma}^2} \right)\left\langle \frac{d}{1 + \left(\bar{h}_2/\sqrt{3\bar{\sigma}} \right)d^2} \right\rangle + \left(3\sqrt{3}m\bar{\sigma}\bar{L} \right)\left\langle \frac{dG}{d^2 + \left(\sqrt{3\bar{\sigma}}/\bar{h}_2 \right)} \right\rangle + \frac{1}{d}$$

Hence, in dimensionless form this frictional force takes the form

$$\bar{F} = \left(\frac{3\bar{h}_2\bar{L}}{2m} \right)\ln\left\{ \frac{1 + \left(\bar{h}_2/\sqrt{3\bar{\sigma}} \right)}{1 + (1 + m)^2\left(\bar{h}_2/\sqrt{3\bar{\sigma}} \right)} \right\} + \left(\frac{3\sqrt{3\bar{\sigma}}\bar{L}G}{2} \right)\ln\left\{ \frac{(1 + m)^2 + \left(\sqrt{3\bar{\sigma}}/\bar{h}_2 \right)}{1 + \left(\sqrt{3\bar{\sigma}}/\bar{h}_2 \right)} \right\} + \frac{1}{m}\ln(1 + m)$$

… … … … … … … (4)

where, $\bar{L} = L/h_2$

At Y=1(fixed plate) one finds that

$$\bar{\tau} = \frac{1}{2}\frac{dP}{dX}\bar{L}\{1+m(1-X)\} + \frac{1}{[1+m(1-X)]}$$

which leads to

$$\bar{\tau} = \frac{1}{2}\bar{L}d\left[\left(\frac{2\bar{h}_2^3}{\bar{\sigma}^2}\right)\left\{\frac{1}{1+\left(\bar{h}_2/\sqrt{3}\bar{\sigma}\right)^2 d^2}\right\} + \left(-6\sqrt{3}m\bar{\sigma}\right)\left\{\frac{G}{d^2+\left(\sqrt{3}\bar{\sigma}/\bar{h}_2\right)^2}\right\}\right] + \frac{1}{d}$$

In turn, giving

$$\bar{\tau} = \left(\frac{\bar{h}_2^3\bar{L}}{\bar{\sigma}^2}\right)\left\langle\frac{d}{1+\left(\bar{h}_2/\sqrt{3}\bar{\sigma}\right)^2 d^2}\right\rangle - \left(3\sqrt{3}m\bar{\sigma}\bar{L}\right)\left\langle\frac{dG}{d^2+\left(\sqrt{3}\bar{\sigma}/\bar{h}_2\right)^2}\right\rangle + \frac{1}{d}$$

Consequently the non-dimensional frictional force is obtained as

$$\bar{F} = \left(\frac{3\bar{h}_2\bar{L}}{2m}\right)\ln\left\{\frac{1+(1+m)^2\left(\bar{h}_2/\sqrt{3}\bar{\sigma}\right)^2}{1+\left(\bar{h}_2/\sqrt{3}\bar{\sigma}\right)^2}\right\} + \left(\frac{3\sqrt{3}\bar{\sigma}G\bar{L}}{2}\right)\ln\left\{\frac{1+\left(\sqrt{3}\bar{\sigma}/\bar{h}_2\right)^2}{(1+m)^2+\left(\sqrt{3}\bar{\sigma}/\bar{h}_2\right)^2}\right\} + \frac{1}{m}\ln(1+m)$$

… … … … … … … (5)

Results and discussion

The pressure distribution of the bearing system is determined by equation (2) while equation (3) presents the variation of load carrying capacity. The friction at the runner plate is calculated from the equation (4) while equation (5) gives friction at the bearing surfaces. Thus these above performance characteristics depend on various parameters such as s, m and h2. Taking, standard deviation to be zero this study reduces to the performance of an infinitely long slider bearing.

It is observed from Figure 2 that the effect of standard deviation is significantly adverse. It is noticed that the aspect ratio has significantly positive effect in the sense that the load carrying capacity increases and friction decreases at the bearing surfaces and the runner plate with increasing value of the aspect ratio which can be seen respectively from Figure 3, 4 and 5.

Further the ratio of the outlet film thickness to bearing system which is manifest in Figures 6 and 7.

Some of the Figures make it clear that the adverse effect of standard deviation can be minimized up to a considerable extent by choosing proper combination of the aspect ratio and the ratio of the outlet film thickness to the length of the bearing. Hence this investigation makes it mandatory to account for roughness while designing this bearing system.

REFERENCE

[1]Lord Rayleigh (1918), "Notes on the theory of lubrication", Philosophical Magazino. And Journal of Science, Vol. 53, p.p.1-12.

[2]Boegli, C. P. (1947), "Hydrodynamic lubrication of finite slider", Journal of Applied Physics, Vol. 18, p.p. 482.

[3]Purday, H. P. F. (1949), Streamline Flow, Constable, London.

[4]Archibald F. R. (1950), "A simple hydrodynamic thrust bearing", ASME Vol. 72, p.p.393.

[5]Charnes A. and Seibel E. (1952), "On the solution of the Reynolds' equation for slider bearing lubrication- Part1", ASME Vol. 74, p.p.867.

[6]Archibald F. R. (1956), "Load capacity and time relations for squeeze films", Jour. Basic Engg. Trans. ASME. Sear D 78, p.p. 231-245.

[7]Pinkus O. and Sternlitcht B. (1961), "Theory of hydrodynamic lubrication", McGraw Hill Book Company, New York.

[8]Cameron A (1966), "Principles of lubrication", Longmans, London.

[9]Tzeng S. T. and Seibel E. (1967.a), "Surface roughness effect on slider bearing lubrication", Trans. ASME, J. Lub. Tech., 10, p.p. 334-338.

[10]Christensen,H.and Tonder,K.C. (1969.a), "Tribology of rough surfaces: Stochastic models of hydrodynamic lubrication". SINTEF report no. 10/69 – 18.

[11]Christensen, H. and Tonder, K.C. (1969.b), "Tribology of rough surfaces: Parametric study and comparison of lubrication models". SINTEF report no. 22/69 -18.

[12]Christensen, H. and Tonder, K.C.(1970), "The hydrodynamic lubrication of rough bearing surfaces of finite width". ASME-ASLE Lubrication conference, Cincinnati, Ohio, paper no. 70-Lub-7.

[13]Prakash J. and Vij S. K. (1973), "Hydrodynamic lubrication of a porous slider", J. Mech. Engg. Sc., 15, p.p. 232-234.

[14]Ting, L.L.(1975), "Engagement behavior of lubricated porous annular disks. Part 1: Squeeze film phase, surface roughness and elastic deformation effects". Wear, 34, p.p. 159-182.

[15]Gross. W. A., Matsch Lee A., Castelli V., Eshel A., Vohr J. H. and Wildmann M. (1980), "Fluid film lubrication", A Wiley-Interscience Publication, John Wiley and Sons, NewYork.

[16]Patel, K.C. and Gupta, J. L. (1983), "Hydrodynamic Lubrication of a porous slider bearing with slip velocity", WEAR, 85, p.p. 309-317.

[17]Prakash, J. and Tiwari, K., Roughness effects in porous circular squeeze plates with arbitrary wall thickness. Lubr. Technol., (1983), 105, p.p. 90-95.

[18]Prajapati, B.L.(1991), "Behavior of squeeze film between rotating porous circular plates: surface roughness and elastic deformation". Pure Appl. Math. Sci.,33(1-2), p.p. 27-36.

[19]Guha, S.K. (1993), "Analysis of dynamic characteristic of hydrodynamic journal bearings with isotropic roughness effects". Wear, 167, p.p. 173-179.

[20]Gupta, J.L. and Deheri, G.M. (1996), "Effect of roughness on the behavior of squeeze film in a spherical bearing", Tribology Transactions, 39, p.p. 99-102.

[21]Andharia, P.I., Gupta, J.L. and Deheri, G.M. (1997), "Effect of longitudinal surface roughness on hydrodynamic lubrication of slider bearings". In Proceedings of Tenth International Conference on Surface modification Technologies, The Institute of Materials, p.p. 872-880.

[22]Andharia, P.I., Gupta, J.L. and Deheri, G.M.(2001), " Effect of surface roughness and hydrodynamic lubrications of slider bearings", Tribology Transaction, 44, No.2, p.p. 291-297.

[23]Basu S. K., Sengupta S. N. and Ahuja B.B. (2005), "Fundamentals of Tribology", Prentice-Hall of India Private Limited, New Delhi.

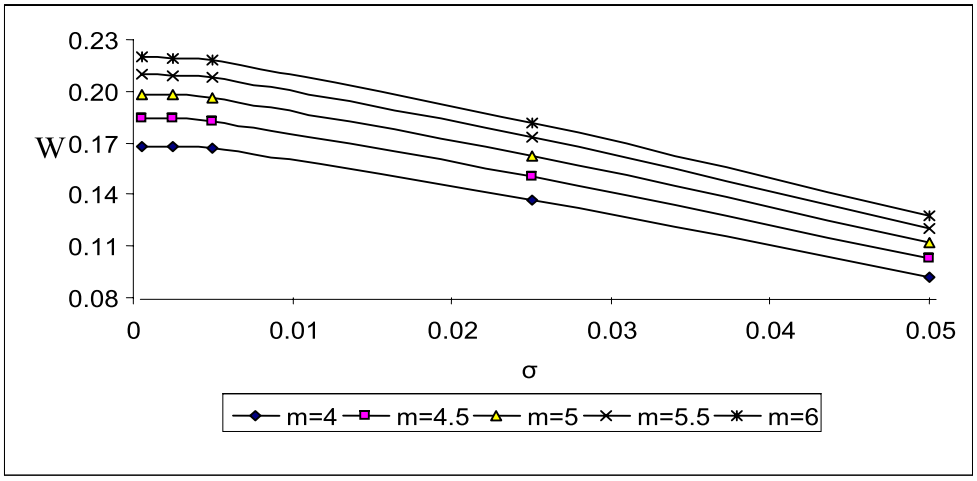

Figure 2: Load carrying capacity with respect to σ and m

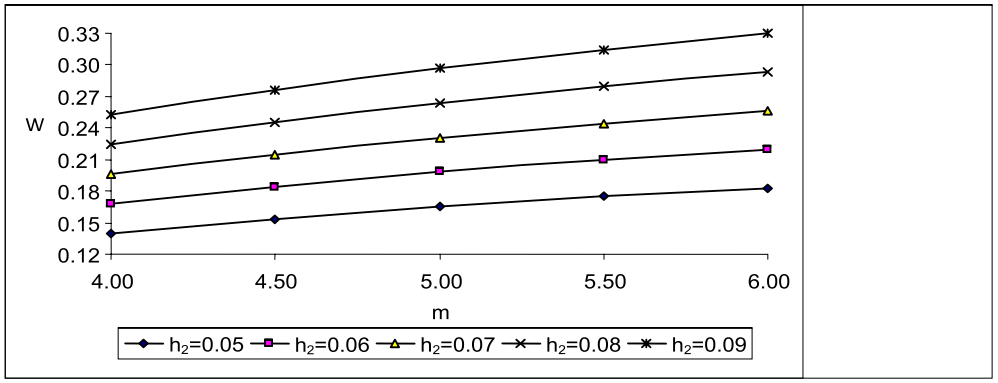

Figure 3: Load carrying capacity with respect to m and h_2

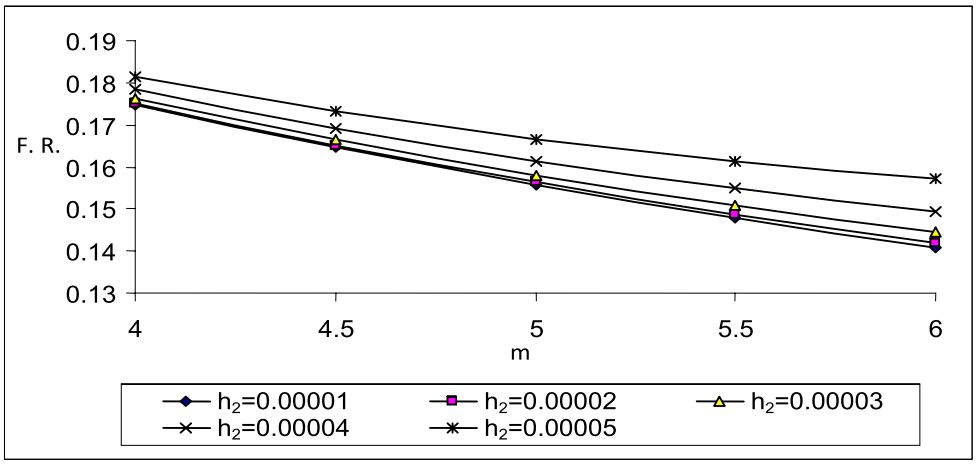

Figure 4: Friction at runner plate with respect to m and h_2

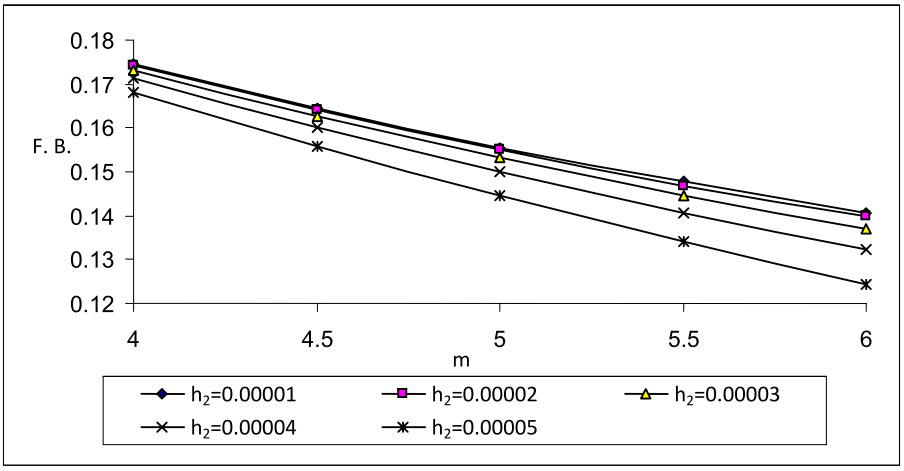

Figure 5: Friction at bearing plate with respect to m and h_2

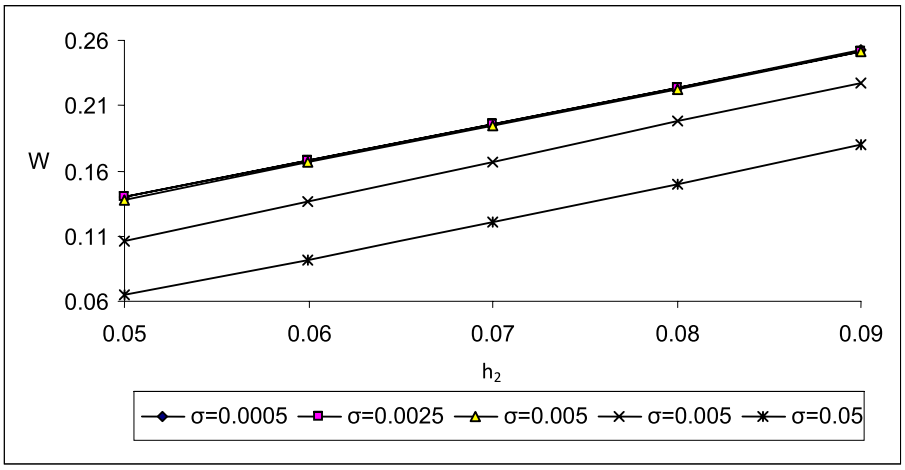

Figure 6: Load carrying capacity with respect to h_2 and σ

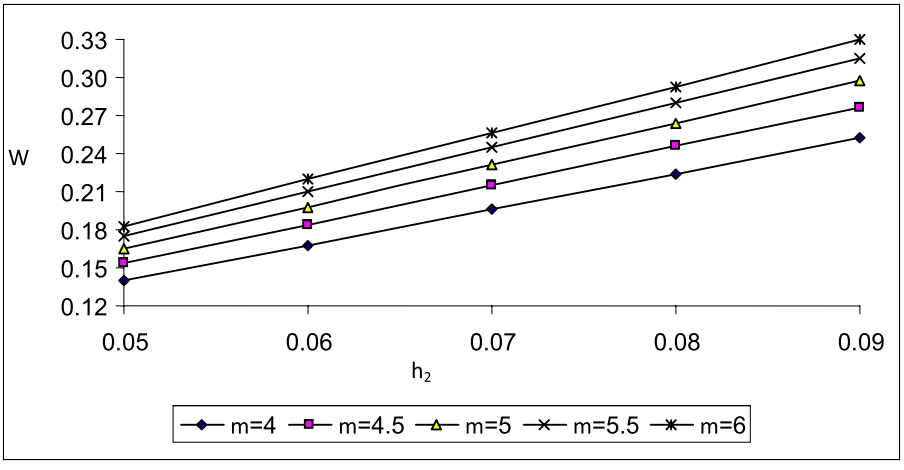

Figure 7: Load carrying capacity with respect to h_2 and m

A COMPARATIVE ANALYSIS OF TRAVELLING SALESMAN PROBLEMS USING NON-DOMINATED SORTING GENETIC ALGORITHM AND NICHED PARETO GENETIC ALGORITHM METHODS

Kinjal U. Adhvaryu
Assistant Professor
Department of Computer Engineering,
Ahmedabad Institute of Technology
Ahmedabad

ABSTRACT

Evolutionary algorithms (EAs) are often well suited for optimization problems involving several coupled parameters objectives. Since 1985, various evolutionary approaches to multiobjective optimization have been developed, capable of searching for multiple solutions in a single iteration. These methods differ in the fitness assignment function obtained, however the decision to which method is best suited for a given problem depends mainly upon the nature of problem and its complexity. As most of the real time applications utilize the multiobjective EAs which makes multiobjective EA as a technique for different applications. Here in this paper, this paper utilize two multiobjective EAs and compared the results for the multiobjective Traveling Salesman Problem (MOTSP). And concluded that NPGA algorithm is comparatively best suited for any TSP type transportation applications.

Keywords: Genetic algorithms, search, optimization, optimal control, stochastic process, multimodal problems, multiobjective problems.

INTRODUCTION

The Traveling Salesman Problem (TSP) is one which has commanded much attention of mathematicians and computer scientists specifically because it is so easy to describe and so difficult to solve. The problem can simply be stated as: if a traveling salesman wishes to visit exactly once each of a list of m cities and then return to the home city, what is the least costly tour the traveling salesman can take? And the Multi-objective traveling salesman problem (MOTSP) is one in which a traveling salesman wishes to visit exactly once each of a list of m cities and then return to the home city but with more than one constraint like minimize distance, cost, time or increase touring attractiveness etc.

Here the problem is symmetric multi-objective traveling salesman problem.

Much of the work on the MOTSP is not motivated by direct applications, but rather by the fact that the MOTSP provides an ideal platform for the study of general methods that can be applied to a wide range of discrete optimization problems. This is not to say, however, that the MOTSP does not find applications in many fields. Indeed, the numerous direct applications of the MOTSP bring life to the research area and help to direct future work Different multi-objective genetic algorithm methods

[2] Have been proposed by the researchers and have been used for multi-objective optimization for number of years. Yet, in general, no method is superior to all others in all the

performance aspects. Different methods have their advantages and disadvantages. But still there is a scope for finding out which method is appropriate for particular Multi-objective Traveling Salesman Problem. A comparative analysis of these methods is a new research area. The methods are mainly compared on the basis of diversity of solutions and closeness to the Pareto front. This paper takes up two different multi-objective genetic algorithms and compares their performance by applying them to a Multi-objective Traveling Salesman problem. Hence, the name of the project appeared as "A Comparative Analysis of Traveling Salesman Problems using Non-dominated Sorting Genetic Algorithm and Niched Pareto Genetic Algorithm Methods".

GENETIC ALGORITHM

Since the idea of genetic algorithms was introduced by John Holland in the early 1970's. GAs has been applied to a lot of optimization problems. Search and optimization techniques can be categorized into three classes: calculus based, enumerative, and random. Calculus based approaches usually require the existence of derivatives and the continuity. Therefore it is difficult to apply them to realistic problems where these assumptions often do not hold. Enumerative methods are straightforward search schemes. They can be applied to optimization problems when the number of feasible solutions is small. Most optimization problems in the real world, however, have countless possible solutions. Therefore they cannot be applied to such complex problems. As for random searches, while they search in solution spaces without any kind of information, it may not be efficient.

Therefore the search direction should be specified in order to improve their search ability. GAs is one of random searches because they use a random choice as a tool in there searching process.

While a random choice performs an important role in GAs, the environment directs the search in GAs. That is, they utilize information from the environment in their searching process.

Differences between Genetic Algorithms and Traditional Methods The Genetic Algorithms differ with traditional methods in the following ways:

1. Genetic algorithms work with a coded form of the function values (parameter set), rather than with the actual values themselves.
2. Genetic algorithms use a set, or population, of points to conduct a search, not just a single point on the problem space. This gives Genetic Algorithms the power to search noisy spaces littered with local optimum points. Instead of relying on a single point to search through the space, the Genetic Algorithms looks at many different areas of the problem space at once, and uses all of this information to guide it.
3. Genetic Algorithms use only payoff information to guide themselves through the problem space. Many search techniques need a variety of information to guide them. The only information a Genetic Algorithm needs is some measure of fitness about a point in the space. Once the Genetic Algorithm knows the current measure of "goodness" about a point, it can use this to continue searching for the optimum.
4. Genetic Algorithms are probabilistic in nature, not deterministic. This is a direct result of the randomization techniques used by Genetic Algorithms.
5. Genetic Algorithms are inherently parallel. Here lies one of the most powerful features of genetic algorithms. Genetic Algorithms, by their nature, are very parallel, dealing with a large number of points (strings) simultaneously.

MULTI-OBJECTIVE OPTIMIZATION PROBLEMS

Besides having multiple objectives, there are a number of fundamental differences between single-objective and multi-objective optimization as follows:

1) Two goals instead of one
2) Dealing with two search spaces
3) No artificial fix-ups

A striking difference between a classical search and optimization method [2, 3] and a Genetic Algorithm is that in the latter a population of solutions is processed in each iteration (or generation). This feature alone gives Genetic Algorithms a tremendous advantage for its use in solving multi-objective optimization problems. Recall that one of the goals of an ideal multi-objective optimization procedure is to find as many Pareto-optimal solutions as possible. Since a Genetic Algorithm works with a population of solutions, in theory we should be able to make some changes to the basic Genetic Algorithm so that a population of Pareto-optimal solutions can be captured in one single simulation run of a Genetic Algorithm. This is the powerful feature of Genetic Algorithms that makes them particularly suitable to solve multiobjective optimization problems. We don't need to perform a series of separate runs as in the case of the traditional mathematical programming techniques.

The first real implementation of a multi-objective genetic algorithm (vector Evaluated Genetic Algorithm, VEGA) was suggested by David Schaffer in 1984. The name VEGA is appropriate for multi-objective optimization, because his GA evaluated an objective vector (instead of a scalar objective function), with each element of the vector representing each objective function.

Although VEGA is simple to implement, it does not find diverse solutions in the population and converges to individual champion solutions only. Surprisingly, no significant study was performed for almost a decade after the pioneering work of Schaffer. Thereafter, several independent groups of researchers have developed different versions of multi-objective evolutionary algorithms [2, 3, 4]. Some of them are:-

i) Multi-objective GA (MOGA) by Fonseca and Fleming (1993)
ii) Non-dominated Sorting Genetic Algorithms (NSGA) by Srinivas and Deb (1994)
iii) Niched-Pareto Genetic Algorithm (NPGA) by Horn, Nafploitis and Goldberg (1994).

Non-dominated Sorting Genetic Algorithm (NSGA)

The Non-dominated Sorting Genetic Algorithm (NSGA) was proposed by Srinivas and Deb [4], and is based on several layers of classifications of the individuals. Before the selection is performed, the population is ranked on the basis of non-domination: all non-dominated individuals are classified into one category. Then this group of classified individuals is ignored and another layer of non-dominated individuals is considered. The process continues until all individuals in the population are classified. This classifies the population P into a number of mutually exclusive equivalent classes called non-dominated sets Pj:

$$P = \bigcup_{j=1}^{\rho} Pj$$

It is important to realize that any two members from the same class cannot be said to be better than one another with respect to all objectives.

The total number of classes (or fronts), denoted as ρ in the above equation, depends on the population P and the underlying problem.

NSGA Fitness Assignment

1. Choose sharing parameter σshare and a small positive number ε and initialize $F_{min} = N + \varepsilon$. Set front counter j = 1.
2. Classify population P according to non-domination to create non-dominated sets P1, P2, … , Pρ.
3. For each q Є Pj

a) Assign fitness $Fj^{(q)} = F_{min} - \varepsilon$.

b) Calculate niche count nc_q using above equation among solutions of P_j only.

c) Calculate shared fitness $Fj'^{(q)} = Fj^{(q)} / nc_q$.

4. $F_{min} = \min (Fj'^{(q)} : q \in P_j)$ and set j = j + 1.
5. If j ≤ ρ, go to step 3. Otherwise, the process is complete.

Niched Pareto Genetic Algorithm (NPGA)

Horn and Nafploitis proposed a tournament selection scheme based on Pareto dominance [2,4]. Instead of limiting the comparison to two individuals, a number of other individuals in the population were used to help determine dominance (typically around 10). When both competitors were either dominated or non-dominated (i.e., there was a tie), the result of the tournament was decided through fitness sharing. Population sizes considerably larger than usual with other approaches were used so that the emerging niches in the population could tolerate the noise of the selection method.

NPGA Tournament Selection Procedure

Arguments – i, j, Q.

Returns – winner

1. Pick a sub-population T_{ij} of size t_{dom} from the parent population P.
2. Find αi as the number of solutions in T_{ij} that dominated i. Calculate αj as the number of solutions in T_{ij} that dominates j.
3. If αi = 0 and αj > 0, then i is the winner. The process is complete.
4. Otherwise, if αi > 0 and αj = 0, then j is the winner. The process is complete.
5. Otherwise, if |Q|≤ 2, i or j is chosen as a winner with probability 0.5. The process is complete. Alternatively, the niche counts nci and nc_j are calculated by placing i and j in the current offspring population Q, independently. With the niching parameter σshare, nci is calculated as the number of offspring (k Є Q) within a σshare distance d_{ik} from i. The distance d_{ik} is the Euclidean distance between solutions i and k in the objective space.
6. If nci ≤ ncj, solution i is the winner. Otherwise, solution j is the winner.

NPGA Procedure

1. Shuffle P, set i = 1, and set Q = φ.
2. Perform the above tournament selection and find the first parent, p1 = NPGA-tournament (i, i + 1, Q).
3. Set i = i + 2 and find the second parent, p2 = NPGA-tournament (i, i + 1, Q).
4. Perform crossover with p1 and p2 and create offspring c1 and c2. Perform mutation on c1 and c2.
5. Update offspring population Q = Q U {c1, c2}.
6. Set i = i + 1. If i < N, go to step 2. Otherwise, if |Q| = N / 2, shuffle P, set I = 1, and go to step 2. Otherwise, the process is complete.

PERFORMANCE COMPARISON

In the following, the case study is described that has been carried out using the above four multiobjective EAs for solving an extended Multiobjective Traveling Salesman Problem. There are two distinct goals in multi-objective optimization:-

(1) discover solutions as close to the Pareto-optimal solutions as possible, and (2) find solutions as diverse as possible in the obtained non-dominated front. An MOEA will be termed a good MOEA, if both goals are satisfied adequately. For that Set Coverage Metric and Maximum Spread Metric are used.

Implementation Details

This work describes implementation of different instances of two different numbers of objectives for Traveling Salesman Problem. All the programs were coded in C. It uses Turbo C in DOS environment. This paper takes 4 instances of each 4 algorithms for bi-objective traveling salesman problem. Also 4 instances of each 4 algorithms for three-objective symmetric traveling salesman problem. In bi-objective TSP, the objectives are to minimize distance and cost. In three-objective TSP, the objectives are to minimize distance and cost and maximize touring attractiveness. I solve the problem for 10-cities, 25-cities, 50-cities and 60-cities.This analysis work contains total 32 graph for bi-objective and three-objective TSP. Apart from these results, the paper contains only 60-cities instance for three-objective TSP.

Simulation for 3-objective TSP

This paper uses the MOTSP with the problem-instances for 10-cities, 25-cities, 50-cities and 60-cities.This analysis work contains total 32 graph for bi-objective TSP and three-objective TSP. Apart from these results, the paper contains only 60-cities instance for three-objective TSP. Results are compared on the basis of performance metrics.

There are two distinct goals in multi-objective optimization: 1) Discover solutions as close to the pareto -optimal solutions as much as possible and 2) Find solutions as diverse as possible in the obtained non-dominated front. An MOEA will be termed a good MOEA, if both goals are satisfied adequately. Comparatively NPGA shows good results.

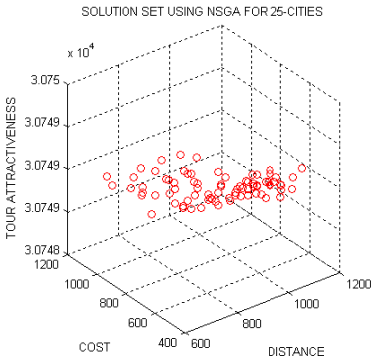

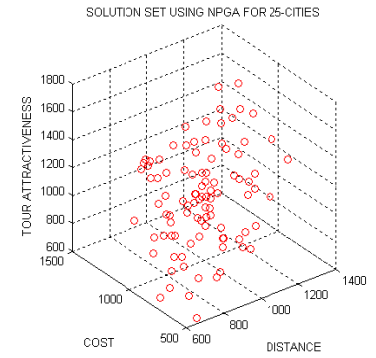

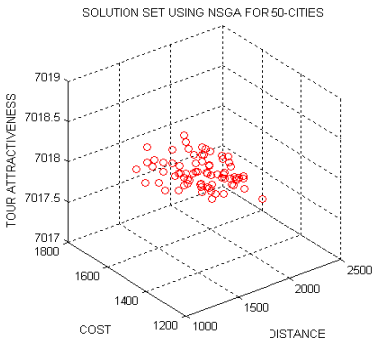

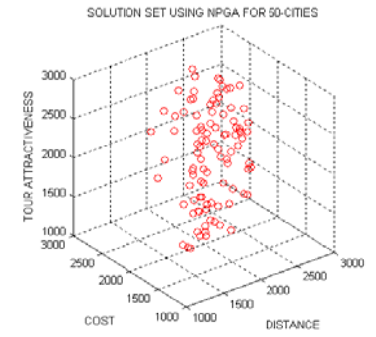

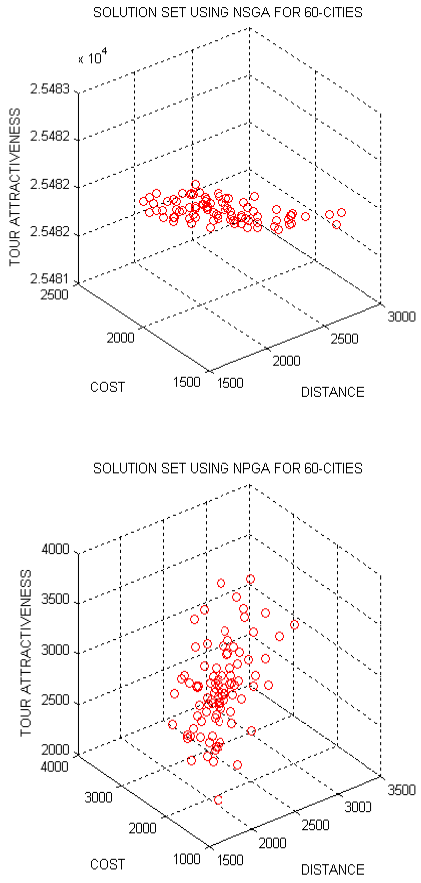

(Fig 4.1 3-objective TSP for 25,50, 60-cities instance)

CONCLUSIONS

Looking at the results of Average Set Coverage, NPGA and NSGA give the best results but from the results of Maximum Spread NPGA is best since it selects individuals by directly checking them for the non-domination compared to NSGA. Also, from solution sets, we can see that NPGA gives more solution sets compared to NSGA which is the most important parameter in deciding the performance of Evolutionary Algorithm. And also from different performance matric it is clear that there is no effect of no. of objectives on performance of NPGA and NSGA. From all above reasons we can say that NPGA is the best suitable algorithm compared to NSGA for Multi-objective traveling salesman problem.

REFERENCES

[1] Goldberg, D.E. (1989). Genetic Algorithms in Search, Optimization, and Machine Learning. Singapore: Pearson Education.

[2] Deb, K. (2002). Multi-objective Optimization using Evolutionary Algorithms. West Sussex: John Wiley and Sons, Ltd.

[3] Coello, Carlos A. and Christiansen, Alan D. An Approach to Multi-objective Optimization using Genetic Algorithms. Department of Computer Science, Tulane University, New Orleans, LA, USA.

[4] D. S. Johnson and L. A. McGeoch, The Traveling Salesman Problem: A Case Study in Local Optimization, Local Search in Combinatorial Optimization, E. H. L. Aarts and J.K. Lenstra (ed), John Wiley and Sons Ltd, 1997, pp 215-310.

[5] Chang Wook Ahn. Advances in Evolutionary Algorithms. Theory, Design and Practice, Springer, ISBN 3-540-31758-9, 2006

[6] Zitzler, E. and Thiele, L. An Evolutionary Algorithm for Multi-objective Optimization: The Strength Pareto Approach. Computer Engineering and Networks Laboratory, Swiss Federal Institute of Technology, Zurich, Switzerland.

[7] Ajith Abraham, Lakhmi Jain and Robert Goldberg (editors).Evolutionary Multiobjective Optimization. Theoretical Advances and Applications, Springer, USA, 2005, ISBN 1-85233-787-7

A SURVEY OF IMAGE REGISTRATION METHODS

Ms. Mehfuza Holia, Lecturer
Electronics Engineering Department
BVM Engineering College
Vallabh Vidyanagar, Gujarat

Dr. V. K. Thakar, Professor
ECE Department,
A.D.Patel Institute of Technology
New Vallabh Vidyanagar, Gujarat

ABSTRACT

This paper presents a preliminary survey of the image registration methods and algorithms as applied to various applications. Image registration is a critical and versatile step in the image processing which has not attracted as many researchers as other issues involved in image processing. In computer vision system sets of data acquired by sampling of the same scene or object at different times or from different perspectives, will be in different coordinate systems. Image registration is the process of transforming the different sets of data into one coordinate system. Registration is necessary in order to be able to compare or integrate the data obtained from different measurements such as different viewpoints, different times, different sensors etc. Image Registration is an important problem and a fundamental task in image processing technique. Hence, an attempt has been made in this paper to presents a survey of recent as well as classical image registration methods. The work is in progress to provide possible solutions to the existing problems. Intuitive comments are presented with each of the methods.

Introduction

Image registration is the process of spatially aligning two images of a scene (1 Reference and 2) sensed. Image Registration is a crucial step in all image analysis tasks in which the final information is gained from the combination of various data sources like in image fusion, change detection, and multi channel image restoration. The differences present there between images are introduced due to different imaging conditions, detection, and multi channel image restoration. One of the reasons that image registration is an extremely challenging problem is the large degree of variability of the input data. The images that are to be registered and mosaicked may contain visual information belonging to very different domains and can undergo many geometric and photometric distortions such as scaling, rotations, projective transformations, non rigid perturbations of the scene structure, temporal variations, and photometric changes due to different acquisition modalities and lighting conditions. All the innovative and significant contributions to the registration problem have found immediate application in many disparate areas such as remotely sensed image processing, medical image analysis, scene reconstruction, surveillance, image fusion, target recognition, target localization, depth perception, image mosaicing and Motion estimation .The outline of the paper is as follows. Section II presents image registration based on acquisition methods. Steps involved in image registration have been outline in section III. Section IV briefs about transport model estimation.

Image Registration Based on Acquisition Methods

Image registration can be divided into main four groups
according to the manner of image acquisition [8].

● **Different viewpoints**: Images of the same scene are acquired from different viewpoints.
Applications: Remote sensing, shape recovery
● **Different times**: Images of the same scene are acquired at different times, often on regular basis, and possibly under different conditions. Applications: automatic change detection for security monitoring, maps from satellite images, remote sensing, healing therapy in medicine, monitoring of the tumor growth, Growth of food products
●**Different sensors**: Images of the same scene are acquired by different sensors. The aim is to integrate of information obtained from different to gain detailed scene presentation.
Applications: offering better spatial resolution in Medical imaging for combination of sensors recording the anatomical body structure like magnetic resonance image (MRI), CCD image sensors, CMOS image sensors, Bayer sensor are different image sensors for better resolution.
● **Scene to model registration**: Images of a scene and a model of the scene are registered. The model can be a computer representation of the scene, for instance maps or digital elevation models (DEM), another scene with similar content (another patient).

The aim is to localize the acquired image in the scene/model and/or to compare them.

Applications: automatic quality inspection, comparison of the patient's image with digital anatomical Atlases, specimen classification.

Steps involved in Image Registration

Different modules for registration are Feature detection, Feature matching, Transform model estimation, Image re-sampling and transformation.

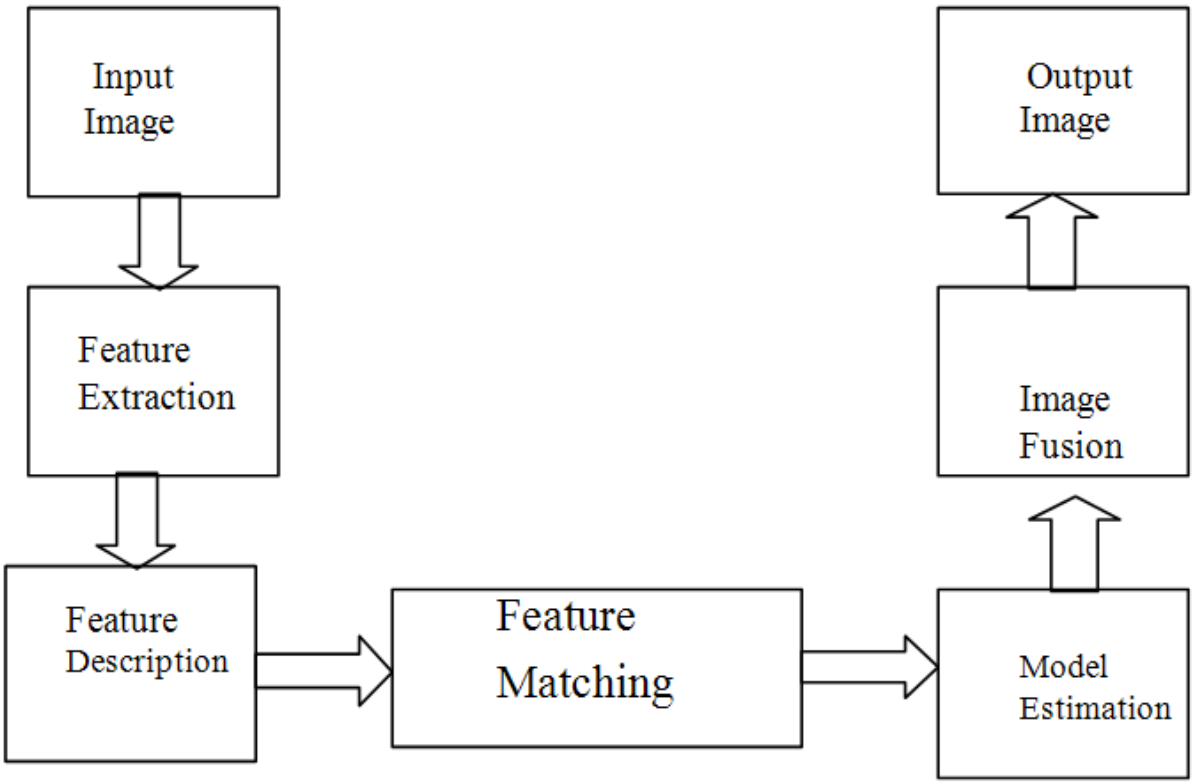

Fig .1 Steps involved in Image Registration

3.1 Feature Detection

Feature detection consists of feature extraction and feature description. Salient and distinctive objects (close boundary regions, edges, contours, line intersections, corners etc) are manually or preferably, automatically detected. For further processing, these features can be represented by their point representatives (centers of gravity, line endings, distinctive points), which are called control lines [8]. Following methods are available for the same as mentioned in the literature:

- **Area- based methods:** Area based methods put emphasis rather on the feature matching step than on their detection [22]

- **Feature-Based methods:** Significant regions (forests and fields), lines (region boundaries, coastlines (road, lakes, mountains, rivers) or points (region corners, line intersections, points or curves with high curvature) are features here. They should be distinct, spread all over the image and efficiently detectable. They are expected to be stable in time to stay at fixed positions during the whole experiment [22].

Region features can be detected by using segmentation methods. Methods proposed in [1], used refinement of the segmentation process to improve the registration quality. The segmentation of the image has been done iteratively together with the registration; in every iteration, the rough estimation of the object correspondence has been used to tune the segmentation parameters. It has been claimed there that the sub pixel accuracy of registration could be achieved using the proposed method.

Kamel et al [2] proposed the idea of virtual circles, using distance transform for selection of region features.

In this approach, the selections of features are invariant with respect to change of scale.

Line features can be the representation of general line segments, object contours, coastal lines, and roads. Standard edge detection methods have been proposed by Canny [3] and D.Marr et al [4] investigated method based on the Laplacian of Gaussian are employed for the line feature detection. D.Ziou et al [5] has given overview of edge detection techniques and also its evaluation in terms of merits and relationships between the wide variety of existing techniques and for assisting in the selection of the most suitable technique for a specific problem.

Point features-group consists of methods working with the intersections, road crossings, centroid of water regions, oil and gas pads, high variance points, local curvature discontinuities, inflection point of curves, local extrema of wavelet transform and corners. Corners are widely used as control points mainly because of their invariance to imaging geometry since they are well perceived by a human observer. In [6] it has been shown that localization properties of direct corner detectors can used for point feature detection. Z.Zheng [7] has provided analysis of gray level corner detection. Kitchen and Rosenfeld [10] proposed to exploit the second-order partial derivatives of the image function for corner detection. But this method is sensitive to noise. From a survey of image registration methods presented in [8] it was concluded that the use of feature based method is recommended if the image contain enough distinctive and easily detectable objects. This is usually the case of applications in remote sensing and computer vision. On the other hand, medical images are not so rich in such details and thus area based methods are used here.

So the, fusion of both the methods is a current research trends to come out with universal method for detection.

3.2 Feature Matching:

The detected features in the reference and sensed images can be matched by means of image intensity values in their close neighborhoods,
the feature spatial distribution or the feature symbolic description.

● Area based methods:

Area based methods are correlation like methods or template matching.

These methods deal with the images without attempting to detect salient objects. W.K.Pratt [9], has given correlation techniques of image registration. Windows of predefined size or even entire images are used for the correspondence estimation. Available area based methods are: correlation-like methods, Fourier methods, Mutual information methods and optimization methods**.**

● Correlation-like methods:

In Correlation-like methods, measure of similarity is computed for window pairs from the sensed and reference images and its maximum is searched. The window pairs for which the maximum is achieved are set as the corresponding ones. The cross-correlation (CC) based registration can also be successfully applied when slight rotation and scaling are present. S.kaneko and I.Murase [11] has given the extended CC methods based on increment sign correlation for the images/objects to be registered are partially occluded. Huttenlocher [13] proposed a method in which they registered binary images (the output of an edge detector) transformed by translation or translation plus rotation, by means of Hausdorff distance.

According to Pratt [9], two drawbacks of correlation like methods: the flatness of the similarity measure maxima and high computational complexity.

● Fourier methods:

They are preferred when acceleration of the computational speed is needed if the images were acquired under varying conditions or they are corrupted by frequency-dependent noise, then Fourier methods are preferred rather than the correlation like methods. They exploit the Fourier representation of the images in the frequency domain. R.N.Bracewell [12] has proposed the phase correlation method based on the Fourier Shift Theorem and was originally proposed for the registration of translated images. The method shows strong robustness against the correlated and frequency dependent noise and non-uniform, time varying illumination disturbances. The computational savings are more significant if the images, which are to be registered, are large. E.D. Castro, C.Morandi [13] introduced an extension of the phase correlation for additional rotation information.

● Mutual information methods

The mutual information (MI) has appeared recently and represents the leading technique in multimodal registration. Registration of multimodal images is the difficult task but often necessary to solve, especially in medical imaging. The MI, originating from the information theory, is a measure of statistical dependency between two data sets and it is particularly suitable for Registration of images from different modalities. P.Viola, W.M.Wells [14] describes the application of MI for the matching to the real scene. Thevenaz and Unser [15] tried to combine various approaches, solving individual steps of MI registration.

The relation of MI to other area based similarity (correlation coefficients, correlation ratio) is given by A.Roche, G.Malalndain [16] using the formulation of maximum likelihood estimation problem.

● Optimization methods

Finding the minimum of dissimilarity measure or the maximum of similarity measure is a multidimensional optimization problem, where the number of dimensions corresponds to the degrees of freedom of the expected geometrical transformation. The only method yielding global extreme solution is an exhaustive search over the entire image. Although it is computationally demanding, it is often used if only translations are to be estimated. In case of transformation with more degrees of freedom or in case of more complex similarity measures, sophisticated optimization algorithms are required, which help to localize the maxima or minima, respectively. R.Sharma and M.Pavel [17] has given the application of Gauss-Newton numerical minimization algorithm for minimizing the sum of squared differences, where the projective geometric deformation has been used.

● Feature–Based Methods

Two sets of features in the reference and sensed images represented by the CPs (points themselves, end points or centers of line features and centers of gravity of regions) have been detected. The aim is to find the pair wise correspondence between them using their spatial relations or various descriptors of features.

● Methods using spatial relations

Methods based primarily on the spatial relations among the features are usually applied if detected features are ambiguous or if their neighborhoods are locally distorted. A.Goshtasby et al [18] described the registration method based on the graph matching algorithm.

He was evaluating the number of features in the sensed image that after the particular transformation, fall within a given range next to the features in the reference image. The transformation parameters with the highest score were then set as a valid estimate

- **Methods using invariant descriptors:**

Here the correspondence of features can be estimated using their description; preferably invariant to the expected image deformation the description should fulfill several conditions. The most important ones are invariance (the descriptions of the corresponding features from the reference and sensed image have to be the same), uniqueness (two different features should have different descriptions), stability (the description of a feature which is slightly deformed in an unknown manner should be close to the description of the original feature), and independence (if the feature description is a vector, its elements should be functionally independent). However, usually not all these conditions have to (or can) be satisfied simultaneously and it is necessary to find an appropriate trade-off.

- **Relaxation methods**

A large group of the registration methods is based on the relaxation approach, as one of the solutions to the consistent labeling problem (CLP): to label each feature from the sensed image with the label of a feature from the reference image, so it is consistent with the labeling given to the other feature pairs. The process of recalculating the pair figures of merit, considering the match quality of the feature pairs and of matching their neighbors, is iteratively repeated until a stable situation is reached. S.Ranade and A.Rosenfiel proposed point pattern matching by relaxation pattern recognition.[19]

4. Transform Model estimation

Once the feature correspondence has been established the mapping function is generally constructed. It is expected to transform the sensed image to overlay it over reference one.

The correspondence of the CPs from the sensed and reference images together with the fact that corresponding CP pairs should be as close as possible after the sensed image transformation are employed in the mapping function region. The task to be completed consists of choosing the type of the mapping function and its parameter estimation.

The type of the mapping function should correspond to the assumed geometric deformation of the sensed Image, to the method of image acquisition (e.g. scanner dependent distortions and errors) and to the required accuracy of the registration [8]. For transform model estimation available models are global mapping models, local mapping models, mapping highest score were then set as a valid estimate. In [20] use of radial basis function for image rectification has been demonstrated.

5. Image Resampling and Transformation

The mapping functions constructed during the previous step are used to transform the sensed image and thus to register the images. The transformation can be realized in a Forward or backward manner. Each pixel from the sensed image can be directly transformed using the estimated mapping functions. This approach, called a forward method, is complicated to implement, as it can produce holes and/or overlaps in the output image (due to the discretization and rounding). Hence, the backward approach is usually chosen. The registered image data from the sensed image are determined using the coordinates of the target pixel (the

same coordinate system as of the reference image) and the inverse of the estimated mapping function. The image interpolation takes place in the sensed image on the regular grid. In this way neither holes nor overlaps can occur in the output image.

A detailed investigation and comparison of resampling techniques was carried out by J.A.Parker [21]. He has given comparisons of interpolating methods for image resampling.

6. Conclusion and Future Work

The paper has outlined basics of image registration with brief survey of the methods and algorithms available in the literature. It has been pointed out that the there are potential open problem in the fusion of feature based and area based methods with a common method of registration of an image. It can be also intuitively commented that with rotating image acquisition device and spatial data be located in memory in three dimensional with correlation amongst coordinates image registration may be successfully done for the majority of the images. Additionally by adjusting thresholds in adaptive manner may take care of illumination with high resolution devices for acquisition for image registration. Various optimizing algorithms can explored for representative images from the image database of interest. Investigations are going on for programmable logic devices based and system on chip based algorithm implementations for segmentation, edge detection and feature based methods for speed, configurability and portability related issues.

References:

[1] A. Goshtasby, G.C. Stockman, C.V. Page, “A region-based approach to digital image registration with sub pixel accuracy”, IEEE Transactions on Geoscience and RemoteSensing 24 (1986) 390-399.

[2] H.S. Alhichri, M. Kamel, “Virtual circles: a new set of features for fast image registration”, Pattern Recognition Letters 24 (2003) 1181-1190.

[3] J. Canny, “A computational approach to edge detection”, IEEE Transactions on Pattern Analysis and Machine Intelligence 8 (1986) 678-698.

[4] D. Marr, E. Hildreth, “Theory of edge detection, Proceedings of the Royal Society of London”, B 207 (1980) 187-217.

[5] Ziou . S. and Tabbone,“Edge detection techniques-an overview ”//citeseer.nj.nec.com/ziou97edge.html, 1997.

[6] K. Rohr, “Localization properties of direct corner detectors”, Journal of Mathematical Imaging and Vision 4 (1994) 139-150.

[7] Z. Zheng, H. Wang, E.K. Teoh, “Analysis of gray level corner detection”, Pattern Recognition Letters 20 (1999) 149-162.

[8] Barbara Zitova and Jan Flusser “Image registration methods: A survey ”. Department of Image Processing, Institute of Information Theory and Automation, Academy of Sciences of the Czech Republic, Image and vision computing 21(2003) 977-1000.

[9] W.K. Pratt, Correlation techniques of image registration, IEEE Transactions on Aerospace and Electronic Systems 10 (1974) 353-358.

[10] L. Kitchen, A. Rosenfeld, Gray-level corner detection, Pattern Recognition Letters 1 (1982) 95-102.

[11] S. Kaneko, I. Murase, S. Igarashi, Robust image registration by increment sign correlation, Pattern Recognition 35 (2002) 2223-2234.

[12] R.N. Bracewell, the Fourier Transform and Its Applications, McGraw-Hill, New York, 1965.

[13] E.D. Castro, C. Morandi, “Registration of translated and rotated images using finite Fourier transform”, IEEE Transactions on Pattern Analysis and Machine Intelligence 9(1987) 700–703.

[14] P.Viola, W.M.Wells, Alignment by maximization of mutual information, International Journal of Computer Vision 24 (1997) 137-154.

[15] P.The´venaz, M. Unser, “An efficient mutual information optimizer for multi resolution image registration”, Proceedings of the IEEE International Conference onImage Processing ICIP’98, Chicago, IL, 2000 833-837.

[16] A. Roche, G. Malandain, N. Ayache, Unifying maximum likelihood approaches in medical image registration, International Journal of Imaging Systems and Technology 11(2000) 71-80.

[17] R.K. Sharma, M. Pavel, Multisensor image registration, Proceedings of the Societyfor Information Display XXVIII (1997) 39-52.

[18] A. Goshtasby, G.C. Stockman, Point pattern matching using convex hull edges,IEEE Transactions on Systems, Man and Cybernetics (1985), 631-637.

[19] S. Ranade, A. Rosenfeld, Point pattern matching by relaxation, Pattern Recognition12 (1980) 269-275.

[20] D.N. Fogel, Image rectification with radial basis functions: Application to RS/GISdata integration, Proceedings of the Third International Conference on Integrating GISand Environmental Modeling, CDROM, Santa Fe, New Mexico, 1996, 19 pp.

[21] J.A. Parker, R.V. Kenyon, D.E. Troxel, Comparison of interpolating methods for image resampling, IEEE Transactions on Medical Imaging 2 (1983) 31–39

[22] Object Recognition, Fundamentals and Case studies, M.Bennamoun and G.J.Mamic Advance in Pattern Recognition. Springer publication.

EXTENT OF HAZARDS OF HAZARDOUS WASTE

Dr. K. N. Sheth
Director
Gandhinagar Institute of Technology
Moti Bhoyan, Gandhinagar

Jalpa Patel
P.G. student of Environmental Science
ISTAR, Vallabh Vidya Nagar, (Gujarat)

ABSTRACT

In the present study an attempt has been made to evaluate the hazards of the waste sludge produced by Common Effluent Treatment Plant managed by Environ Infrastructure Co. Ltd., Baroda (EICL, Umraya). The investigation has been made based on the characterization studies of effluent including metal analysis and sludge generated from equalization tank, primary settling tank and aeration tank. The results show that the quality of treated effluent does not show any characteristics of the hazardous waste. The primary sludge as well biological sludge is also free from any toxicity, reactivity, corrosivity or ignitibility. In accordance with the hazardous waste management handling rules – 1989, (amended upto 2003). The sludge generated by EICL cannot be termed as hazardous in its legal perspective. The GPCB considers waste of the sludge generated by CETP as hazardous (Category – 12). However, this is not true in this case.

Keywords: Hazardous, CETP, pH, Toxicity, Corrosivity, Reactivity, Ignitability

INTRODUCTION

The handling and disposal of hazardous chemicals from the moment of manufacture to their ultimate disposal has become great matter of environmental concern. This is because hazardous waste cause health effects by entering into body through inhalation or skin absorption or puncture wounds. The temporary effects include dizziness, headache and nausea and the permanent effects such as cancer disability and death. These effects may be evident immediately or they may not be apparent for months together or even years. The impact on health is also dependent on the amount and duration of hazardous waste exposure.[1] Hazardous waste includes those wastes that are ignitable, such as solvents, and can cause fires; corrosive, such as acids and can corrode metals drums; reactive, which are unstable and cause explosions; and toxic, which are harmful or fatal when ingested or absorbed.[2]

In accordance with the 'Hazardous Waste Management Handling Rules', 1989 (and amended from time to time latest by 2003), Waste category no.18 specifies that sludges arising from treatment wastewater containing heavy metals, oils and emulsions and spent chemicals and incineration ash irrespective of any quantity is hazardous.[3]

In order to confirm whether the waste is hazardous there is a procedure laid down by Resource Conservation Recovery Act (RCRA). In a case of Common Effluent Treatment Plant (CETP) the sludges generated are considered under category 12 and therefore they are referred as, "Hazardous". The sludges from the CETP is not specifically included in 40 CFR 261.[4]

The next step is to determine whether the waste is listed under F,P,K,& U series.[5] The sludges from CETP are not specifically listed under any series.

The solution, therefore, lies in determining whether the waste exhibits the properties of ignitability, corrosivity, reactivity or toxicity. In a common effluent treatment plant, the knowledge of the materials used or processes employed may not help in concluding whether the waste is hazardous. Thus the testing of the sludge is the only alternative left for the investigators. The testing has to be carried out in accordance with the specified methods. As usual the waste generated by EICL managed CETP is considered hazardous as a part of waste category 12.

An attempt is proposed to be made to investigate the extent of hazards of so called hazardous waste. This, therefore starts the investigation right from influent to the sludges for various characteristics of hazardous waste i.e. the characterization studies has to be both for effluent as well as primary and secondary sludge. It is the testing protocol which may help determining as to whether so called hazardous waste is really hazardous.

MATERIALS AND METHODS

The prime objective of the present study is to evaluate the hazards of the waste-sludge produced by Common Effluent Treatment Plant of EICL, Umaraya. The samples were collected every 15 days constantly for 3 times for sludge analysis and for 2 times for Effluent analyses. The details showing the number of samples collected date, time and such other details have been reported in Table 1. The samples taken were discrete samples and as they were collected without regard to any time as well as flow. In order to study the basic characteristics of wastewater, physico chemical sludge and the biological sludge grab samples may yield sufficient results. Composites samples were not required as the aim is not to design the sludge treatment facilities.

To study broadly the variation in the characteristics of the samples grab samples would suffice. The material used for collection of samples was inert in nature and were not capable of making any reaction with the material of sample. So, far as preservation is concerned the samples were brought to laboratory and immediately stored in the refrigerator. The analysis of the effluent was carried out in Environmental Engineering Lab of BVM Engineering College, Vallabh Vidyanagar whereas its metal analysis was carried out using Inductive Plasma (ICP) Technique of SICART, Vallabh Vidyanagar. The flash point test for physico chemical as well as biological sludge was carried out in Industrial Chemistry Lab, ISTAR, Vallabh Vidyanagar.

The methods for determination of various parameters for the effluent was strictly as directed in “Standard Methods for Water and Wastewater Examination”. The analyses of the samples collected on 10th February, 2004 have been reported in this paper.

Results and Discussion

There are 3 general classes of RCRA waste that are defined as hazardous.

- **Characteristic wastes.**[7]
  Characteristic wastes exhibit the characteristics of corrosivity, reactivity, ignitability and toxicity codes D001 to D0043.

- **Listed wastes**[8]
  Listed wastes are hazardous waste stream from specific and nonspecific sources listed under codes F, K, P and U.

- **Hazardous debris**[6]
  The same classes are also considered hazardous by GPCB.

Normally for determining whether a waste stream exhibit toxicity characteristic is an

important criteria to determine whether waste is hazardous under RCRA.

Toxicity characteristics leaching procedure for 24 organic compound, 6 pesticides, 2 herbicides and 8 metals are described both by RCRA as well as Hazardous Waste Management Handling Rules, 1989.

In the present study there is no possibility of organic compound, pesticides, and herbicides as the wastewater reaching to treatment plant is either from the dyes and intermediates or pharmaceuticals. Metal analysis both from the effluent as well as sludge have been analysed through Inductive Couple Plasma (ICP) and have been reported in Table – 2.

The pH which may give rise to corrosivity has also been analysed both for effluent and sludge. The waste oil and grease has been measured both for effluent as well as sludge and interestingly they get reduced during the treatment to the acceptable limits.

The results have been reported in Table – 3

The analysis shows the presence of refractory organics which may or may not be hazardous. The pH of the effluent right from equalization tank to final outlet remains within the limit.

The oil and grease in equalization tank is 26.18 mg/L which stagewise reduces and final reaches to 7.72 mg/L in the final outlet which is within the limit. The VOC and oil & grease are almost removed during aeration.

The Chemical Oxygen Demand (COD), Biological Oxygen Demand (BOD) and Total Organic Carbon (TOC) are getting reduced stage wise and the final values are found to be within limit. The BOD and COD are formed to be almost nearly same i.e. BOD from 580 mg/L reduces to 90 mg/L whereas TOC 551 mg/L reduces to 63 mg/L.

The final COD value is 176 mg/L it therefore shows the presence of some refractory organics.

As evident from Table – 4 the sludge samples have been carried out from equalization tank, primary treatment and biological treatment. The pH of equalization sludge, primary sludge and biological sludge are 7.6, 8.3 and 7.9 respectively.

It is crystal clear that it does not show any corrosivity because the pH is neither below 2 nor above 12.5. From Table – 4 it is also clear that the value of TOC of influent sludge which is 163 mg/L. The TOC of primary sludge is 217 mg/L whereas of biological sludge is 1162 mg/L.

This shows that the TOC increases in the sludge of the secondary clarifier due to presence of microbial cells. In order to dispose the sludge to the landfill site the TOC value must be < 5%. The present sludge therefore can be disposed off in landfill site. So far as metal content is concerned they are in negligible amount. It can be considered as 'nil' as they are present in extremely low quantity. The Table – 5 exhibits the concentration sludge tank, primary sludge and biological sludge. Arsenic, Selenium, Cadmium, Mercury are absolutely absent. The trace amount of the metals have been analysed in ICP. It would have been impossible to analyse by any other means as they are in extremely low concentration. EPA methods used for Inductive Coupled Argon as a source of the excitation to produce emission spectra of metals and metal alloys.[2]

A confirmatory test both for primary sludge as well as biological sludge were carried out. Results have been reported in Table – 6. The number of samples analysed were 9. However, the entire test shows negative results. To retreat following aspects may be noted.

a. pH of 10% solution is found to be between 7.3 to 7.89 i.e. 5.5 to 12.
b. TOC has been found to be always < 5%.

c. During ignitability test, the sludge samples never getting ignited when exposed to open flame. The flash point of the ignited waste to be hazardous should be < 60^0 C. However, the flash point of present sludge is found to be > 200^0 C. It has been found that the different samples of sludge are not capable of causing fire under temperature and pressure existing in room.
d. The sludge samples were not found to be odorous.
   During the experimentation it is observed that the sludge has not shown any reaction with water. The sludges are stable, as they also don't from any gas or fume during reaction.

SUMMARY OF CONCLUSIONS

In light of results obtained and the inferences drawn, following conclusions can be made:

1. The quality of the treated effluent doesn't show any characteristics of the hazardous waste.
2. The primary sludge also doesn't exhibit any characteristic of hazardous waste.
3. The biological sludge is also free from any toxicity, reactivity, corrosivity or ignitability.
4. In accordance with the Hazardous Waste Management Handling Rules 1989 (and amended up to 2003), the sludge generated by EICL can't be termed as hazardous. The sludge therefore can be returned as solid waste which is not strictly hazardous in its legal perspective.
5. The GPCB considers all the waste of the sludge generated by CETP as hazardous (category 12). However, it is not true for all the cases. It is beyond doubt that EICL sludge can't be said as hazardous under RCRA legislation or Hazardous Waste Management Handling Rules, 1989 under Environment Protection Act (EPA), 1986.

REFERENCES

1. Jeanne Mager stellman, "Encyclopedia of occupational Health & safety ", 4th edition, Vol – II, labour office Geneva. PP – 53.12 -53.14
2. EMMA P. POPEK, "Sampling & Analysis of Environmental Chemical Pollutants", Academic Press
3. Charles A. Wentz, "Hazardous Waste Management", 2nd Edition, McGraw-Hill, Inc., PP – 96-102.
4. Michael D. Cagregs, Philip C. Buekingham, Jeffrey C. Evans & Environmental Resource Management, "Hazardous Waste Management", 2nd Edition, McGraw-Hill International Edition, PP – 13, 15.
5. Richard J. Watts, "Hazardous Waste : Sources, Pathways, Receptars", John Willey & Sons, Inc. PP- 20-23
6. Rahul Kar, "Management of Hazrdous Wastes", Journal IAEM, Vol.25, (1998) PP- 10
7. William P. Cunningham, Terence M. Cooper, Entle Gerham, Malcolm T. Hepworth, "Environmental Eneyclopedia", 2nd Edition, Jaico Pulishing House.
8. Nicholas P. Chosemisinoff and Paul N. Chosemisinoff, "Encylopedia of Environment and Pollution Control, Hazardous Materialsand Waste Management", Vol. III, Jaico Publishing House, PP – 38-40, 51.

TABLE – 1
DETAILS SHOWING THE SAMPLING OF COLLECTION OF EFFLUENT AND SLUDGE

Sr. No.	Date of Sampling	Time	Volume of Sample collected		Dried Sludge	Material of Container
			Effluent	Slurry		
1.	10-02-2004	16.00 hrs	5 litres	-	1 kg.	Effluent in LDPE Carboy and Sludge in plastic container
2.	24-02-2004	14.10 hrs	5 litres	-	1 kg.	
3.	09-03-2004	17.30 hrs	5 litres	-	1 kg.	

TABLE – 2
METAL ANALYSIS OF EFFLUENT - 10.02.2004

Sr. No.	Parameter	Eq. Tank	Final Outlet
1.	Arsenic	0.0	0.0
2.	Barium	0.046	0.014
3.	Cadmium	0.0005	0.0
4.	Chromium	0.009	0.001
5.	Lead	0.074	0.032
8.	Mercury	0.0	0.0
7.	Selenium	0.0	0.0
8.	Silver	0.0	0.0

All parameters in mg/L

TABLE – 3
EFFLUENT ANALYSIS - 10.02.2004

Sr. No.	Parameter	Eq.T	PST	AT	FC	Final Outlet
1.	PH	7.6	7.3	7.5	7.5	7.89
2.	TDS	6908	6600	5792	4291	3974
3.	SS	2232	1050	625	254	119
4.	COD	960	451	304	311	176
5.	BOD	580	423	170	114	90
6.	TOC	551.6	443	334	109	83.51
7.	Oil and Grease	26.18	21.81	12.23	7.70	7.72

All parameters in mg/L except pH

Eq.T = Equalization Tank
PST = Primary Settling Tank
AT = Aeration Tank
FC = Final Clarifier

TABLE – 4
SLUDGE ANALYSIS - 10.02.2004

Sr. No.	Parameter	Eq. Sludge	Primary Sludge	Biological Sludge
1.	pH	7.6	8.3	7.9
2.	COD	1040	800	336
3.	BOD	829	390	257
4.	TOC	162.7	216.6	1162
5.	Oil and Grease	14	8	6

All parameters in mg/L except pH

TABLE – 5
METAL ANALYSIS - 10.02.2004

Sr. No.	Parameter	Eq. Sludge	Primary Sludge	Biological Sludge
1.	Arsenic	0.0	0.0	0.0
2.	Barium	0.0388	0.027	0.012
3.	Cadmium	0.0	0.0	0.0
4.	Chromium	0.006	0.004	0.001
5.	Lead	0.037	0.037	0.032
6.	Mercury	0.0	0.0	0.0
7.	Selenium	0.0	0.0	0.0
8.	Silver	0.005	0.002	0.0

All parameters in mg/L

TABLE – 6
CONFIRMATORY TEST ANALYSIS

Sr. No.	Parameters	Observation (Average Values)
1.	pH	Found between 7.3 to 7.89
2.	TOC	83.51 to 551.6 mg/L
3.	Ignitability	Not ignited when exposed to flame (flash point 7200^{0}C). Not capable of causing fire under normal temperature and pressure.
4.	Odour	Odourless.
5.	Ractivity	No reaction observed with water i.e. the sludges are stable. It does not form any gas or fume during the reaction.

Releasing of First State Level GIT-Jet, Research Journal
on 1st April, 2008 by Prof. Dr. B. G. Patel, Vice Chancellor, S P University,
Dr. K. N. Sheth, Convener & Editor in Chief and Dr. Y. P. Kosta, Member of Editorial Board

Trustees of Platinum Foundation

Shri Harishbhai Rohera

Shri Ghanshyambhai Thakkar

Smt. Varshaben M. Pandhi

Shri Deepakbhai Ravani

Shri Pravinbhai Shah

CONTENTS

Gandhinagar Institute of Technology, M.B.A. Programme

Published by Platinum Foundation
Printed at Dharmanandan Press, Isanpur, Ahmedabad

Designed by
Hiren Trivedi